



HAL
open science

Generalized Osteosclerotic Condition in the Skeleton of *Nanophoca vitulinoides*, a Dwarf Seal from the Miocene of Belgium

Leonard Dewaele, Olivier Lambert, Michel Laurin, Tim de Kock, Stephen Louwye, Vivian de Buffrénil

► **To cite this version:**

Leonard Dewaele, Olivier Lambert, Michel Laurin, Tim de Kock, Stephen Louwye, et al.. Generalized Osteosclerotic Condition in the Skeleton of *Nanophoca vitulinoides*, a Dwarf Seal from the Miocene of Belgium. *Journal of Mammalian Evolution*, 2019, 26 (4), pp.517-543. 10.1007/s10914-018-9438-9 . hal-02550689

HAL Id: hal-02550689

<https://hal.sorbonne-universite.fr/hal-02550689>

Submitted on 22 Apr 2020

HAL is a multi-disciplinary open access archive for the deposit and dissemination of scientific research documents, whether they are published or not. The documents may come from teaching and research institutions in France or abroad, or from public or private research centers.

L'archive ouverte pluridisciplinaire **HAL**, est destinée au dépôt et à la diffusion de documents scientifiques de niveau recherche, publiés ou non, émanant des établissements d'enseignement et de recherche français ou étrangers, des laboratoires publics ou privés.

Journal of Mammalian Evolution

Generalized osteosclerotic condition in the skeleton of *Nanophoca vitulinoides*, a dwarf seal from the Miocene of Belgium --Manuscript Draft--

Manuscript Number:	JOMM-D-17-00063R2	
Full Title:	Generalized osteosclerotic condition in the skeleton of <i>Nanophoca vitulinoides</i> , a dwarf seal from the Miocene of Belgium	
Article Type:	Original Article	
Keywords:	Neogene; Phocidae; <i>Nanophoca vitulinoides</i> ; osteohistology; microanatomy; osteosclerosis	
Corresponding Author:	Leonard Dewaele Universiteit Gent Ghent, BELGIUM	
Corresponding Author Secondary Information:		
Corresponding Author's Institution:	Universiteit Gent	
Corresponding Author's Secondary Institution:		
First Author:	Leonard Dewaele	
First Author Secondary Information:		
Order of Authors:	Leonard Dewaele	
	Olivier Lambert	
	Michel Laurin	
	Tim De Kock	
	Louwye Stephen	
	Vivian de Buffr�enil	
Order of Authors Secondary Information:		
Funding Information:	Fonds Wetenschappelijk Onderzoek (11V9117N)	Mr. Leonard Dewaele
	Society of Vertebrate Paleontology (2016 Steven Cohen award for excellent student research)	Mr. Leonard Dewaele
	Fonds Wetenschappelijk Onderzoek	dr. Tim De Kock
Abstract:	<p>In the fossil record, it has been shown that various clades of secondarily aquatic tetrapods experienced an initial densification of their bones in the early stages of their evolution, and developed spongier and lighter bones only later in their evolution, with the acquisition of more efficient swimming modes. Although the inner bone structure of most secondarily aquatic tetrapods has already been studied, no research hitherto focused on true seals, or Phocidae. However, preliminary observations previously made on a Miocene species, <i>Nanophoca vitulinoides</i>, suggested that this taxon showed pronounced specialization of bone structure as compared to other seals. This feature justifies a specific comparative study, which is the purpose of this article. Microanatomical analysis of bones of <i>N. vitulinoides</i> shows compactness values nearing 100%, which is much higher than in other semi-aquatic mammals, pinnipeds included. Osteohistological analyses show virtually complete remodeling of the medullary territory by Haversian substitution. Extreme bone compactness locally resulted from an imbalance, towards reconstruction, of this process. Cortical regions were less intensely remodeled. In a number of specimens, the cortex shows clear growth marks as seasonal lines of arrested growth. The results suggest that, despite the extreme compactness of long bones of <i>N. vitulinoides</i> and the small size of this</p>	

taxon, the growth rate of the cortex, and that of the bones in general, did not differ strongly from that of other, larger phocids. Extreme skeletal compaction and densification must have increased body density in *Nanophoca*. Consequently, speed, acceleration, and maneuverability must have been low, and this taxon was most likely a near-shore bottom-dwelling seal. Consequently, dietary preferences were most likely oriented towards benthic food sources.

Leonard Dewaele
Department Geology
281 Krijgslaan
Ghent 9000
Belgium

Ghent, 2018/03/28

Dear Editor,

Please find attached the revised version of our manuscript "Generalized osteosclerotic condition in the skeleton of *Nanophoca vitulinoides*, a dwarf seal from the Miocene of Belgium." After minor revisions, we would like to resubmit the final manuscript to the *Journal of Mammalian Evolution*. We would also like to thank you for your helpful comments.

We implemented all grammar and spelling suggestions and comments. Although few in number, we made a limited number of changes that have not been requested by the Editor:

- 1) On two occasions, we wrote "*Phocanella pumilla*." This has been changed to "*Phocanella pumila*" with one "l".
- 2) We changed the position of Canoville and Laurin (2010) and Canoville et al. (2016) in the reference list in order to make it alphabetical.
- 3) The Editor did not explicitly request that "annuli" should not be in italics in the caption of Fig. 10. However, we adjusted this in order to be consistent with the other comments in the manuscript.

We added the paragraph "Data Availability" where the Editor requested it, and we hope that it fulfils the requirements for publication.

Although we adhere to the comments of the Editor, we wish to draw the attention to the abbreviations of genus names. For instance, in some instances, *Nanophoca vitulinoides* is abbreviated in some paragraphs before it is spelled out. This is the case in all paragraphs of the microanatomical part of the results. On other occasions, the Editor requests to spell out names after the first mention in a paragraph. This applies for instance to *Callophoca obscura* and *Phocanella pumila* in the caption for Fig. 12, and for *Phocanella pumila* on l.442, 447, and 449 of the returned manuscript, in the "Comparative data" section.

Although we follow the instructions of the Editor in the revised manuscript, we feel that this contradicts with the guidelines to spell out names only the first time they are mentioned in each paragraph.

We hope that the revised manuscript is in fulfillment for publication in *Journal of Mammalian Evolution*.

Sincerely,

Leonard Dewaele and co-authors

[Click here to view linked References](#)

1 **Generalized osteosclerotic condition in the skeleton of *Nanophoca***
2
3 ***vitulinoides*, a dwarf seal from the Miocene of Belgium**
4
5
6

7 3

8
9
10 4 Leonard Dewaele^{1,2*}, Olivier Lambert², Michel Laurin³, Tim De Kock⁴, Stephen
11
12 Louwye¹, Vivian de Buffrénil³
13
14

15
16 6 ¹Vakgroep Geologie, Universiteit Gent, Ghent, Belgium
17

18
19 7 ²Directorate “Earth and History of Life”, Institut Royal des Sciences Naturelles de Belgique,
20
21 Brussels, Belgium
22

23
24 9 ³Département Origines et Evolution, Muséum National d’Histoire Naturelle, Paris, France
25
26

27
28 10 ⁴PProGRess, Vakgroep Geologie, Universiteit Gent, Ghent, Belgium
29
30

31 11 *Corresponding author: leonard.dewaele@ugent.be
32
33

34 12

35
36
37 13 **ABSTRACT**
38
39

40 14 In the fossil record, it has been shown that various clades of secondarily aquatic tetrapods
41
42 15 experienced an initial densification of their bones in the early stages of their evolution, and
43
44 16 developed spongier and lighter bones only later in their evolution, with the acquisition of
45
46 17 more efficient swimming modes. Although the inner bone structure of most secondarily
47
48 18 aquatic tetrapods has already been studied, no research hitherto focused on true seals, or
49
50 19 Phocidae. However, preliminary observations previously made on a Miocene species,
51
52 20 *Nanophoca vitulinoides*, suggested that this taxon showed pronounced specialization of bone
53
54 21 structure as compared to other seals. This feature justifies a specific comparative study, which
55
56 22 is the purpose of this article. Microanatomical analysis of bones of *N. vitulinoides* shows
57
58
59
60
61
62
63
64
65

23 compactness values nearing 100%, which is much higher than in other semi-aquatic
24 mammals, pinnipeds included. Osteohistological analyses show virtually complete
25 remodeling of the medullary territory by Haversian substitution. Extreme bone compactness
26 locally resulted from an imbalance, towards reconstruction, of this process. Cortical regions
27 were less intensely remodeled. In a number of specimens, the cortex shows clear growth
28 marks as seasonal lines of arrested growth. The results suggest that, despite the extreme
29 compactness of long bones of *N. vitulinoides* and the small size of this taxon, the growth rate
30 of the cortex, and that of the bones in general, did not differ strongly from that of other, larger
31 phocids. Extreme skeletal compaction and densification must have increased body density in
32 *Nanophoca*. Consequently, speed, acceleration, and maneuverability must have been low, and
33 this taxon was most likely a near-shore bottom-dwelling seal. Consequently, dietary
34 preferences were most likely oriented towards benthic food sources.

35
36 Keywords: Neogene, Phocidae, *Nanophoca vitulinoides*, osteohistology, microanatomy,
37 osteosclerosis

38
39
40
41
42
43
44
45
46
47
48
49
50
51
52
53
54
55
56
57
58
59
60
61
62
63
64
65

39 **INTRODUCTION**

1
2
3 40 Numerous studies have shown the existence of a general relationship between the bone
4
5 41 microanatomy and the ecology of tetrapods (e.g., Wall 1983; Stein 1989; Fish and Stein,
6
7 42 1991; Turner 1998; Ricqlès and Buffrénil 2001; Germain and Laurin 2005; Liu et al. 2009;
8
9 43 Amson et al. 2014). Several lineages of tetrapods returned to the aquatic environment (e.g.,
10
11 44 Uhen 2007; Pyenson et al. 2014; and references therein), and data available hitherto suggest
12
13 45 that, in such forms, fast and agile swimming amniotes have lighter and spongier bones than
14
15 46 slow bottom-dwellers, which generally have heavy and compact (osteosclerotic) bones
16
17 47 (Buffrénil et al. 1988, 1989; Webb and Buffrénil 1990; Taylor 2000; Laurin et al. 2011;
18
19 48 Houssaye et al. 2013). In slow secondarily aquatic tetrapods, such as sirenians, the heavy
20
21 49 bones passively compensate the buoyancy generated by lung volume and help conserve
22
23 50 energy during swimming at shallow depth (Domning and Buffrénil 1991; Ricqlès and
24
25 51 Buffrénil 2001; Houssaye 2009; see also Taylor 2000). Two mechanisms may increase
26
27 52 skeletal mass: thickening of the cortex (pachyostosis), or increased inner compactness of the
28
29 53 bones (osteosclerosis); both can also occur simultaneously to form pachyosteosclerosis (e.g.,
30
31 54 Buffrénil et al. 2010; Houssaye et al. 2016). However, most marine tetrapod clades show an
32
33 55 initial evolutionary stage of pachyosteosclerosis prior to the regression of this feature in pace
34
35 56 with the development of more efficient swimming modes (Ricqlès 1989).

36
37 57 Although pinnipeds are “marine mammals,” they retain some terrestrial mobility,
38
39 58 which makes them an interesting model for studying the modification of bone structure in the
40
41 59 course of an evolutionary adaptation to marine life. However, bone histology and
42
43 60 microanatomy in these animals has received little attention in the past, with few exceptions
44
45 61 (e.g., Stein 1989). Indeed, while the osteohistology and microanatomy of other marine
46
47 62 mammal clades was specifically studied from an evolutionary point of view, pinnipeds were
48
49 63 considered only in the context of broad comparative datasets including extensive taxonomic
50
51
52
53
54
55
56
57
58
59
60
61
62
63
64
65

64 sampling, at the scale of Mammalia or marine tetrapods (e.g., Laurin et al. 2011; Dumont et
65 al. 2013; Canoville et al. 2016; Houssaye and Fish 2016; Houssaye et al. 2016). Two
66 contributions specifically dealing with pinnipeds can be mentioned: the preliminary study of
67 the extinct walrus *Valenictus*, showing pachyosteosclerosis in this taxon (Deméré 1994a, b),
68 and the publication on pachyosteosclerosis in the seal *Pachyphoca*, from the middle Miocene
69 of the Ukraine (Eastern Paratethys), by Koretsky and Rahmat (2017). Unfortunately, this
70 study gives only a very brief microanatomical description, without histological, quantitative
71 data or informative figures relevant to this topic. Existing information suggests that bone
72 structure of the pinnipeds differs little from that of most other mammals, because they display
73 none of the conspicuous specializations of bone inner architecture often encountered in
74 marine tetrapods. Indeed, their appendicular long bones, though not strictly tubular
75 (tubularity sensu stricto is a peculiar adaptation of the diaphyseal region of some limb bones
76 to a terrestrial locomotion), have compact periosteal cortices framing a nearly open medullary
77 cavity with only few slender trabeculae (see e.g., Quemeneur et al. 2013 for the femur;
78 Canoville and Laurin 2010 for the humerus; Germain and Laurin 2005 for the radius; see also
79 Nakajima and Endo 2013). Moreover, the structure of their ribs (comparative data in
80 Canoville et al. 2016) and vertebrae (Dumont et al. 2013; Houssaye et al. 2014) merely
81 reflects the common condition observed in most mammals. This situation may seem
82 paradoxical considering the intermediate habitat and mode of locomotion that characterizes
83 this taxon. Miscellaneous observations nevertheless suggest that the question may be more
84 complex and that in the pinnipeds, and more generally within a given clade and a general
85 habitat (e.g. coastal, pelagic, etc.), bone structure may differ between taxa according to the
86 detailed characteristics of their ecological adaptations (see also on this topic Houssaye et al.
87 2016). Such is the case, for example, of the bones of *Nanophoca vitulinoides*, a small phocid
88 from the middle Miocene (late Langhian–late Serravallian; ca. 14.2–11.6 Ma) of Antwerp

89 region, in Belgium. From broken and fractured specimens, the internal structure of bones in
90 this taxon appears extremely compact and lacks a differentiated medullary cavity. These
91 intriguing preliminary observations call for further analysis.

92 The aim of the present study is to describe and interpret the osseous structure of
93 *Nanophoca* at both the microanatomical and histological levels, and compare it with similar
94 data from other phocids and more distantly related taxa. *Nanophoca vitulinoides* is the best-
95 known extinct seal from the Neogene (Miocene + Pliocene, 23.03 – 2.58 Ma) of the North
96 Sea Basin, and represents more than half the fossil seal specimens at the Royal Belgian
97 Institute of Natural Sciences, or RBINS (Dewaele et al. 2017a). Its postcranial skeleton is the
98 most complete described hitherto (Fig. 1); however, cranial elements are still lacking.
99 *Nanophoca vitulinoides* is remarkable in two respects: first, with a total estimated length of
100 approximately one meter, it is one of the smallest known Phocidae (Dewaele et al. 2017a); in
101 this family, only *Batavipusa neerlandica* from the early to middle Tortonian (8–11.5 Ma) of
102 the Netherlands, *Monachopsis* from the early to middle Tortonian (c. 8.4–11.4 Ma) of
103 Moldova, and *Pachyphoca chapskii* from the late Serravallian to early Tortonian (11.2–12.3
104 Ma) of Ukraine are about as small or smaller, based on humeral length (Koretsky 2001;
105 Koretsky and Peters 2008; Koretsky and Rahmat 2013; Dewaele et al. 2017a). Second, most
106 late Neogene seal taxa found in Belgium also occur in the Lee Creek Mine of the Yorktown
107 Formation, Aurora, North Carolina, USA; *N. vitulinoides* is the only one restricted to Belgian
108 strata (Koretsky and Ray 2008; Dewaele et al. 2017a). Studying bone structure in this taxon,
109 and comparing it with other seals could, on the one hand, bring basic data (still missing
110 hitherto) on bone histology in phocids and, on the other hand, show the nature of the
111 structural specialization of the *Nanophoca* skeleton, which would help in inferring its
112 development and possible functional/ecological significance.

114 **MATERIAL AND METHODS**

115 **BIOLOGICAL SAMPLE**

116 This study rests on two main methodological approaches: A) gross (macro-anatomic)
117 morphometry for assessing the presence or absence of pachyostosis in *Nanophoca*; B)
118 microanatomy and histology for describing the inner structure of the bones.

119 For the morphometric part, 29 humeri from 13 phocid species and 25 femora from 12
120 species were measured by one of us (LD), roughly following the procedure used by Buffr nil
121 et al. (2010) for sirenian ribs. Similar data from the literature were also considered (Tables 1,
122 2). The new morphometric data presented below include three extant taxa: the grey seal
123 *Halichoerus grypus* from the cold temperate and subarctic zones of the North Atlantic, the
124 harbor seal *Phoca vitulina* from the temperate to arctic zones of the North Atlantic and North
125 Pacific, and the Baikal seal *Pusa sibirica* from Lake Baikal. All bones included in the study
126 were from adult or subadult individuals, judging from the degree of epiphyseal fusion in
127 associated long bones (see Stor  2000). The comparative sample of extinct phocids is largely
128 dependent on the published fossil record; this is why some taxa are represented in the dataset
129 by both humeri and femora, while others are only represented by measurements of either
130 humeri or femora.

131 Because the dataset used for the morphometric study depends on the literature, the
132 dataset employed for the microanatomical and histological studies is necessarily different as it
133 is based on first-hand analyses of actual specimens available for scanning and/or sectioning.
134 (see Tables 1, 2 versus Table 3). The microanatomical dataset includes measurements on the
135 extant phocine *Phoca vitulina*, the extinct phocids *Nanophoca vitulinoides*, including the
136 neotype specimen IRSNB M2276, *Callophoca obscura* from the Tortonian to Zanclean (late
137 Miocene – early Pliocene) of Belgium and North Carolina (LD pers. obs.), *Leptophoca*
138 *proxima* from the late Aquitanian to late Serravallian (late early Miocene – late middle

139 Miocene) of Belgium and the North American Chesapeake Bay area (Koretsky 2001;
140 Dewaele et al. 2017b), and *Phocanella pumila* from the Tortonian to Zanclean (late Miocene
141 – early Pliocene) of Belgium and North Carolina (LD pers. obs.). Two additional small extinct
142 Neogene phocids from the southern North Sea Basin are also considered: *Batavipusa*
143 *neerlandica*, from the early to middle Tortonian (8 – 11.5 Ma) of the Netherlands, and
144 *Praepusa boeska*, from the late Miocene to late Pliocene of Belgium and the Netherlands
145 (Koretsky and Peters 2008; Koretsky et al. 2015). However, the fossil record of these taxa is
146 extremely scarce and the attribution of the various specimens to each taxon is questionable
147 (e.g., Koretsky and Peters 2008, Koretsky et al. 2015, Dewaele et al. 2017a). Tomographic
148 (CT) data for *B. neerlandica* and *Pr. boeska* are of moderate quality. Distinction between the
149 internal structures of the bone and the sediment infill proved unpractical, and both taxa are
150 only considered qualitatively. Additional data (from either classical thin sections or micro-CT
151 scans) already published by Buffrénil and Schoevaert (1989), Buffénil et al. (2010), Canoville
152 and Laurin (2010), Canoville et al. (2016), and Amson et al. (2014) about the inner structure
153 of long bones in various extant and extinct aquatic mammals (otters, marine sloths, polar bear,
154 and sirenians) were also considered for the comparisons (Table 3). In extinct phocid taxa, the
155 osteohistological dataset is limited to three species, in addition to *N. vitulinoides*: the
156 monachine *Callophoca obscura*, and the phocines *Leptophoca proxima* and *Phocanella*
157 *pumila* (Table 3). The bone samples for these taxa include femora, humeri, radii, ribs, tibiae,
158 and lumbar vertebrae with both transverse and longitudinal sections. These bones are also
159 known in the fossil record of *N. vitulinoides* and can therefore allow detailed comparisons.

160

161 **PROCESSING OF THE SPECIMENS**

162 **Morphometric features.** Buffrénil et al.'s (2010) study focused on the discrimination of
163 pachyostosis sensu stricto (cortical hyperplasy) in ribs and used, among other measurements,

164 rib length. Unfortunately, very few entire ribs are available for fossil seals, and the so-called
165 Cortical Development index used by these authors (the calculation of this index requires
166 measurements of total length, chord, and mean circumference of the ribs) could not be applied
167 to the ribs of *N. vitulinoides*; conversely, this index, called here “bulkiness index,” or BI,
168 could be used for the humeri and femora in the same conditions as for the other phocid
169 specimens (Fig. 2). For the humerus, two measurements were taken: A) absolute sagittal
170 length of the bone between the most proximal point and most distal point, or BL, and B)
171 transverse width at mid-shaft, or TW. For the femur, three measurements were taken: A)
172 absolute sagittal length (BL), B) transverse width at the narrowest portion of the diaphysis
173 (TW), and C) anteroposterior width of the diaphysis in the same portion (APW), which is
174 perpendicular to transverse width. For the humerus, the calculated ratio is $BI = TW/BL$. A
175 low BI value indicates a relatively narrow diaphysis, and a high value indicates a relatively
176 thick diaphysis. For the femur, the ratio is $BI = [0.5(TW+APW)]/BL$. Similarly, a low value
177 of BI indicates a relatively narrow diaphysis, and a high value indicates a relatively thick
178 diaphysis.

179 **Thin section analysis (microanatomy and histology).** Thin section preparation was carried
180 out according to the classical procedures used for this kind of preparations (Lamm 2013). All
181 the sections made for this study are now part of the Histotheque (i.e., thin section collection)
182 housed in the Muséum national d’Histoire naturelle in Paris, where they are recorded under
183 various numbers within the Histos database. These sections include transverse mid-diaphyseal
184 and metaphyseal sections, with additional longitudinal sections through the epiphyses.
185 Microscopy was performed using a Zeiss Axioskop microscope, with ordinary and polarized
186 transmitted light at low (x25) to medium (x400) magnifications. All measurements of
187 sectional dimensions were performed with the software ImageJ (National Institute of Health,
188 USA) on microphotographs. For microanatomy, only mid-diaphyseal transverse sections were

189 considered. The terminology used in microanatomical and histological descriptions refers to
190 Francillon-Vieillot et al. (1990) and Prondvai et al. (2014).

191 **X-ray computed microtomography (micro-CT)**. A part of the biological sample (see Table
192 4–8) consists of specimens scanned at the Ghent University Centre for X-ray Tomography
193 (www.ugct.ugent.be) with a custom-built microtomograph HECTOR (Masschaele et al.
194 2013). Depending on the sample, the tube was operated at 140 to 160 kV and 40 to 45 W. A 1
195 mm Al filter was applied to reduce beam hardening, which was then further filtered during the
196 reconstruction process. The reconstruction was performed with OCTOPUS
197 RECONSTRUCTION (XRE Belgium). Resulting images had a voxel size of approximately
198 30 μm , 46 μm , or 84 μm , depending on the magnification (see Table 4–8).

199 **Cross-section analysis using *BONE PROFILER***—All cross-sections (be they material thin
200 sections or virtual micro-CT Scan sections) were analyzed using BONE PROFILER Version
201 4.5.8 (Girondot and Laurin 2003). BONE PROFILER is a freeware dedicated to the analysis
202 of bone compactness in sections, i.e., the area actually occupied by mineralized bone tissue
203 divided by total sectional area, and designed to calculate relevant parameters describing the
204 compactness profile. To do so, the entire cross-section is divided in 3060 cells created by the
205 intersection of 60 sectors ($360^\circ/60 = 6^\circ$ per sector) and 51 concentric rings parallel to the
206 section outline (Laurin et al. 2004: fig. 3). Compactness distribution and variation from the
207 ontogenetic center of the sections to cortical surface are presented as the ‘compactness
208 profile’. The compactness profile is characterized by four parameters S, P, Min, and Max. S is
209 the reciprocal of the slope at the curve inflection point, and it is proportional to the relative
210 width of the transition zone between the medulla and the cortical regions. P is the position of
211 the curve inflection point on the x-axis, and it represents the position of the transition area
212 between the medulla and the cortical region. Min and Max are the minimum and maximum
213 asymptotes, respectively, representing the minimum and maximum values of bone

214 compactness in a section. Other parameters can be calculated using BONE PROFILER
1
2 215 (Laurin et al. 2004; Quemeneur et al. 2013), but these were not used in the current study.
3
4 216 More elaborate analyses with BONE PROFILER including parameters Minrad, Maxrad, Srad,
5
6
7 217 and Prad are not used in the present study, but are provided as Supporting Information
8
9 218 (Appendix 1). These are similar to the abovementioned parameters, but are the radial
10
11 219 versions, i.e., the average values of the measurements for the 60 sectors. Hence, standard
12
13 220 deviations (SD) are also calculated for these values.
14
15
16
17
18 221
19
20

21 222 **PHYLOGENETIC FRAMEWORK**

22
23

24 223 For the phylogenetic position of *N. vitulinoides* in the current study, we follow the
25
26 224 phylogenetic analysis by Dewaele et al. (2017a), which is, to date, the only published analysis
27
28 225 including this species (Fig. 3). According to Dewaele et al. (2017a: fig. 25; Fig 3. in the
29
30 226 current study), *N. vitulinoides* is a relatively late-branching stem-phocine; it is the closest
31
32 227 known relative of crown Phocinae. Evidently, it should be noted that this phylogenetic
33
34 228 position is only relative to the other Operational Taxonomic Units (OTUs) included in this
35
36 229 analysis. The phylogenetic relationships of other small phocids, such as *Batavipusa*
37
38 230 *neerlandica*, *Pontophoca sarmatica*, *Praepusa boeska*, or –most notably– *Monachopsis*
39
40 231 *pontica* has been studied by Koretsky (2001) and Koretsky and Rahmat (2013). However,
41
42 232 their fossil record is too scarce (e.g., *B. neerlandica* is only known from one isolated humerus,
43
44 233 an isolated ilium, and an isolated partial femur tentatively assigned to it; *M. pontica* is only
45
46 234 known from multiple isolated humeri and femora) to be confident about their phylogenetic
47
48 235 position. Not surprisingly, previous phylogenetic analyses including those taxa show little
49
50 236 consensus and confidence on their phylogenetic position (Koretsky 2001; Koretsky and
51
52 237 Rahmat 2013). For the phylogeny of other, extant Pinnipedia included in this study, we refer
53
54 238 to Higdon et al. (2007). The extinct *Callophoca obscura*, *Leptophoca proxima*, and
55
56
57
58
59
60
61
62
63
64
65

239 *Phocanella pumila* have all been considered in phylogenetic analyses. There is little
1
2 240 consensus about the phylogenetic position of the monachine *C. obscura*. Some researchers
3
4 241 consider *C. obscura* most closely related to the extant elephant seal *Mirounga*, while others
5
6 242 group it with the late Pliocene *Pliophoca etrusca* from Italy, or consider it as a stem
7
8 243 monachine (compare Muizon 1981; Koretsky and Ray 2008; Koretsky and Rahmat 2013;
9
10 244 Amson and Muizon 2014; Berta et al. 2015). Therefore, we consider *C. obscura* a monachine
11
12 245 phocid, but we do not make genus-level phylogenetic inferences for this taxon. The
13
14 246 phylogenetic position of *L. proxima* (or as *Leptophoca lenis*) has been first analyzed by
15
16 247 Koretsky (2001) and Koretsky and Rahmat (2013), but without consensus. Cozzuol (2001)
17
18 248 interpreted *L. lenis* as an early-branching phocine, while Berta et al. (2015) suggested that the
19
20 249 taxon was an early-branching stem monachine. However, the latter expressed doubt over their
21
22 250 phylogenetic results for *Leptophoca*. More recent studies by Dewaele et al. (2017a, b) placed
23
24 251 *L. proxima* as a stem phocine with strong statistical support. The phylogenetic position of *P.*
25
26 252 *pumila* has only been analyzed once, by Koretsky and Rahmat (2013). However, they neither
27
28 253 present the character matrix nor a list of synapomorphies to support their analysis. In addition,
29
30 254 this analysis differs on key nodes from other, widely-accepted phylogenetic analyses (e.g.
31
32 255 Bininda-Emonds and Russell 1996), inhibiting us of considering this analysis to elucidate the
33
34 256 phylogenetic position of *Phocanella pumila*. The phylogenetic position of the latter remains
35
36 257 unclear, pending future discoveries of more complete material and new analyses. This
37
38 258 information is provided only as contextual information; we did not perform any phylogeny-
39
40 259 informed statistical tests in this study given that the focus is on only three early pinniped taxa.
41
42
43
44
45
46
47
48
49
50
51

260

261 **INSTITUTIONAL ABBREVIATIONS**

262 **IRSNB/RBINS**, Institut royal des Sciences naturelles de Belgique, Brussels, Belgium; **MAB**,
263 Oertijdmuseum Groene Poort, Boxtel, the Netherlands; **MNHN**, Muséum national d'Histoire

264 naturelle, Paris, France; **MSC**, Smithsonian Institution Museum Support Center, Suitland,
265 Maryland, USA; **USNM**, National Museum of Natural History, Washington, DC, USA.

266

267 **DATA AVAILABILITY**

268 All data used in this study is presented within the main text. Additional results from the radial
269 analysis with BONE PROFILER are provided as Supporting Information (Appendix 1). Thin
270 sections that are used in this study are housed at the MNHN. Specimens that have been CT-
271 scanned are housed at the IRSNB. Specimens are available for consultation and access should
272 be requested at the respective institutions.

273

274 **RESULTS**

275 **MORPHOMETRIC DATA**

276 Although no complete ribs of *N. vitulinoides* are preserved to perform morphometric
277 measurements, the sub-circular morphology of the cross-section from these bones differs from
278 that of related taxa (Fig. 5A versus Fig. 5B, C). For a similar rib length (a parameter that
279 unfortunately is lacking), it could possibly be indicative of some incipient tendency toward
280 pachyostosis. Morphometric results for the humerus and femur are listed as Tables 1 and 2.
281 The diaphysis of the humerus of *Nanophoca* is relatively slender, as compared to other extant
282 and extinct Phocidae. BI ratio for the humerus of two specimens of *N. vitulinoides* is 0.121
283 and 0.135, which is at the lower half of the range of the 29 calculated values (0.109 – 0.210)
284 (Table 1). Apart from the extinct *Batavipusa neerlandica* (0.182), *Monachopsis pontica*
285 (0.169), and *Pachyphoca ukrainica* (0.210), extinct Phocidae in our sample tend to have a

286 relatively slender humeral diaphysis, as compared to extant forms. This rules out the eventual
287 occurrence of pachyostosis in the humerus of *N. vitulinoides*.

288 Bulkiness index values indicate that the femoral diaphysis of *N. vitulinoides* (0.200,
289 0.207, and 0.208) and other extinct Phocidae (0.173 – 0.240) is overall relatively thick, as
290 compared to extant Phocidae (0.158 – 0.187) (Table 2). This contrasts with the measurements
291 of the humeri. As for the humerus, the taxon with the bulkiest femur is *Pachyphoca*, returning
292 a value of 0.240 for *Pachyphoca ukrainica*, based on the average of three specimens
293 presented by Koretsky and Rahmat (2013), and a value of 0.229 for one specimen of
294 *Pachyphoca chapskii*. Given that the femora of the extinct taxa in our sample have
295 consistently higher values, i.e., suggestive of pachyostosis, it remains difficult to find
296 conclusive evidence on the presence or absence of pachyostosis in the femur of *N. vitulinoides*
297 in comparison to contemporaneous taxa.

298

299 MICROANATOMY

300 *Vertebrae*

301 [Table 4]

302 [Figure 4]

303 Bone compactness in the centra of the two lumbar vertebrae of *N. vitulinoides*, ranges from
304 93.8% for the adult, to 63.6% for the juvenile. (Table 4; Fig. 4). These values are much higher
305 than those observed in the other pinnipeds and semi-aquatic mammals included in this study
306 (Table 4): compactness values indeed range for these taxa from 22.3% (hooded seal,
307 *Cystophora cristata*) to 44.3% (sea otter, *Enhydra lutris*). Apart from *N. vitulinoides*, the
308 compactness values for the vertebrae of the Phocinae (22.3% for *C. cristata* and 29.3% for the

309 harp seal, *Pagophilus groenlandicus*) are lower than the values calculated for Monachinae and

310 Otariidae.

311

312 **Rib**

313 [Table 5]

314 [Figure 5]

315 With an overall compactness of 99.8%, the rib of *N. vitulinoides* is almost completely

316 ossified, and much more compact than that of other semi-aquatic mammals (Table 5; Fig. 5).

317 The Cape fur seal *Arctocephalus pusillus* and the Californian sea lion *Zalophus californianus*

318 have the second and third most compact ribs in the biological sample, with compactnesses of

319 78.4% and 78.2%, respectively. While there is no differentiated medullary cavity in the rib of

320 *N. vitulinoides* (Fig. 5A), the medullary cavity in the ribs of other taxa in the biological

321 sample is occupied by loose spongiosa and surrounded by a compact cortex (Fig. 5B, C).

322

323 **Humerus**

324 [Table 6]

325 [Figure 6]

326 [Figure 7]

327 With an overall compactness of 99.7% for one specimen and 99.9% for the other, the humerus

328 of *N. vitulinoides* is almost completely solid (Table 6; Fig. 6). Only the humerus of

329 *Phocanella pumila* has a comparably (though somewhat lesser) high compactness (95.9%);

330 but unlike *Phocanella pumila*, there is no discernable medullary cavity in the two specimens

331 of *N. vitulinoides* (Fig. 6A, B versus Fig. 6C). Given the poor density differentiation between
332 the mineralized bone tissue and the sediment infill in *Batavipusa neerlandica* and *Praepusa*
333 *boeska*, quantitative microanatomical analysis using BONE PROFILER was precluded. A
334 qualitative analysis reveals the presence of a porous medullary cavity framed by compact
335 cortices in both taxa (Fig. 7A, B).

336

337 ***Femur***

338 [Table 7]

339 [Figure 8]

340 Compactness values for the two femora of *N. vitulinoides*, i.e., 97.1% and 99.4%, are much
341 higher than those of all extant and most extinct semi-aquatic taxa considered in this study
342 (Table 7; Fig. 8A, B versus Fig. 8C, D, F-I). Only the femur of *Phocanella pumila* shows a
343 compactness approaching the condition in *N. vitulinoides* (Table 7; Fig. 8A, B versus Fig.
344 8E).

345

346 ***Other bones***

347 [Table 8]

348 [Figure 9]

349 Other long bones of *N. vitulinoides*, i.e., the radius and the tibia, have been studied as well and
350 show very high compactness ratios, similar to the condition observed in the rib, humerus, and
351 femur (Table 8; Fig. 9). There is no discernable medullary cavity present, unlike, for example,
352 the extant *Phoca vitulina* (Table 8; Fig. 9A, C versus Fig. 9B, D).

353

1
2
3
4
5
6
7
8
9
10
11
12
13
14
15
16
17
18
19
20
21
22
23
24
25
26
27
28
29
30
31
32
33
34
35
36
37
38
39
40
41
42
43
44
45
46
47
48
49
50
51
52
53
54
55
56
57
58
59
60
61
62
63
64
65

354 **BONE HISTOLOGY**

355 In cross and sagittal sections, all bones of *N. vitulinoides* examined in this study share the
356 same basic histological features (in addition to their microanatomical similarity), with only
357 few differences most likely related to ontogenetic age. In most of the bones, except one of the
358 radii (Histos 2142) and one of the vertebral centra (Histos 2150), Haversian remodeling is
359 mild in the cortex; the characteristics of primary periosteal deposits thus remain visible
360 (Fig.10A, B). They consist in layers of woven-parallel tissue (according to Prondvai et al.'s
361 2014 terminology) with longitudinal primary osteons, separated by very birefringent annuli
362 made of parallel-fibered or lamellar bone (Fig.10C). Short Sharpey's fibers (60-80 μm long)
363 colonize the basal parts of the woven-parallel layers (Fig.10C). The annuli are wide (up to 180
364 μm) in the cortical depth, and thinner (some 60-70 μm) towards the cortical periphery. The
365 bone displaying the greatest number of visible growth marks is the humerus, with five sharp
366 annuli (Fig.10A) associated with lines of arrested growth. Of course, in this specimen, several
367 annuli were erased by remodeling in the depth of the cortex. In the long bones where they
368 occur, the annuli tend to be more tightly spaced towards the cortical periphery, but they
369 nevertheless maintain a significant spacing, e.g., 320 μm between the fourth and fifth annuli
370 in the humerus (Fig.10A). In the femur and the humerus, in which cortical structure is
371 perfectly preserved up to the outer margin of the diaphysis, the last growth mark is an annulus
372 (Fig.10A). The nature of the last growth mark is less evident in the other long bones, due to
373 the impregnation of superficial layers by a dark substance during fossilization. However, there
374 is no clear indication of the presence of an external fundamental system (EFS) that could have
375 shown that the growth of the bones, at least in diameter, had dropped to a very low level and
376 that skeletal growth was ending by the time the animals died. In the two specimens (radius
377 Histos 2142 and centrum of the vertebra Histos 2150) where the structure of primary

1
2 378 periosteal deposits is no longer visible, bone cortices are entirely occupied by a particularly
3 379 dense Haversian tissue (Fig.10E) that extends continuously towards the central (medullary)
4
5 380 region of the bones.

6
7 381 The medullary territory of all bones is entirely compact, with the exception of some
8
9 382 scarce, vaguely circular cavities measuring generally less than 300-400 μm in diameter. The
10
11 383 dense Haversian tissue occupying this region (Fig.10F) has three basic characteristics: A) Its
12
13 384 secondary osteons are roughly longitudinal, but their orientation can be locally variable;
14
15 385 moreover, their central canals (Havers' canals) develop numerous transversal anastomoses
16
17 386 (Wolkman's canals), suggesting high BMU (Bone Multicellular Units, i.e., the populations of
18
19 387 cells responsible for the formation of secondary osteons; Frost 1969) activation frequency,
20
21 388 i.e., parameter *Ac.f* in classical histomorphometric nomenclature (cf. Dempster 2013). B)
22
23 389 Most of the secondary osteons show evidence of particularly intense remodeling (Fig.10G,
24
25 390 H), with the presence of two to four cycles of resorption and reconstruction centered on the
26
27 391 Haversian canal. By this process, several generations of osteons with decreasing diameters
28
29 392 were formed inside ontogenetically older secondary osteons. This situation is general in *N.*
30
31 393 *vitulinoides*; it occurs in all secondary bone deposits, be they localized in the medullary or
32
33 394 cortical regions of the bones. C) Such a process resulted in extreme thinning of the lumens of
34
35 395 Havers' canals, which are very seldom wider than 10 μm , and most often less than 5 μm .
36
37 396 Havers' canals in numerous osteons are so drastically reduced that they seem to be completely
38
39 397 occluded (Fig.10H).

40
41 398 This special Haversian tissue, characteristic of the medullary (and occasionally
42
43 399 cortical) region, can be observed in all parts of the long bones: in the mid-diaphyseal region as
44
45 400 well as in metaphyses, from which it extends continuously into the whole epiphyseal regions,
46
47 401 up to the proximal and distal extremities of the bones, where it merges into the thin layers of
48
49 402 calcified cartilage covering articular surfaces (Fig.11A-C). None of the longitudinal sections
50
51
52
53
54
55
56
57
58
59
60
61
62
63
64
65

1
2
3
4
5
6
7
8
9
10
11
12
13
14
15
16
17
18
19
20
21
22
23
24
25
26
27
28
29
30
31
32
33
34
35
36
37
38
39
40
41
42
43
44
45
46
47
48
49
50
51
52
53
54
55
56
57
58
59
60
61
62
63
64
65

403 (which were made in all specimens) reveal the presence of a functional growth plate or a lack
404 of fusion of primary and secondary centers of ossification (Fig.11A, B). We thus conclude
405 that the growth in length of long bone specimens in our sample was complete.

406 With the exception of the vertebral centra (considered below), there is only one
407 variation to this general pattern. In the radius Histos 2174, the medullary territory (51% of the
408 total area in cross section) is occupied by a compacted spongiosa whose former trabeculae,
409 still clearly distinguishable, show numerous reversion lines (created by a strong resorption –
410 reconstruction activity), but no secondary osteons (Fig.11D, E). Conversely, inter-trabecular
411 spaces are entirely filled by endosteal lamellar tissue showing evidence of intense Haversian
412 substitution. This process resulted in several generations of concentric secondary osteons
413 (Fig.10E). Such a detailed topographical difference in remodeling patterns, through which the
414 initial architecture of the medullary spongiosa was preserved, is unknown in all other
415 specimens studied here.

416 The femur, humerus, and ulna examined here display a strong off-centering of growth
417 (Fig.11F) that provoked, on the one hand, the development of a thick primary cortex on the
418 lateral side of these bones and, on the other hand, the superficial outcropping of remodeled
419 medullary regions, due to extensive resorption on their medial side. The result of this double
420 process was a lateral drift of growth. Moreover, several of the long bones show, on cross
421 sections, variably oriented fissures 120 to 200 μm long (Fig.11E). These cracks are observed
422 only in deep cortical regions and in the medullary territory; they never reach the peripheral
423 margins of the bones. Their possible nature and the causes of their occurrence are discussed
424 below (see Discussion).

425 The trabeculae occupying the centrum of the largest vertebra (specimen IRSNB prov.
426 16), as well as the lamellar bone that partly fills inter-trabecular spaces, have a histological
427 structure similar to that observed in the medullary region of long bones: they are formed of

1
2
3
4
5
6
7
8
9
10
11
12
13
14
15
16
17
18
19
20
21
22
23
24
25
26
27
28
29
30
31
32
33
34
35
36
37
38
39
40
41
42
43
44
45
46
47
48
49
50
51
52
53
54
55
56
57
58
59
60
61
62
63
64
65

428 intensively-remodeled tissue (Fig.11G). Remodeling is less intensive in the smaller vertebra;
429 therefore, the growth pattern of this bone remains legible. It was a normal endochondral
430 osteogenesis, with complete resorption of epiphyseal calcified cartilages and active
431 remodeling of primary trabeculae, at a small distance away from the zone of cartilage
432 hypertrophy. In general, none of the bones examined in this study displays the slightest
433 residue of calcified cartilage outside a narrow band (200 to 400 μm) localized just under the
434 epiphyseal surface (Fig.11C). The largest centrum retains only a thin layer of primary
435 periosteal bone tissue spared by remodeling on the walls of the neural arch (Fig.11I). Six
436 tightly spaced growth marks (mean spacing $< 50 \mu\text{m}$) forming an external fundamental
437 system are visible in this layer: the bone was thus reaching the end of its growth.

438

439 **Comparative data**

440 The vertebrae of pinniped taxa other than *N. vitulinoides* show relatively little
441 microanatomical or histological differences from other mammals. Moreover, the diaphyses of
442 their long bones, though presenting some few, slender medullary trabeculae, do not display
443 typical microanatomical or histological peculiarities (very high or very low global
444 compactness, lack of a medullary cavity, cortical hyperplasy, diaphyseal persistence of
445 calcified cartilage, etc.) likely to distinguish these taxa unambiguously from other mammals
446 (see also the Introduction). The only exception is the small development of the medullary
447 cavity in the femur of *Phocanella pumila* (Fig.12A). When primary periosteal cortices in long
448 bones, are partly spared by Haversian substitution (as observed in the femur of *Phocanella*
449 *pumila* and a rib from *Monachus monachus*), they are composed, like those of *N. vitulinoides*,
450 of a woven-parallel complex containing longitudinal primary osteons, annuli and lines of
451 arrested growth (Fig.12B–D). Otherwise, remodeling is intense and spreads to the totality of
452 bone cortices; however, extreme remodeling resulting in the closure of vascular canals does

1
2
3
4
5
6
7
8
9
10
11
12
13
14
15
16
17
18
19
20
21
22
23
24
25
26
27
28
29
30
31
32
33
34
35
36
37
38
39
40
41
42
43
44
45
46
47
48
49
50
51
52
53
54
55
56
57
58
59
60
61
62
63
64
65

453 not occur (Fig.12D, E). In all taxa, except *Phocanella pumila*, the thin trabeculae occurring in
454 the medullary cavity are made of remodeled lamellar bone, framing wide inter-trabecular
455 spaces (Fig.12E, F). In *Phocanella pumila*, medullary trabeculae are also intensely remodeled,
456 but they are much thicker than in other pinnipeds (compare Fig.12A and 12F). As a
457 consequence, they divide the medullary cavity into small lacunae and strongly increase its
458 compactness (on cross sections).

460 **DISCUSSION**

461 **MORPHOMETRICS AND MICROANATOMY**

462 Based on the sample of specimens used for the morphometric analysis, the diaphysis of the
463 humerus of extinct Phocidae is generally more slender than in extant specimens, apart from
464 the late Miocene *Pachyphoca ukrainica*, which shows pachyostotic ‘swelling’ of the humeral
465 diaphysis. However, the femoral diaphysis of the sampled extinct Phocidae is generally a little
466 thicker than that of extant Phocidae. The femoral diaphysis in *Pachyphoca* and, to a lesser
467 extent, *N. vitulinoides* is also relatively bulky, without appearing swollen. Thus, we detected
468 no clear pachyostotic trend in our sample.

469 Despite the absence of pachyostosis in the humerus and the femur of *N. vitulinoides*,
470 osteosclerosis appears to be extreme in this taxon, and occurs also in *Phocanella pumila*. For
471 the studied specimens of *N. vitulinoides*, namely one rib, two humeri, one radius, two femora,
472 and one tibia, actual bone compactness (0.971 – 0.999) approaches 1 (100%). Similarly,
473 although slightly lower (0.959 – 0.977), compactness values in the humerus and femur of
474 *Phocanella pumila* are much above the common situation of other specimens. The relatively
475 high compactness of the lumbar vertebrae of both the juvenile and the adult specimens of *N.*
476 *vitulinoides* shows that osteosclerosis in the taxon extends to the entire postcranial skeleton.

477 Moreover, differences in compactness between the adult (93.8%) and the juvenile (63.6%)
478 suggest that the increase in compactness is an ongoing process during the growth of the
479 animal. In addition to that, it is noteworthy that the compactness observed in the vertebrae of
480 Phocinae (excluding *N. vitulinoides*) is noticeably lower than the compactness observed in
481 Monachinae and Otariidae. This may hypothetically be related to differences in locomotion
482 (Pierce et al. 2011; Kühn and Prey 2012) or differences in maternal care (Boness and Bowen
483 1996). However, this is beyond the scope of the current study and should be treated in a future
484 studies.

485 Considering the entire set of microanatomical observations made on the bones of
486 *Nanophoca*, it seems obvious that osteosclerosis touches most (and perhaps all) of the
487 appendicular elements. This contrasts with the situation prevailing in the sirenian *Dugong*
488 *dugon*, in which there is a gradual decrease in compactness from the more proximal portion of
489 the forelimb towards its distal portion (Buffrénil and Schoevaert 1989). A similar condition
490 has been described in the marine sloth *Thalassocnus* (Amson et al. 2014) in which the radius
491 is noticeably less compact than the humerus.

492

493 **GROWTH PATTERN OF THE BONES AND MECHANISM OF THEIR COMPACTION**

494 ***Growth pattern of bone cortices.*** According to the experimental data presently available
495 about the relationship between the structure of periosteal bone deposits and their accretion
496 rate, the so-called Amprino's (1947) rule, the growth in thickness of *N. vitulinoides* bone
497 cortices proceeded at relatively moderate speed. The woven-parallel bone with longitudinal
498 primary osteons that compose them is generally associated, in extant mammals and birds, with
499 apposition rates ranging between 4 and 8 μm per day (Castanet et al. 1996, 2000). All other
500 forms of woven-parallel bone, i.e., reticular, plexiform, laminar, or radial tissues, correspond
501 to higher growth rates. This question is nevertheless complex; it remains incompletely settled

502 and contrasting results have been presented by Margerie et al. (2002). To our knowledge,
1
2 503 there are neither experimental data on bone apposition rate in pinnipeds nor precise
3
4 504 histological descriptions of the structure of periosteal cortices in their bones. The comparative
5
6
7 505 observations made in the present study suggest that, despite its modest size, *N. vitulinoides*
8
9
10 506 did not grow at a rate very different from that of larger species.

11
12 507 The growth of primary bone cortices was cyclic in *Nanophoca* with, as in most
13
14 508 mammals for which accurate data exist, the yearly alternation of a fast growth phase
15
16
17 509 (accretion of the woven-parallel layers) when food was abundant, and a slow growth phase,
18
19 510 corresponding to unfavorable environmental conditions, during which the annuli were
20
21
22 511 formed. In one specimen at least, the humerus Histos 2139, a total arrest of growth occurred
23
24 512 each year, resulting in the formation of lines of arrested growth. The comparative sample
25
26
27 513 reveals that *Nanophoca* did not differ from other pinnipeds for these characteristics. More
28
29 514 generally, several recent studies (e.g., Castanet 2006; Köhler et al. 2012) show that the
30
31 515 presence of growth cycles of annual periodicity (supposed so in fossils) is a general,
32
33
34 516 plesiomorphic feature in vertebrates (it primarily depends on endogenous rhythms), whatever
35
36 517 their phylogenetic position, physiological characteristics, or ecological adaptations, as shown
37
38
39 518 by the occurrence of cyclic growth marks in Silurian placoderms (Giles et al. 2013).

40
41 519 The ontogenetic transformation of primary cortices in *Nanophoca* was basically due to
42
43 520 intense Haversian remodeling, a situation also observed in other pinnipeds and otherwise
44
45
46 521 common to most mammals. Cortical remodeling presented some delay as compared to that
47
48
49 522 occurring in the medullary region, which explains that non-remodeled primary cortices co-
50
51 523 existed with a densely remodeled medulla in most bones.

52
53 524 ***Mechanism of medullary compaction.*** Our histological observations suggest that the
54
55
56 525 fundamental process of endochondral osteogenesis was not significantly modified in *N.*
57
58 526 *vitulinoides*. Contrary to the situation prevailing in numerous secondarily aquatic tetrapods
59
60
61
62
63
64
65

527 (reviewed in e.g., Ricqlès and Buffrénil 2001), the calcified cartilage formed in growth plates
1
2 528 was entirely eroded and the formation of primary trabeculae was apparently normal.
3
4 529 Compaction of the medullary region basically resulted from the mode of remodeling of these
5
6
7 530 trabeculae. The erosion and reconstruction process involved in bone remodeling is generally
8
9
10 531 balanced, the amount of bone resorbed by osteoclasts being approximately compensated by an
11
12 532 equivalent amount of reconstructive (secondary) osseous tissue (Parfitt 1981, 1982). In *N.*
13
14 533 *vitulinoides*, imbalance visibly existed in favor of the reconstructive stage: the amount of
15
16 534 secondary deposits produced by endosteal osteoblasts exceeded the volume of tissue
17
18
19 535 previously eroded by the osteoclasts. The detailed histogenetical mechanism controlling this
20
21
22 536 peculiar functioning of the osteoblasts is, of course, beyond reach of this study. The regulation
23
24 537 of osteoblast activity during Haversian remodeling is a complex, still poorly elucidated
25
26
27 538 question (e.g., Martin 2000; Burr and Allen 2014). It nevertheless remains that the cause
28
29 539 responsible for osteosclerosis in *N. vitulinoides* obviously resided in a modification of this
30
31
32 540 regulation mechanism. Occlusion of intra-osseous cavities due to this process was extremely
33
34 541 pronounced because several, successive peri-vascular remodeling cycles occurred locally
35
36 542 (over-remodeling), up to a quasi-total closure of vascular canals. Vascular canals reduced to
37
38
39 543 diameters less than 10 μm , and a fortiori the thinner capillaries housed in them, are unlikely to
40
41 544 have remained functional, as the mean diameter of mammalian erythrocytes (not to speak of
42
43
44 545 other blood cells) is 7 to 8 μm (e.g., Fawcett and Jensch 1997). In humans, the lumen of the
45
46 546 Haversian canal of a normal, fully developed, secondary osteon is 20 – 50 μm in diameter
47
48
49 547 (Jaworski 1993; Fiala 1980; see also Polig and Jee 1990). For example, in the ribs of male
50
51 548 humans aged 20 – 25 years, mean Haversian canal perimeter (variable *Hc.Pm* in classical
52
53 549 nomenclature) is 0.165 mm, and Haversian canal area (*Hc.Ar*) is 0.002 mm² (Qiu et al. 2003);
54
55
56 550 these parameters indeed correspond to a diameter of some 50 μm .
57
58
59
60
61
62
63
64
65

551 The compaction process described here in *N. vitulinoides* is known also from other
1
2 552 marine tetrapods; it was observed in the femur and humerus of *Clausiosaurus germaini*
3
4 553 (Buffrénil and Mazin 1989), the rostral region of the skull of several ziphiid whales (Buffrénil
5
6
7 554 and Casinos 1995; Zylberberg et al. 1998; Lambert et al. 2011; Dumont et al. 2016), and the
8
9 555 five species of the xenarthran genus *Thalassocnus* (Amson et al. 2014). Conversely, it was not
10
11 556 observed in other pinnipeds, albeit our data suggest that *Phocanella pumila* might have
12
13 557 displayed a similar specialization, though far less pronounced than in *N. vitulinoides*.
14
15
16

17 558 ***Remark on the timing of somatic growth in Nanophoca vitulinoides***—The results of the
18
19 559 present study reveal a paradoxical situation in which two conditions, which can be considered
20
21 560 contradictory, coexist. A) In several long bones (humerus, femur, ulna), primary periosteal
22
23 561 cortices display rather broadly spaced annuli up to bone periphery and, although the outer
24
25 562 margins of the bones are bordered by an annulus, there is no clearly characterized external
26
27 563 fundamental system. This situation should normally indicate that, on the one hand, the growth
28
29 564 of the bones was still actively progressing when the animals died and that, on the other hand,
30
31 565 death occurred during the unfavorable season, when annuli were formed. B) However, in all
32
33 566 long bones, growth plates are entirely erased by remodeling; therefore, no further growth in
34
35 567 length could occur. A possible explanation for these contrasted data is that the growth in
36
37 568 diameter of the bones remained active by the time their growth in length was already stopped.
38
39 569 This hypothesis is not convincing because such a process would have created a great diversity
40
41 570 in the shape of the bones of *N. vitulinoides*, a situation that does not exist (see Dewaele et al.
42
43 571 2017a). Another hypothesis is to consider that growth ceased abruptly, with both the
44
45 572 destruction of growth plates and a sudden stop in periosteal apposition, when a certain size
46
47 573 was reached. In this situation, peripheral annuli should be viewed as functional equivalents of
48
49 574 EFS. For each individual, this double process of growth cessation is likely to have occurred
50
51 575 during the unfavorable season, when annuli were deposited. Depending on the age when this
52
53
54
55
56
57
58
59
60
61
62
63
64
65

576 process normally occurred (this age cannot be determined because early growth marks were
1
2 577 erased by remodeling) it could explain the small size of *N. vitulinoides*. This issue requires the
3
4
5 578 examination of a larger sample of *Nanophoca* bones and cannot be settled for the present.
6
7 579 Moreover, slight local differences in the timing of the growth dynamics are not to be
8
9
10 580 excluded, as suggested by the occurrence of an EFS in the largest vertebra.

11
12 581 ***Possible consequence of compaction on bone biomechanics***—The unusual frequency of the
13
14 582 short fissures observed in several specimens of *N. vitulinoides* cannot be readily explained by
15
16 583 the effect of taphonomic constraints because *N. vitulinoides* fossils do not show traces of
17
18
19 584 crushing or deformation (although they can be broken). Moreover, the cracks are restricted to
20
21
22 585 the central region of the bones, and never extend towards their peripheral margins; such
23
24 586 extensions should nevertheless have occurred if an external constraint had been exerted on the
25
26
27 587 bones. The aspect of the fissures observed here is strongly reminiscent of the fatigue micro-
28
29 588 fractures, as they are classically described and illustrated in the skeleton of *Homo* (e.g.,
30
31 589 Schaffer et al. 1995; Lee et al. 2003; Landrigan et al. 2011) and numerous domestic and wild
32
33
34 590 animals such as, e.g., dogs (Burr et al. 1985), rats (Voide et al. 2011), sheep (Mohsin et al.
35
36 591 2006), etc. In the absence of another plausible interpretation, the fissures observed in bones of
37
38
39 592 *N. vitulinoides* are considered as genuine fatigue micro-fractures. The accumulation and
40
41 593 coalescence of these small lesions, caused by long-lasting, repetitive mechanical stress,
42
43
44 594 constitute the major processes responsible for the degradation of bone mechanical properties
45
46 595 (Danova et al. 2003). Their relative abundance in *N. vitulinoides* could have been indirectly
47
48
49 596 induced by the compaction of bone tissue that occurred in this taxon. It is indeed possible that
50
51 597 the pronounced reduction, or even the total occlusion, of the lumen of vascular canals by
52
53
54 598 excessive secondary deposits resulted in a local cessation of Haversian remodeling, as the
55
56 599 precursors of the osteoclasts (monocytes), cells of the blood lineage, arrive in situ via vascular
57
58 600 networks (syntheses in Marks and Popoff 1988; Charles and Aliprantis 2014; see also Lafage-
59
60
61
62
63
64
65

601 Proust et al. 2015). It is therefore likely that the extreme and imbalanced remodeling in bones
1
2 602 of *N. vitulinoides* was a self-blocking process, a hypothesis that could additionally explain
3
4 603 why open resorption cavities are so scarce in the bones of *N. vitulinoides* observed in this
5
6
7 604 study. One of the functions most commonly attributed to remodeling, be it of the Haversian
8
9
10 605 type or not, is precisely to operate a local replacement of the osseous tissue damaged by the
11
12 606 proliferation of fatigue micro-fractures (Burr 1993; Burr et al. 1995; Lieberman et al. 2003).
13
14 607 In *N. vitulinoides*, this process might have been hampered by local restriction to blood supply.
15
16
17 608 If a strong increase in bone compactness in this taxon was positively selected for the
18
19 609 functional benefit that it could provide, the “price to pay” was a decrease in the mechanical
20
21
22 610 resistance of the bones. This result is maladaptive because a total closure of vascular canals
23
24 611 actually provided negligible gain in mass (which was not the case for the closure of larger
25
26 612 bone cavities). This situation suggests that such an extreme degree of bone compaction might
27
28
29 613 have resulted from developmental constraints that could have prevented compaction of the
30
31
32 614 skeleton to be optimal throughout. Several, relatively common, disorders of the skeleton
33
34 615 likely to have a genetic origin provoke increased and imbalanced remodeling, e.g., Paget’s
35
36 616 disease, osseous mastocytosis, etc. (Ralston 2008; Michou and Brown 2011; see also Evans et
37
38
39 617 al. 1983), and can produce symptoms reminiscent of, though not strictly identical to, the
40
41 618 situation observed in *N. vitulinoides*. It seems possible that the peculiarities of bone structure
42
43
44 619 in *Nanophoca* could have initially resulted from a process akin to such pathological processes.
45
46 620 Pending an actual genetic causality, the latter could have been selected and subsequently
47
48
49 621 increased during evolution for its adaptive consequences, if the resulting general compactness
50
51 622 increase of the skeleton of *N. vitulinoides* was advantageous. Such a process might have
52
53 623 occurred also in other aquatic tetrapods showing the same bone structural peculiarities as
54
55
56 624 *Nanophoca*. Future studies should address this issue and point out the frequency of this
57
58 625 putative process.
59
60
61
62
63
64
65

626

1
2
3 **627 FUNCTIONAL CONSIDERATIONS**
4
5

6 628 One of the obvious consequences of the osteosclerotic-like process described here was to
7
8 629 increase the overall mass of the *N. vitulinoides* skeleton. In the absence of pachyostosis, this
9
10
11 630 increase was relatively moderate, as compared to the extreme situations encountered in the
12
13 631 Sirenia (Kaiser 1974; Buffrénil et al. 2010) or the marine squamates (the so-called limbed
14
15 632 snakes) from the Cenomanian of Europe and North Africa (Buffrénil and Rage 1993;
16
17
18 633 Houssaye, 2013). Nevertheless, it necessarily provoked an increase in the density and inertia
19
20
21 634 of the body, and proportionally reduced its buoyancy and maneuverability in the water as well
22
23 635 as on land (Taylor 2009; Domning and Buffrénil 1991). It is thus likely that, as compared to
24
25 636 the other pinnipeds devoid of osteosclerosis, (e.g., *Arctocephalus*, *Phocarctos*, and *Zalophus*:
26
27
28 637 Godfrey 1985; Beentjes 1990; Fish et al. 2003), the locomotor capabilities of *N. vitulinoides*
29
30
31 638 were characterized by a lower swimming speed and a poor aptitude for steep accelerations or
32
33 639 sudden direction changes (maneuverability). Until now, no skull of this taxon has been
34
35 640 discovered; thus, its feeding strategy and food preferences cannot be determined. The extreme
36
37
38 641 compactness of postcranial elements strongly suggests that *N. vitulinoides* was not adapted to
39
40 642 the capture of fast and mobile prey in open seas. Rather, it must have fed upon benthic or
41
42
43 643 fixed animals in coastal shallow waters. One well-known extant benthic feeder is the walrus,
44
45 644 *Odobenus rosmarus* (e.g., Fay 1982; Gjertz and Wiig 1992; Dehn et al. 2006). However, bone
46
47
48 645 densification in the walrus is limited to pachyostosis in certain cranial regions (Kaiser 1967),
49
50 646 while the postcranial skeleton is largely untouched by pachyosteosclerosis (e.g., Canoville et
51
52 647 al. 2016: fig. 7O). In addition, Deméré (1994a, b) showed that the skeleton of the extinct
53
54
55 648 walrus *Valenictus* was pachyosteosclerotic and that this taxon most likely had an even more
56
57 649 pronounced benthic foraging lifestyle than the extant *Odobenus*. Moreover, the interpretation
58
59
60 650 of *N. vitulinoides* as a benthic feeder closely fits the conclusions drawn by Dewaele et al.
61
62
63
64
65

651 (2017a) from extensive anatomical clues and reconstructions of the appendicular musculature:
1
2 652 pectoral and pelvic girdles were used by *N. vitulinoides* in a different way than in other
3
4
5 653 Phocidae, presumably for grasping and crawling on the substrate. For instance, the strong
6
7 654 development of the greater tubercle of the humerus, the weak development of the lesser
8
9 655 tubercle of the latter, and the strong development of the olecranon process on the ulna point
10
11 656 toward powerful extension and abduction of the foreflippers, contrasting with the conditions
12
13 657 displayed by extant phocids. In this functional context, even a limited buoyancy decrease (as
14
15 658 compared to other taxa such as the sirenians or some Cenomanian aquatic squamates; the
16
17 659 bone ballast of *Nanophoca* is moderate) must have facilitated a passive control, with little
18
19 660 energy expense, of body position and trim in the water column. The same may apply to the
20
21 661 contemporaneous late Miocene–early Pliocene *Phocanella pumila*, given the similar trend
22
23 662 toward density increase in the humerus and femur. Hence, a comparable feeding pattern might
24
25 663 have existed in these two taxa. Unfortunately, no dental remains are known from *Phocanella*
26
27 664 *pumila*, which precludes elucidating the feeding habits of this species and, indirectly, that of
28
29 665 *N. vitulinoides*. Both are nevertheless found in the same geological context, and might
30
31 666 therefore have shared close ecological adaptations. Although our analysis includes only two
32
33 667 specimens of the latter taxon (the extent of bone compaction in the rest of the skeleton cannot
34
35 668 be assessed), a similar ecology to that of *N. vitulinoides* can be expected. The presence of a
36
37 669 (thick) spongy trabecular network in the medullary cavity of *Batavipusa neerlandica* and
38
39 670 *Praepusa boeska*, two small, roughly contemporaneous (late Miocene–early Pliocene) species
40
41 671 from the southern margin of the North Sea Basin, shows that the extreme compactness of the
42
43 672 long bones of *N. vitulinoides* is not strictly correlated with the small body size of the taxon.
44
45
46
47
48
49
50
51
52
53
54
55
56

57 674 CONCLUSIONS

58
59
60
61
62
63
64
65

675 *Nanophoca vitulinoides* from the middle Miocene of the North Sea Basin is the first extinct
1
2 676 phocid taxon to undergo a detailed microanatomical and osteohistological description. Its long
3
4 677 bones are extremely compact, lacking a differentiated medullary cavity and exhibiting
5
6 678 compactness values close to 100%. Apart from the extinct phocine seal *Phocanella pumila*,
7
8 679 such structural peculiarities are unknown among pinnipeds. The spine of *Nanophoca* was also
9
10 680 touched by this process, which is a unique case among mammals. The high compactness is
11
12 681 not observed in any other semi-aquatic mammal. The high compactness observed in the
13
14 682 skeleton of *Nanophoca* resulted from an imbalanced remodeling process located in the
15
16 683 medullary region. Positively selected during evolution, this process might have been rooted in
17
18 684 an initial genetic condition akin to one form of the so-called “metabolic bone diseases.” It
19
20 685 increased body density, thus reducing buoyancy and facilitating long-lasting underwater stays.
21
22 686 Conversely, it limited speed and maneuverability. Although more complete fossils, and
23
24 687 especially cranial remains, are needed to draw definite conclusions on *Nanophoca* ecology,
25
26 688 the results of this study strongly suggest that *N. vitulinoides* was a bottom-dwelling seal,
27
28 689 living in shallow waters close to the shore in the Miocene North Sea Basin, and feeding on
29
30 690 benthic prey.
31
32
33
34
35
36
37
38
39
40
41

691

692 **ACKNOWLEDGEMENTS**

42
43
44
45 693 The research presented in this study is in partial fulfillment of the PhD research of LD,
46
47 694 conducted at Ghent University, Ghent, Belgium, and in collaboration with the Royal Belgian
48
49 695 Institute of Natural Sciences, Brussels, Belgium. This PhD research is funded by the Research
50
51 696 Foundation – Flanders (FWO) through an FWO PhD Fellowship to LD. This research is also
52
53 697 partly funded by the Society of Vertebrate Paleontology’s 2016 Steven Cohen Award for
54
55 698 Excellent Student Research, awarded to LD. TDK holds a postdoctoral Fellowship at the
56
57 699 FWO.
58
59
60
61
62
63
64
65

1
2
3
4
5
6
7
8
9
10
11
12
13
14
15
16
17
18
19
20
21
22
23
24
25
26
27
28
29
30
31
32
33
34
35
36
37
38
39
40
41
42
43
44
45
46
47
48
49
50
51
52
53
54
55
56
57
58
59
60
61
62
63
64
65

700 We also want to thank S Bruaux, C Cousin, and A Folie from the RBINS for providing access
701 to the collections. We thank R Fraaije and N Peters from the Oertijdmuseum Groene Poort,
702 Boxtel, Netherlands, for allowing access to the holotypes of *Batavipusa neerlandica* and
703 *Praepusa boeska*. We are grateful to M Bosselaers for donating specimens from his private
704 collection for the elaboration of thin sections. Special thanks to JR Wible (editor-in-chief), A
705 Houssaye (reviewer), and a second anonymous reviewer for helpful comments that improved
706 the quality of this work.

707

708 REFERENCES CITED

- 709 Amprino R (1947) La structure du tissu osseux envisagée comme expression de différences
710 dans la vitesse de l'accroissement. Arch Biol 58:315–330
- 711 Amson E, Muizon C de (2014) A new durophagous phocid (Mammalia: Carnivora) from the
712 late Neogene of Peru and considerations on monachine seal phylogeny. J Syst
713 Paleontol 12:523–548. doi: 10.1080/14772019.2013.799610
- 714 Amson E, Muizon C de, Laurin M, Argot C, Buffrénil V de (2014) Gradual adaptation of
715 bone structure to aquatic lifestyle in extinct sloths from Peru. Proc Biol Soc
716 281:20140192. doi: 10.1098/rspb.2014.0192
- 717 Beentjes MP (1990) Comparative terrestrial locomotion of the Hooker's sea lion (*Phocarcos*
718 *hookeri*) and the New Zealand fur seal (*Arctocephalus forsteri*): evolutionary and
719 ecological implications. Zool J Linn Soc 98:307–325. doi: 10.1111/j.1096-
720 3642.1990.tb01204.x
- 721 Berta A, Kienle S, Bianucci G, Sorbi S (2015) A reevaluation of *Pliphoca etrusca*
722 (Pinnipedia, Phocidae) from the Pliocene of Italy: phylogenetic and biogeographic
723 implications. J Vertebr Paleontol 35:e88944. doi: 10.1080/02724634.2014.889144

- 724 Bininda-Emonds ORP, Russell AP (1996) A morphological perspective on the phylogenetic
1
2 725 relationships of the extant phocid seals (Mammalia: Carnivora: Phocidae). Bonn Zool
3
4 726 Monogr 41:1–256
5
6
7 727 Boness DJ, Bowen WD (1996) The evolution of maternal care in pinnipeds. Bioscience
8
9 728 46:645–654
10
11
12 729 Buffrénil V de, Canoville A, D'Anastasio R, Domning DP (2010) Evolution of sirenian
13
14 730 pachyosteosclerosis, a model-case for the study of bone structure in aquatic tetrapods.
15
16 731 J Mammal Evol 17:101–120.doi: 10.1007/s10914-010-9130-1
17
18
19
20 732 Buffrénil V de, Casinos A (1995) Observations histologiques sur le rostre de *Mesoplodon*
21
22 733 *densirostris* (Mammalia, Cetacea, Ziphiidae): le tissu osseux le plus dense connu. Ann
23
24 734 Sci Nat Zool 13ème Ser 16:21–32
25
26
27
28 735 Buffrénil V de, Mazin J-M (1989) Bone histology of *Claudiosaurus germaini* (Reptilia,
29
30 736 Claudiosauridae) and the problem of pachyostosis in aquatic tetrapods. Hist Biol
31
32 737 2:311–322.doi: 10/1080/08912968909386509
33
34
35
36 738 Buffrénil V de, Rage J-C (1993) La ‘pachyostose’ vertébrale de *Simoliophis* (Reptilia,
37
38 739 Squamata): données comparatives et considérations fonctionnelles. Ann Paleontol
39
40 740 (Vertebr) 79:315–335
41
42
43
44 741 Buffrénil V de, Ricqlès A de, Ray CE, Domning, DP (1990) Bone histology of the ribs of the
45
46 742 archaeocetes (Mammalia: Cetacea). J Vertebr Paleontol 10:455–466.doi:
47
48 743 10/1080/02724634.1990.10011828
49
50
51
52 744 Buffrénil V de, Schoevaert D (1989) Données quantitatives et observations histologiques sur
53
54 745 la pachyostose du squelette du dugong, *Dugong dugon* (Müller) (Sirenia,
55
56 746 Dugongidae). Can J Zool 67:2107-2119. doi: 10.1139/z89-300
57
58
59
60
61
62
63
64
65

- 747 Burr DB (1993) Remodeling and the repair of fatigue damage. *Calcif Tissue Internatl* 53
1
2 748 (suppl 1):S75–S81. doi: 10.1007/BF01673407
3
4 749 Burr DB, Allen MR (eds) (2014) *Basic and Applied Bone Biology*. Elsevier/Academic Press,
5
6 London
7 750
8
9 751 Burr DB, Martin RB, Schaffler MB, Radin EL (1985) Bone remodeling in response to *in vivo*
10
11 fatigue microdamage. *J Biomech* 18:189–200. doi:10.1016/0021-9290(85)90204-0
12 752
13
14 753 Canoville A, Buffrénil V de, Laurin M (2016) Microanatomical diversity of amniote ribs: an
15
16 exploratory quantitative study. *Biol J Linn Soc* 118:706–733. doi: 10.1111/bij.12779
17 754
18
19 755 Canoville A, Laurin M (2010) Evolution of humeral microanatomy and lifestyle in amniotes,
20
21 and some comments on palaeobiological inferences. *Biol J Linn Soc* 100:384–406.
22 756
23 doi: 10.1111/j.1095-8312.2010.01431.x
24 757
25
26 758 Castanet J (2006) Time recording in bone microstructures of endothermic animals; functional
27
28 relationships. *CR Palevol* 5:629–636. doi: 10.1016/j.crpv.2005.10.006
29 759
30
31 760 Castanet J, Grandin A, Abourachid A, Ricqlès A de (1996) Expression de la dynamique de
32
33 croissance dans la structure de l’os périostique chez *Anas platyrhynchos*. *CR Acad Sci*
34 761
35 Paris, *Sci Vie* 319:301–308
36 762
37
38 763 Castanet J, Curry Rogers C, Cubo J, Boisard J (2000) Periosteal bone growth rates in extant
39
40 ratites (ostrich and emu). Implications for assessing growth in dinosaurs. *CR Acad Sci*
41 764
42 Paris, *Sci Vie* 323:543–550. doi: 10.1016/S0764-4469(00)00181-5
43 765
44
45 766 Charles JF, Aliprantis AO (2014) Osteoclasts: more than ‘bone eaters’. *Trends Mol Med*
46
47 20:449–459. doi: 10.1016/j.molmed.2014.06.001
48 767
49
50 768 Cozzuol MA (2001) A “northern” seal from the Miocene of Argentina: implications for
51
52 phocid phylogeny and biogeography. *J Vertebr Paleontol* 21:415–421. doi:
53 769
54 10.1671/0272-4634(2001)021[0415:ANSFTM]2.0.CO;2
55 770
56
57
58
59
60
61
62
63
64
65

- 771 Danova NA, Colopy SA, Radtke CL, Kalscheur VL, Markel MD, Vanderby R Jr, McCabe
1
2 772 RP, Escarcega AJ, Muir P (2003) Degradation of bone structural properties by
3
4 773 accumulation and coalescence of microcracks. *Bone* 33:197–205. doi: 10.1016/S8756-
5
6 774 3282(03)00155-8
7
8
9
10 775 Dehn L-A, Sheffield GG, Follmann EH, Duffy LK, Thomas DL, O’Hara TM (2006) Feeding
11
12 776 ecology of phocid seals and some walrus in the Alaskan and Canadian Arctic as
13
14
15 777 determined by stomach contents and stable isotope analysis. *Polar Biol* 30:167–181.
16
17 778 doi: 10.1007/s00300-006-0171-0
18
19
20 779 Deméré TA (1994a) Two new species of fossil walruses (Pinnipedia: Odobenidae) from the
21
22 780 upper Pliocene San Diego Formation. *Proc San Diego Soc Nat Hist* 29:77–98
23
24
25 781 Deméré TA (1994b) The family Odobenidae: a phylogenetic analysis of fossil and living taxa.
26
27 782 *Proc San Diego Soc Nat Hist* 29:99–123
28
29
30
31 783 Dempster, DW, Compston JE, Drezner MK, Glorieux FH, Kanis JA, Malluche H, Meunier
32
33 784 PJ, Ott SM, Recker RR, Parfitt AM (2013) Standardized nomenclature, symbols, and
34
35 785 units for bone histomorphometry: a 2012 update of the report of the ASBMR
36
37 786 Histomorphometry Nomenclature Committee. *J Bone Miner Res* 28:1–16. doi:
38
39 787 10.1002/jbmr.1805
40
41
42
43 788 Dewaele L, Amson E, Lambert O, Louwye S (2017a) Reappraisal of the extinct seal “*Phoca*”
44
45 789 *vitulinoides* from the Neogene of the North Sea Basin, with bearing on its geological
46
47 790 age, phylogenetic affinities, and locomotion. *PeerJ* 5:e3316. doi: 10.7717/peerj.3316
48
49
50
51 791 Dewaele L, Lambert O, Louwye S (2017b) On *Prophoca* and *Leptophoca* (Pinnipedia,
52
53 792 Phocidae) from the Miocene of the North Atlantic realm: redescription, phylogenetic
54
55 793 affinities and paleobiogeographic implications. *PeerJ* 5:e3024. doi: 10.7717/peerj.3024
56
57
58
59
60
61
62
63
64
65

- 1
2
3
4
5
6
7
8
9
10
11
12
13
14
15
16
17
18
19
20
21
22
23
24
25
26
27
28
29
30
31
32
33
34
35
36
37
38
39
40
41
42
43
44
45
46
47
48
49
50
51
52
53
54
55
56
57
58
59
60
61
62
63
64
65
- 794 Domning D, Buffrénil V de (1991) Hydrostasis in the Sirenia: quantitative data and functional
795 interpretation. *Mar Mammal Sci* 7:331–368. doi: 10.1111/j.1748-7692.1991.tb00111.x
- 796 Dumont M, Buffrénil V de, Mijan I, Lambert O (2016) Structure and growth pattern of the
797 bizarre hemispheric prominence of the rostrum of the fossil beaked whale *Globicetus*
798 *huberus* (Mammalia, Cetacea, Ziphiidae). *J Morphol* 277:1292–1308. doi:
799 10.1002/jmor.20575
- 800 Dumont M, Laurin M, Jacques F, Pellé E, Dabin W, Buffrénil V de (2013) Inner architecture
801 of vertebral centra in terrestrial and aquatic mammals: a two-dimensional comparative
802 study. *J Morphol* 274:570–584. doi: 10.1002/jmor.20122
- 803 Evans RA, Hughes WG, Dunstan CR, Lennon WP, Kohan L, Hills E, Wong SYP(1983)
804 Adult osteosclerosis. *Metab Bone Dis Relat* 5:111–117. doi: 10.1016/0221-
805 8747(83)90011-5
- 806 Fawcett DW, Jensch RP (1997) Bloom and Fawcett: Concise Histology. Chapman and Hall,
807 New York
- 808 Fay FH (1982) Ecology and biology of the Pacific walrus, *Odobenus rosmarus divergens*
809 Illiger. *N Am Fauna* 74:1–279. doi: 10.3996/nafa.74.0001
- 810 Fiala P (1980) Structure of the long limb bones and its significance in determining age in
811 man. *Folia Morphol* 28:259–263
- 812 Fish FE, Stein BR (1991) Functional correlates of differences in bone density among
813 terrestrial and aquatic genera in the family Mustelidae (Mammalia). *Zoomorphology*
814 110:339–345. doi: 10.1007/BF01668024
- 815 Fish FE, Hurley J, Costa DP (2003) Maneuverability by the sea lion *Zalophus californianus*:
816 turning performance of an unstable body design. *J Exp Biol* 206:667–674. doi:
817 10.1242/jeb.00144

- 1
2
3
4
5
6
7
8
9
10
11
12
13
14
15
16
17
18
19
20
21
22
23
24
25
26
27
28
29
30
31
32
33
34
35
36
37
38
39
40
41
42
43
44
45
46
47
48
49
50
51
52
53
54
55
56
57
58
59
60
61
62
63
64
65
- 818 Francillon-Vieillot H, de Buffrénil V, Castanet J, Geraudie J, Meunier JF, Sire JY, Zylberberg
819 L, Ricqlès A de (1990) Microstructure and mineralization of vertebrate skeletal
820 tissues. In: Carter JG (ed) Skeletal Biomineralizations: Patterns, Processes and
821 Evolutionary Trends, Vol. 1. Van Nostrand Reinhold, New York, pp 471–530.
- 822 Frost HM (1969) Tetracycline-based histological analysis of bone remodeling. Calc Tiss Res
823 33:211–237. doi: 10.1007/BF02058664
- 824 Fulton TL, Strobeck C (2010) Multiple markers and multiple individuals refine true seal
825 phylogeny and bring molecules and morphology back in line. Proc Roy Soc B–Biol
826 Sci 277:1065–1070. doi: 10.1098/rspb.2009.1783
- 827 Germain D, Laurin M (2005) Microanatomy of the radius and lifestyle in amniotes
828 (Vertebrata, Tetrapoda). Zool Scr 34:335–350. doi: 10.1111/j.1463-
829 6409.2005.00198.x
- 830 Giles S, Rücklin M, Donoghue PCJ (2013) Histology of “placoderm” dermal skeletons:
831 implications for the nature of the ancestral gnathostomes. J Morphol 274:627–644.
832 doi: 10.1002/jmor.20119
- 833 Girondot M, Laurin M (2003) Bone Profiler: a tool to quantify, model and statistically
834 compare bone section compactness profiles. J Vertebr Paleontol 23:458-461. doi:
835 10.1671/0272-4634(2003)023[0458:BPATTQ]2.0.CO;2
- 836 Gjertz I, Wiig Ø (1992) Feeding of walrus *Odobenus rosmarus* in Svalbard. Polar Record
837 28:57–59. doi: 10.1017/S0032247400020283
- 838 Godfrey SJ (1985) Additional observations of subaqueous locomotion in the California Sea
839 Lion (*Zalophus californianus*). Aquat Mammal 11:53–57

- 1
2
3
4
5
6
7
8
9
10
11
12
13
14
15
16
17
18
19
20
21
22
23
24
25
26
27
28
29
30
31
32
33
34
35
36
37
38
39
40
41
42
43
44
45
46
47
48
49
50
51
52
53
54
55
56
57
58
59
60
61
62
63
64
65
- 840 Gray N-M, Kainec K, Madar SI, Tomko L, Wolfe S (2007) Sink or swim? Bone density as a
841 mechanism for buoyancy control in early cetaceans. *Anat Rec* 290:638–653. doi:
842 10.1002/ar.20533
- 843 Higdon JW, Bininda-Emonds ORP, Beck RMD, Ferguson SH (2007) Phylogeny and
844 divergence of the pinnipeds (Carnivora: Mammalia) assessed using a multigene
845 dataset. *BMC Evol Biol* 7 :216. doi: 10.1186/1471-2148-7-216.
- 846 Houssaye A (2009) “Pachyostosis” in aquatic amniotes: a review. *Integr Zool* 4:325–340. doi:
847 10.1111/j.1749-4877.2009.00146.x
- 848 Houssaye A (2013) Palaeoecological and morphofunctional interpretation of bone mass
849 increase: an example in Late Cretaceous shallow marine squamates. *Biol Rev* 88:117–
850 139.
- 851 Houssaye A, Fish FE (2016) Functional (secondary) adaptation to an aquatic life in
852 vertebrates: an introduction to the symposium. *Integr Comp Biol* 56:1266–1270. doi:
853 10.1093/icb.icw129
- 854 Houssaye A, Lindgren J, Pellegrini R, Lee AH, Germain D, Polcyn MJ (2013)
855 Microanatomical and histological features in the long bones of mosasaurine mosasaurs
856 (Reptilia, Squamata)—implications for aquatic adaptation and growth rates. *PLoS One*
857 8:e76741. doi: 10.1371/journal.pone.0076741
- 858 Houssaye A, Sander PM, Klein N (2016) Adaptive patterns in aquatic amniote bone
859 microanatomy—more complex than previously thought. *Integr Comp Biol* 56:1349–
860 1369. doi: 10.1093/icb/icw120

- 1 861 Houssaye A, Tafforeau P, Muizon C de, Gingerich PD (2015). Transition of Eocene whales
2 862 from land to sea: evidence from bone microstructure. PLoS One 10:e0118409. doi:
3
4 863 10.1371/journal.pone.0118409
5
6
7 864 Jaworski ZFG (1992) Haversian system and Haversian bone. In: Hall BK (ed) Bone
8
9 Metabolism and Mineralization. CRC Press, Boca Raton, pp 21–45.
10
11
12 866 Jefferson TA, Webber MA, Pitman RL (2008) Marine Mammals of the World: A
13
14 Comprehensive Guide to their Identification. Elsevier/Academic Press, Amsterdam
15
16 867
17
18 868 Kaiser HE (1974) Morphology of the Sirenians. A Macroscopic X-Ray Atlas of the
19
20 Morphology of Recent Species. S. Karger, Basel
21
22
23 870 Köhler M, Marin-Moratalla N, Jordana X, Aanes R (2012) Seasonal bone growth and
24
25 physiology in endotherms shed light on dinosaur physiology. Nature 487:358–361.
26
27 871 doi: 10.1038/nature11264
28
29 872
30
31 873 Koretsky IA (2001) Morphology and systematics of the Miocene Phocinae (Mammalia:
32
33 Carnivora) from Paratethys and the North Atlantic Region. Geol Hung Ser Palaeontol
34
35 874 54:1–109
36
37 875
38
39 876 Koretsky IA, Grigorescu D (2002) The fossil monk seal *Pontophoca sarmatica* (Alekseev)
40
41 (Mammalia: Phocidae: Monachinae) from the Miocene of eastern Europe. Smithson
42
43 877 Contrib Paleobiol 93:149–162
44
45 878
46
47 879 Koretsky IA, Peters N (2008) *Batavipusa* (Carnivora, Phocidae, Phocinae): a new genus from
48
49 the eastern shore of the North Atlantic Ocean (Miocene seals of the Netherlands, part
50
51 880 II). Deinsea 12:53–62
52
53 881
54
55 882 Koretsky IA, Peters N, Rahmat SJ (2015) New species of *Praepusa* (Carnivora, Phocidae,
56
57 Phocinae) from the Netherlands supports east to west Neogene dispersal of true seals.
58
59 883
60
61
62
63
64
65

- 884 Vestn Zool 49:57–66
- 1
2
- 3 885 Koretsky IA, Rahmat SJ (2013) First record of fossil Cystophorinae (Carnivora, Phocidae):
4
5 886 middle Miocene seals from the northern Paratethys. Riv Ital Paleontol S 119:325–350.
6
7
8 887 doi: 10.13130/2039-4942/6043
9
- 10
11 888 Koretsky IA, Rahmat SJ (2017). Preliminary report of pachyosteosclerotic bones in seals.
12
13 889 Open Acc Res Anat 1:1–3
14
- 15
16 890 Koretsky IA, Ray CE (2008) Phocidae of the Pliocene of Eastern North America. Virginia
17
18 891 Mus Nat Hist Spec Pub 14:81–140
19
20
- 21 892 Kriloff A, Germain D, Canoville A, Vincent P, Sache M, Laurin M (2008) Evolution of bone
22
23 893 microanatomy of the tetrapod tibia and its use in palaeobiological inference. J Evol
24
25
26 894 Biol 21:807–826. doi: 10.1111/j.1420-9101.2008.01512.x
27
28
- 29 895 Kühn C, Frey E (2012) Walking like caterpillars, flying like bats—pinniped locomotion.
30
31 896 Palaeobio Palaeoenv 92:197–210. doi: 10.1007/s12549-012-0077-5
32
33
34
- 35 897 Lafage-Proust M-H, Roche B, Langer M, Cleret D, Vanden Bossche A, Olivier T, Vico L
36
37 898 (2015) Assessment of bone vascularization and its role in bone remodeling. BoneKEy
38
39 899 Rep 4, art. no. 662:1–8. doi: 10.1038/bonekey.2015.29
40
41
42
- 43 900 Lambert O, Muizon C de, Buffrénil V de (2011) Hyperdense rostral bones of ziphiid whales:
44
45 901 diverse processes for a similar pattern. CR Palevol 10:453–468. doi:
46
47 902 10.1016/j.crpv.2011.03.012
48
49
- 50
51 903 Lamm ET (2013) Preparation and sectioning of specimens. In: Padian K, Lamm ET (eds)
52
53 904 Bone Histology of Fossil Tetrapods: Advancing Methods, Analysis, and Interpretation.
54
55 905 University of California Press, Berkeley, pp 55–160
56
57
58
59
60
61
62
63
64
65

- 1
2
3
4
5
6
7
8
9
10
11
12
13
14
15
16
17
18
19
20
21
22
23
24
25
26
27
28
29
30
31
32
33
34
35
36
37
38
39
40
41
42
43
44
45
46
47
48
49
50
51
52
53
54
55
56
57
58
59
60
61
62
63
64
65
- 906 Landrigan MD, Li J, Turnbull TL, Burr DB, Niebur GL, Roeder RK (2011) Contrast-
907 enhanced micro-computed tomography of fatigue microdamage accumulation in
908 human cortical bone. *Bone* 48:443–450. doi: 10.1016/j.bone.2010.10.160
- 909 Laurin M, Canoville A, Germain D (2011) Bone microanatomy and lifestyle: a descriptive
910 approach. *CR Palevol* 10:381–402. doi: 10.1016/j.crpv.2011.02.003
- 911 Laurin M, Girondot M, Loth M-M (2004) The evolution of long bone microanatomy and
912 lifestyle in lissamphibians. *Paleobiology* 30:589–613. doi: 10.1666/0094-
913 8373(2004)030<0589:TEOLBM>2.0.CO;2
- 914 Lee TC, Mohsin S, Taylor D, Parkesh R, Gunnlaugsson T, O’Brien FJ, Giehl M, Gowin W
915 (2003) Detecting microdamage in bone. *J Anat* 203:161–172. doi: 10.1046/j.1469-
916 7580.2003.00211.x
- 917 Lieberman DE, Pearson OM, Polk JD, Demes B, Crompton AW (2003) Optimization of bone
918 growth and remodeling in response to loading in tapered mammalian limbs. *J Exp Biol*
919 206:3125–3138. doi: 10.1242/jeb.00514
- 920 Liu XS, Bevill G, Keaveny TM, Sajda P, Guo XE (2009) Micromechanical analyses of
921 vertebral trabecular bone based on individual trabeculae segmentation of plates and
922 rods. *J Biomech* 42:249–256. doi: 10.1016/j.biomech.2008.10.035
- 923 Margerie E de, Cubo J, Castanet J (2002) Bone typology and growth rate: testing and
924 quantifying “Amprino’s rule” in the mallard (*Anas platyrhynchos*). *CR Biol* 325:221–
925 230. doi: 10.1016/S1631-0691(02)01429-4
- 926 Marks SC, Popoff SN (1988) Bone cell biology: the regulation of development, structure and
927 function of the skeleton. *Am J Anat* 183:1–44. doi: 10.1002/aja.1001830102

- 928 Martin RB (2000) Toward a unifying theory of bone remodeling. *Bone* 26:1–6. doi:
1
2 929 10.1016/S8756-3282(99)00241-0
3
4
5 930 Masschaele B, Dierick M, Loo DV, Boone MN, Brabant L, Pauwels E, Cnudde V, Hoorebeke
6
7 931 LV (2013) HECTOR: A 240kV micro-CT setup optimized for research. *J Phys Conf*
8
9 932 Ser 463:012012. doi: 10.1088/1742-6596/463/1/012012.
10
11
12
13 933 Michou L, Brown JP (2011) Genetics of bone diseases: Paget’s disease, fibrous dysplasia,
14
15 934 osteopetrosis and osteogenesis imperfecta. *Joint Bone Spine* 78: 252–258. doi:
16
17 935 10.1016/j.bspin.2010.07.010
18
19
20
21 936 Mohsin S, O’Brien FJ, Lee TC (2006) Osteonal crack barriers in ovine compact bone. *J Anat*
22
23 937 208: 81-89
24
25
26
27 938 Muizon C de (1981) Les vertébrés fossiles de la Formation Pisco (Pérou). Première partie:
28
29 939 deux nouveaux Monachinae du Pliocène de Sud Sacaco. *Inst Franc Etud Andines*
30
31 940 Mem 6 20–161
32
33
34
35 941 Nakajima Y, Endo H (2013). Comparative humeral microanatomy of terrestrial, semiaquatic,
36
37 942 and aquatic carnivorans using micro-focus CT scan. *Mammal Study* 38:1–8
38
39
40 943 Parfitt AM (1981) Bone effect of spaceflight: analysis by quantum concept of bone
41
42 944 remodeling. *Acta Astronaut* 8:1083–1090. doi: 10.1016/0094-5765(81)90082-5
43
44
45 945 Parfitt AM (1982) The coupling of bone formation to bone resorption: a critical analysis of
46
47 946 the concept and of its relevance to the pathogenesis of osteoporosis. *Metab Bone Dis*
48
49 947 *Relat* 4:1–6. doi: 10.1016/022-8747(82)90002-9
50
51
52
53 948 Pierce SE, Clack JA, Hutchinson JR (2011) Comparative axial morphology in pinnipeds and
54
55 949 its correlation with aquatic locomotory behaviour. *J Anat* 219:502–514. doi:
56
57 950 10.1111/j.1469-7580.2011.01406.x
58
59
60
61
62
63
64
65

- 1
2
3
4
5 951 Polig E, Jee WSS (1990) A model of osteon closure in cortical bone. *Calcif Tissue Internatl*
6
7 952 47:261–269. doi: 10.1007/BF02555907
8
9
10 953 Prondvai E, Stein KHW, Ricqlès A de, Cubo J (2014) Development-based revision of bone
11
12 954 tissue classification: the importance of semantics for science. *Biol J Linn Soc*
13
14 955 112:799–816. doi: 10.1111/bio.12323
15
16
17 956 Pyenson, ND, Kelley NP, Parham JF (2014) Marine tetrapod macroevolution: physical and
18
19 957 biological drivers on 250 Ma of invasions and evolution in ocean ecosystems.
20
21 958 *Palaeogeogr Palaeoclimatol Palaeoecol* 400:1–8. doi:10.1016/j.palaeo.2014.02.18
22
23
24 959 Qiu S, Fyhrie DP, Palnitkar S, Sudhaker Rao D (2003) Histomorphometric assessment of
25
26 960 Haversian canal and osteocyte lacunae in different-sized osteons in human ribs. *Anat*
27
28 961 *Rec* 272A:520–525. doi: 10.1002/ar.a.10058
29
30
31 962 Quemeneur S, Buffrénil V de, Laurin M (2013) Microanatomy of the amniote femur and
32
33 963 inference of lifestyle in limbed vertebrates. *Biol J Linn Soc* 109:644–655. doi:
34
35 964 10.1111/bij.12066
36
37 965 Ralston SH (2008) Pathogenesis of Paget’s disease of Bone. *Bone* 43: 819–825. doi:
38
39 966 10.1016/j.bone.2008.06.015
40
41
42
43 967 Ricqlès A de (1989). Les mécanismes hétérochroniques dans le retour des tétrapodes au
44
45 968 milieu aquatique. *Geobios Mem Spec* 12:337–348. doi: 10.1016/S0016-
46
47 969 6995(89)80034-8
48
49
50
51 970 Ricqlès A de, Buffrénil V de (1995) Sur la présence de pachyostéoclérose chez la rhytine de
52
53 971 Steller [*Rhytina (Hydrodamalis) gigas*], sirénien récent éteint. *Ann Sci Nat Zool Paris*,
54
55 972 13e Ser 16:47–53
56
57
58
59
60
61
62
63
64
65

- 1
2
3
4
5
6
7
8
9
10
11
12
13
14
15
16
17
18
19
20
21
22
23
24
25
26
27
28
29
30
31
32
33
34
35
36
37
38
39
40
41
42
43
44
45
46
47
48
49
50
51
52
53
54
55
56
57
58
59
60
61
62
63
64
65
- 973 Ricqlès A de, Buffrénil V de (2001) Bone histology, heterochronies and the return of
974 Tetrapods to life in water: w[h]ere are we? In: Mazin J-M, Buffrénil V de
975 (eds) Secondary Adaptation of Tetrapods to Life in Water. Verlag Dr. Friedrich Pfeil,
976 München, pp 289–310
- 977 Schaffler MB, Choi K, Milgrom C (1995) Aging and matrix microdamage accumulation in
978 human compact bone. *Bone* 17:521–527. doi: 10.1016/8756-3282(95)00370-3
- 979 Stein BR (1989) Bone density and adaptation in semiaquatic mammals. *J Mammal* 70:467–
980 476. doi: 10.2307/1381418
- 981 Storå J (2000) Skeletal development in the Grey seal *Halichoerus grypus*, the Ringed seal
982 *Phoca hispida botnica*, the Harbour seal *Phoca vitulina vitulina* and the Harp seal
983 *Phoca groenlandica*. Epiphyseal fusion and life History. *Archaeozoologia* 11:199–
984 222.
- 985 Taylor MA (2009) Functional significance of bone ballast in the evolution of buoyancy
986 control strategies by aquatic tetrapods. *Hist Biol* 14:15–31. doi:
987 10.1080/10292380009380550
- 988 Thompson DW (1961) *On Growth and Form*. Cambridge University Press, Cambridge
- 989 Turner CH (1998) Three rules for bone adaptation to mechanical stimuli. *Bone* 23:399–407.
990 doi: 10.1016/S8756-3282(98)00118-5
- 991 Uhen MD (2007) Evolution of marine mammals: back to the sea after 300 million years. *Anat*
992 *Rec* 290:514–522. doi:10.1002/ar.20545
- 993 Van Beneden P-J (1871) Les phoques de la mer scaldisienne. *Bul Acad R Sci Let b-Arts Belg*
994 2^{ième} Ser 32:5–19

995 Van Beneden P-J (1877) Description des ossements fossiles des environs d'Anvers, première
1
2 996 partie. Pinnipèdes ou amphithériens. Ann Mus R Hist Nat Belg 1:1–88.
3
4
5 997 Voide R, Schneider P, Stauber M, van Lenthe GH, Stampanoni M, Müller R (2011) The
6
7 importance of murine cortical bone microstructure for microcrack initiation and
8 998
9 propagation. Bone 49:1186–1193. doi: 10.1016/j.bone.2011.08.011
10 999
11
12
13 1000 Wall WP (1983) The correlation between high limb-bone density and aquatic habits in recent
14
15 mammals. J Paleontol 57:197–207
16 1001
17
18
19 1002 Webb P, Buffrénil V de (1990) Locomotion in the biology of large aquatic vertebrates. Trans
20
21 Am Fish Soc 119:629–641. doi: 10.1577/1548-
22
23 8659(1990)119<0629:LITBOL>2.3.CO;2
24 1004
25
26
27 1005 Zylberberg L, Traub W, Buffrénil V de, Alizard F, Arad T, Weiner S (1998) Rostrum of a
28
29 toothed whale: ultrastructural study of a very dense bone. Bone 23:241–247. doi:
30
31 10.1016/S8756-3282(98)00101-X
32
33
34 1008
35
36
37
38
39
40
41
42
43
44
45
46
47
48
49
50
51
52
53
54
55
56
57
58
59
60
61
62
63
64
65

1
2
3 **LEGENDS OF THE FIGURES**
4

5
6 **Fig. 1** – Reconstruction of the skeleton of the phocid *Nanophoca vitulinoides* from the middle
7
8 Miocene of the southern North Sea, with the partial skeleton of specimen IRSNB M2276
9
10 superimposed. Light gray indicates bone types that have been subjected to micro-CT
11
12 scanning exclusively; dark gray indicates bone types that have been subjected to thin
13
14 sectioning exclusively; and intermediate gray indicates bones that have been subjected to
15
16 both micro-CT scanning and thin sectioning. Thin sectioning includes transverse sections
17
18 and longitudinal sections. Note: thin sectioning has been performed on other specimens than
19
20 IRSNB M2276. Modified from Dewaele et al. (2017a: fig. 1).
21
22
23
24

25
26 **Fig. 2** – Line drawing of a humerus and femur of the *Nanophoca vitulinoides* neotype
27
28 specimen IRSNB M2276 showing the measurements taken for the basic morphometric
29
30 analysis. Gray lines on the humerus show total length of the humerus and least transverse
31
32 width of the humeral diaphysis. Gray lines on the femur show total length of the femur and
33
34 least transverse width across the diaphysis. Anteroposterior width is shown as an arrow
35
36 perpendicular to the field of view (circle with diagonal cross).
37
38
39
40

41 **Fig. 3** – Phylogeny of *Nanophoca vitulinoides*, as presented by Dewaele et al. (2017a). Both
42
43 *Leptophoca proxima* and *N. vitulinoides* are shown as stem phocines. Based on the
44
45 literature, the phylogenetic position of *Callophoca obscura* is difficult to ascertain. The
46
47 phylogenetic position of *Batavipusa neerlandica*, *Phocanella pumila*, and *Praepusa boeska*
48
49 remains unclear, in part due to the incompleteness of their respective fossil records.
50
51
52

53
54 **Fig.4** – Microanatomy of the vertebra of *Nanophoca vitulinoides*. Longitudinal
55
56 microanatomical drawings of an **A**) adult (Histos 2150, thin section) and **B**) juvenile (Histos
57
58
59
60
61
62
63
64
65

1
2
3
4
5
6
7
8
9
10
11
12
13
14
15
16
17
18
19
20
21
22
23
24
25
26
27
28
29
30
31
32
33
34
35
36
37
38
39
40
41
42
43
44
45
46
47
48
49
50
51
52
53
54
55
56
57
58
59
60
61
62
63
64
65

2147, thin section) lumbar vertebra. The compactness in the adult specimen is clearly much higher than in the juvenile specimen. Scale bars equal 5 mm.

Fig. 5 – Microanatomy of the rib of *Nanophoca vitulinoides*. Microanatomical drawings of the transverse sections through the ribs of **A)** *N. vitulinoides* (Histos 2152, thin section), **B)** *Callophoca obscura* (Histos 168, thin section), and **C)** *Phoca vitulina* (specimen from Canoville et al. 2016, thin section), and the corresponding compactness profiles. Scale bars equal 5 mm.

Fig.6 – Microanatomy of the humerus of *Nanophoca vitulinoides*. Microanatomical drawings of the transverse sections through the humerus of **A)** *N. vitulinoides* (IRSNB M2276c, micro-CT), **B)** *N. vitulinoides* (Histos 2136, thin section), **C)** *Phocanella pumila* (Histos 163, thin section), **D)** *Phoca vitulina* (IRSNB 1157E, micro-CT), **E)** *Mirounga leonina* (specimen from Canoville and Laurin 2010, thin section), **F)** *Otaria byronia* (specimen from Canoville and Laurin 2010, thin section), and **G)** *Lutra lutra* (specimen from Canoville and Laurin 2010, thin section), and the corresponding compactness profiles. Scale bars equal 5 mm.

Fig.7 – Micro-CT scans of the holotype humeri of *Batavipusa neerlandica* and *Praepusa boeska* from the middle Miocene of the southern North Sea basin. Scans show the diaphyseal cross sections of holotype humeri of **A)** *B. neerlandica* (MAB 3798) and **B)** *P. boeska* (MAB 4686). Anterior end up. White arrows point toward different concentric cortical layers. A spongy medullary region is clearly visible in *B. neerlandica*, but less conspicuous in *P. boeska*. Scale bars equal 5 mm.

Fig.8 – Microanatomy of the femur of *Nanophoca vitulinoides*. Microanatomical drawings of the transverse sections through the femur of **A)** *N. vitulinoides* (Histos 1935, thin section), **B)** *N. vitulinoides* (IRSNB M2276d, micro-CT), **C)** *Leptophoca proxima* (Histos 166, thin

1 section), **D**) *Callophoca obscura* (Histos 170, thin section), **E**) *Phocanella pumila* (Histos
2 160, thin section), **F**) *Phoca vitulina* (IRSNB 1157E, micro-CT), **G**) *Otaria byronia*
3
4 (specimen from Quemeneur et al. 2013, thin section), and **H**) and **I**) *Lutra lutra* (specimen
5 from Quemeneur et al. 2013, thin section), and the corresponding compactness profiles.
6
7 Scale bars equal 5 mm.
8
9

10
11
12 **Fig.9** – Microanatomy of the radius and tibia of *Nanophoca vitulinoides*. Microanatomical
13 drawings of the transverse sections through the radius of **A**) *N. vitulinoides* (Histos 2142,
14 thin section), and **B**) *Phoca vitulina* (IRSNB 1157E, micro-CT), and through the tibia **C**) *N.*
15 *vitulinoides*(IRSNB M2276g, micro-CT), and **D**) *P. vitulina* (IRSNB 1157E, micro-CT),
16
17 and the corresponding compactness profiles. Scale bars equal 5 mm.
18
19
20
21
22
23
24

25 **Fig.10** – Bone structure in the cortex and medulla of *Nanophoca vitulinoides*. **A**) The cortex
26 of the humeral diaphysis (cross section) is composed of a woven-parallel complex with
27 longitudinal primary osteons and conspicuous, broadly spaced annuli (arrows). Left half:
28 ordinary transmitted light, right half: polarized light. **B**) Longitudinal section in the same
29 bone in the metaphyseal region. The primary osteons appear brightly birefringent. **C**) Closer
30 view at the diaphyseal cortex between annuli 2 and 4. The arrows point to short Sharpey's
31 fibers. **D**) Lines of arrested growth (arrows) in the humeral cortex. **E**) Cross-section in the
32 larger radius (Histos 2174). The whole bone area is occupied by a dense Haversian tissue,
33 and no medullary cavity is visible. **F**) Closer view at the remodeled medullary of the radius
34 shown in Fig.10E. **G**) Detail of the structure of the dense Haversian tissue in the medulla of
35 the radius. Remark that vascular canals are extremely thin or occluded. **H**) Close view at
36 over-remodeled bone in the medulla of the radius. The two arrows point at occluded
37 Haversian canals. Scale bars equal 5 μm , except E) 5 mm, and H) 50 μm .
38
39
40
41
42
43
44
45
46
47
48
49
50
51
52
53
54
55
56

57 **Fig.11** – Inner bone remodeling in long bones and vertebrae. **A**) Longitudinal section in the
58 proximal metaphyseal and epiphyseal regions of the femur. The whole bone is compact and
59
60
61
62
63
64
65

1 composed of densely remodeled osseous tissue. **B)** Longitudinal section in the proximal
2 metaphysis and epiphysis of a rib. Same comment as for the femur. **C)** Longitudinal section
3 in the epiphysis of the larger radius (Histos 2174). Epiphyseal surface is covered by a thin
4 layer of calcified cartilage. Under it, the metaphyseal medulla is already compact and
5 densely remodeled (right half: polarized light). **D)** Cross section in the diaphysis of the
6 smaller radius (Histos 2142). The architecture of the spongiosa that once occupied the
7 medulla is still visible, though inter-trabecular spaces are filled. **E)** Detail of the medullar of
8 the smaller radius. The endosteal deposits filling inter-trabecular spaces are densely
9 remodeled and vascular canals (arrows) tend to be occluded. The asterisks indicate micro-
10 cracks. **F)** Off-centered growth of Humeral diaphysis. One face of the bone is under
11 resorption (hollow arrow) while accretion occurs on the other (solid arrow). **G)** Cross
12 section in the centrum of the larger vertebra. Polarized light reveals that the thick trabeculae
13 filling the centrum are densely remodeled. **H)** Longitudinal section in the same specimen
14 (polarized light) showing densely remodeled osseous tissue. **I)** External fundamental system
15 on the outer wall of the neural arch (cross section) in polarized light. Scale bars equal 5 mm
16 for A) and B); 1 mm for D), F), G), H), and I); and 500µm for C), and E).

17
18
19
20
21
22
23
24
25
26
27
28
29
30
31
32
33
34
35
36
37
38
39 **Fig.12** – Comparative data in extant and extinct pinnipeds. **A)** Cross section in the femur of
40 *Phocanella pumila*. Remark the relatively high compactness of this bone, and its non-
41 remodeled cortex. White rectangle: field shown in Fig.11B. **B)** Detail of the cortex showing
42 a woven-parallel tissue with longitudinal primary osteons and annuli. Right half: polarized
43 light. **C)** lines of arrested growth in the femoral cortex of *Phocanella pumila*. **D)** Non-
44 remodeled part of the cortex of a rib in *Monachus monachus* (polarized light). Histology of
45 primary cortices is comparable to that prevailing in *Phocanella pumila* and *Nanophoca*
46 *vitulinoides*. **E)** Remodeling in the deep femoral cortex of *Callophoca obscura*. Remodeling
47 is intense, but Havers' canals remain widely open. **F)** Normal (most frequent) bone
48
49
50
51
52
53
54
55
56
57
58
59
60
61
62
63
64
65

1 architecture in extant and some extinct pinnipeds (here: femur of *Callophoca obscura*). The
2 medullary region is hollow, and contains only a loose spongiosa with thin trabeculae. Scale
3 bars equal 10 mm for A) and F); 1 mm for the inset of F); and 500 μ m for B), C), D), and
4
5
6
7 E).
8
9

10
11
12
13
14
15
16
17
18
19
20
21
22
23
24
25
26
27
28
29
30
31
32
33
34
35
36
37
38
39
40
41
42
43
44
45
46
47
48
49
50
51
52
53
54
55
56
57
58
59
60
61
62
63
64
65

[Click here to view linked References](#)1
2
3
4
5
6
7
8
9
10
11
12
13
14
15
16
17
18
19
20
21
22
23
24
25
26
27
28
29
30
31
32
33
34
35
36
37
38
39
40
41
42
43
44
45
46
47
48
49
50
51
52
53
54
55
56
57
58
59
60
61
62
63
64
65

1 **Generalized osteosclerotic condition in the skeleton of *Nanophoca***
2 ***vitulinoides*, a dwarf seal from the Miocene of Belgium**

3
4 Leonard Dewaele^{1,2*}, Olivier Lambert², Michel Laurin³, Tim De Kock⁴, Stephen
5 Louwye¹, Vivian de Buffrénil³

6 ¹Vakgroep Geologie, Universiteit Gent, Ghent, Belgium

7 ²Directorate “Earth and History of Life”, Institut Royal des Sciences Naturelles de Belgique,
8 Brussels, Belgium

9 ³Département Origines et Evolution, Muséum National d’Histoire Naturelle, Paris, France

10 ⁴PProGRess, Vakgroep Geologie, Universiteit Gent, Ghent, Belgium

11 *Corresponding author: leonard.dewaele@ugent.be

12
13 **ABSTRACT**

14 In the fossil record, it has been shown that various clades of secondarily aquatic tetrapods
15 experienced an initial densification of their bones in the early stages of their evolution, and
16 developed spongier and lighter bones only later in their evolution, with the acquisition of
17 more efficient swimming modes. Although the inner bone structure of most secondarily
18 aquatic tetrapods has already been studied, no research hitherto focused on true seals, or
19 Phocidae. However, preliminary observations previously made on a Miocene species,
20 *Nanophoca vitulinoides*, suggested that this taxon showed pronounced specialization of bone
21 structure as compared to other seals. This feature justifies a specific comparative study, which
22 is the purpose of this article. Microanatomical analysis of bones of *N. vitulinoides* ~~bones~~

1
2
3
4
5
6
7 23 shows compactness values nearing 100%, which is much higher than in other semi-aquatic
8
9 24 mammals, pinnipeds included. Osteohistological analyses show virtually complete
10
11 25 remodeling of the medullary territory by Haversian substitution. Extreme bone compactness
12
13 26 locally resulted from an imbalance, towards reconstruction, of this process. Cortical regions
14
15 27 were less intensely remodeled. In a number of specimens, the cortex shows clear growth
16
17 28 marks as seasonal lines of arrested growth. The results suggest that, despite the extreme
18 29 compactness of long bones of *N. vitulinoides* ~~long bones~~ and the small size of this taxon, the
19
20 30 growth rate of the cortex, and that of the bones in general, did not differ strongly from that of
21
22 31 other, larger phocids. Extreme skeletal compaction and densification must have increased
23
24 32 body density in *Nanophoca*. Consequently, speed, acceleration, and man~~eu~~verability must
25
26 33 have been low, and this taxon was most likely a near-shore bottom-dwelling seal.
27
28 34 Consequently, dietary preferences were most likely oriented towards benthic food sources.
29
30 35

31
32 36 Keywords: Neogene, Phocidae, *Nanophoca vitulinoides*, osteohistology, microanatomy,
33
34 37 osteosclerosis

35
36 38
37
38
39
40
41
42
43
44
45
46
47
48
49
50
51
52
53
54
55
56
57
58
59
60
61
62
63
64
65

1
2
3
4
5
6
7
8
9
10
11
12
13
14
15
16
17
18
19
20
21
22
23
24
25
26
27
28
29
30
31
32
33
34
35
36
37
38
39
40
41
42
43
44
45
46
47
48
49
50
51
52
53
54
55
56
57
58
59
60
61
62
63
64
65

INTRODUCTION

Numerous studies have shown the existence of a general relationship between the bone microanatomy and the ecology of tetrapods (e.g., Wall 1983; Stein 1989; Fish and Stein, 1991; Turner 1998; Ricqlès and Buffrénil 2001; Germain and Laurin 2005; Liu et al. 2009; Amson et al. 2014). Several lineages of tetrapods returned to the aquatic environment (e.g., Uhen 2007; Pyenson et al. 2014; and references therein), and data available hitherto suggest that, in such forms, fast and agile swimming amniotes have lighter and spongier bones than slow bottom-dwellers, which generally have heavy and compact (osteosclerotic) bones (Buffrénil et al. 1988, 1989; Webb and Buffrénil 1990; Taylor 2000; Laurin et al. 2011; Houssaye et al. 2013). In slow secondarily aquatic tetrapods, such as sirenians, the heavy bones passively compensate the buoyancy generated by lung volume and help conserve energy during swimming at shallow depth (Domning and Buffrénil 1991; Ricqlès and Buffrénil 2001; Houssaye 2009; see also Taylor 2000). Two mechanisms may increase skeletal mass: thickening of the cortex (pachyostosis), or increased inner compactness of the bones (osteosclerosis); both can also occur simultaneously to form pachyosteosclerosis (e.g., Buffrénil et al. 2010; Houssaye et al. 2016). However, most marine tetrapod clades show an initial evolutionary stage of pachyosteosclerosis prior to the regression of this feature in pace with the development of more efficient swimming modes (Ricqlès 1989).

Although pinnipeds are “marine mammals,” they retain some terrestrial mobility which makes them an interesting model for studying the modification of bone structure in the course of an evolutionary adaptation to marine life. However, bone histology and microanatomy in these animals has received little attention in the past, with few exceptions (e.g., Stein 1989). Indeed, while the osteohistology and microanatomy of other marine mammal clades was specifically studied from an evolutionary point of view, pinnipeds were considered only in the context of broad comparative datasets including extensive taxonomic

Formatted: Space After: 0 pt

Formatted: Indent: First line: 0.5", Space After: 0 pt

1
2
3
4
5
6
7 64 sampling, at the scale of Mammalia or marine tetrapods (e.g., Laurin et al. 2011; Dumont et
8
9 65 al. 2013; Canoville et al. 2016; Houssaye and Fish, 2016; Houssaye et al. 2016). Two
10
11 66 contributions specifically dealing with pinnipeds can be mentioned: the preliminary study of
12
13 67 the extinct walrus *Valenictus*, showing pachyosteosclerosis in this taxon (Deméré, 1994a, b),
14
15 68 and the publication on pachyosteosclerosis in the seal *Pachyphoca*, from the middle Miocene
16
17 69 of the Ukraine (Eastern Paratethys), by Koretsky and Rahmat (2017). Unfortunately, this
18
19 70 study gives only a very brief microanatomical description, without histological, quantitative
20
21 71 data or informative figures relevant to this topic. Existing information suggests that bone
22
23 72 structure of the pinnipeds differs little from that of most other mammals, ~~since~~ because they
24
25 73 display none of the conspicuous specializations of bone inner architecture often encountered
26
27 74 in marine tetrapods. Indeed, their appendicular long bones , though not strictly tubular
28
29 75 (tubularity sensu stricto is a peculiar adaptation of the diaphyseal region of some limb bones
30
31 76 to a terrestrial locomotion), have compact periosteal cortices framing a nearly open medullary
32
33 77 cavity with only few slender trabeculae (see e.g., Quemeneur et al. 2013 for the femur;
34
35 78 Canoville and Laurin 2010 for the humerus; Germain and Laurin 2005 for the radius; see also
36
37 79 Nakajima and Endo 2013). Moreover, the structure of their ribs (comparative data in
38
39 80 Canoville et al. 2016) and vertebrae (Dumont et al. 2013; Houssaye et al. 2014) merely
40
41 81 reflects the common condition observed in most mammals. This situation may seem
42
43 82 paradoxical considering the intermediate habitat and mode of locomotion that characterizes
44
45 83 this taxon. Miscellaneous observations nevertheless suggest that the question may be more
46
47 84 complex and that in the pinnipeds, and more generally within a given clade and a general
48
49 85 habitat (e.g. coastal, pelagic, etc.), bone structure may differ between taxa according to the
50
51 86 detailed characteristics of their ecological adaptations (see also on this topic Houssaye et al.
52
53 87 2016). Such is the case, for example, of the bones of *Nanophoca vitulinoides*, a small phocid
54
55 88 from the middle Miocene (late Langhian–late Serravallian; ~~e-ca.~~ ca. 14.2–11.6 Ma) of Antwerp

Formatted: Font: Not Italic

Formatted: Font: Not Italic

Formatted: Font: Not Italic

1
2
3
4
5
6
7
8
9
10
11
12
13
14
15
16
17
18
19
20
21
22
23
24
25
26
27
28
29
30
31
32
33
34
35
36
37
38
39
40
41
42
43
44
45
46
47
48
49
50
51
52
53
54
55
56
57
58
59
60
61
62
63
64
65

region, in Belgium. From broken and fractured specimens, the internal structure of bones in this taxon appears extremely compact and lacks a differentiated medullary cavity. These intriguing preliminary observations call for further analysis.

The aim of the present study is to describe and interpret the osseous structure of *Nanophoca* at both the microanatomical and histological levels, and compare it with similar data from other phocids and more distantly related taxa. *Nanophoca vitulinoides* is the best-known extinct seal from the Neogene (Miocene + Pliocene, 23.03 – 2.58 Ma) of the North Sea Basin, and represents more than half the fossil seal specimens at the Royal Belgian Institute of Natural Sciences, or RBINS (Dewaele et al. 2017a). Its postcranial skeleton is the most complete described hitherto (Fig. 1); however, cranial elements are still lacking. *Nanophoca vitulinoides* is remarkable in two respects: first, with a total estimated length of approximately one meter, it is one of the smallest known Phocidae (Dewaele et al. 2017a); in this family, only *Batavipusa neerlandica* from the early to middle Tortonian (8–11.5 Ma) of the Netherlands, *Monachopsis* from the early to middle Tortonian (c. 8.4–11.4 Ma) of Moldova, and *Pachyphoca chapskii* from the late Serravallian to early Tortonian (11.2–12.3 Ma) of Ukraine are about as small or smaller, based on humeral length (Koretsky 2001; Koretsky and Peters 2008; Koretsky and Rahmat 2013; Dewaele et al. 2017a). Second, most late Neogene seal taxa found in Belgium also occur in the Lee Creek Mine of the Yorktown Formation, Aurora, North Carolina, USA; *N. vitulinoides* is the only one restricted to Belgian strata (Koretsky and Ray 2008; Dewaele et al. 2017a). Studying bone structure in this taxon, and comparing it with other seals could, on the one hand, bring basic data (still missing hitherto) on bone histology in phocids and, on the other hand, show the nature of the structural specialization of the *Nanophoca* skeleton, which would help in inferring its development and possible functional/ecological significance.

Formatted: Indent: First line: 0.5"

1
2
3
4
5
6
7
8
9
10
11
12
13
14
15
16
17
18
19
20
21
22
23
24
25
26
27
28
29
30
31
32
33
34
35
36
37
38
39
40
41
42
43
44
45
46
47
48
49
50
51
52
53
54
55
56
57
58
59
60
61
62
63
64
65

MATERIAL AND METHODS

BIOLOGICAL SAMPLE

This study rests on two main methodological approaches: A) gross (macro-anatomic) morphometry for assessing the presence or absence of pachyostosis in *Nanophoca*; B) microanatomy and histology for describing the inner structure of the bones.

For the morphometric part, 29 humeri from ~~thirteen-13~~ phocid species and 25 femora from ~~twelve-12~~ species were measured by one of us (LD), roughly following the procedure used by Buffr n l et al. (2010) for sirenian ribs. Similar data from the literature were also considered (~~TablesTab-~~ 1, 2). The new morphometric data presented below include three extant taxa: the grey seal *Halichoerus grypus* ~~Fabricius-1791~~ from the cold temperate and subarctic zones of the North Atlantic, the harbor seal *Phoca vitulina* ~~Linnaeus-1758~~ from the temperate to arctic zones of the North Atlantic and North Pacific, and the Baikal seal *Pusa sibirica* (~~Gmelin-1788~~) from Lake Baikal. All bones included in the study were from adult or subadult individuals, judging from the degree of epiphyseal fusion in associated long bones (see Stor  2000). The comparative sample of extinct phocids is largely dependent on the published fossil record; this is why some taxa are represented in the dataset by both humeri and femora, while others are only represented by measurements of either humeri or femora.

Because the dataset used for the morphometric study depends on the literature, the dataset employed for the microanatomical and histological studies is necessarily different ~~since-as~~ it is based on first-hand analyses of actual specimens available for scanning and/or sectioning. (see ~~Tab-Tables~~ 1, 2 versus ~~TableTab-~~ 3). The microanatomical dataset includes measurements on the extant phocine *Phoca vitulina*, the extinct phocids *Nanophoca vitulinoides* (~~Van-Beneden-1871~~), including the neotype specimen IRSNB M2276, *Callophoca obscura* ~~Van-Beneden-1876~~ from the Tortonian to Zanclean (late Miocene – early Pliocene) of Belgium and North Carolina (LD pers. obs.), *Leptophoca proxima* (~~Van~~

Formatted: Space After: 0 pt

Formatted: Indent: First line: 0.5", Space After: 0 pt

Formatted: Indent: First line: 0.5"

Formatted: Font: Not Italic

1
2
3
4
5
6
7 139 ~~Beneden 1877~~) from the late Aquitanian to late Serravallian (late early Miocene – late middle
8
9 140 Miocene) of Belgium and the North American Chesapeake Bay area (Koretsky 2001;
10
11 141 Dewaele et al. 2017b), and *Phocanella pumila* from the Tortonian to Zanclean (late Miocene
12
13 142 – early Pliocene) of Belgium and North Carolina (LD pers. obs.). Two additional small extinct
14
15 143 Neogene phocids from the southern North Sea ~~Bb~~ basin are also considered: *Batavipusa*
16
17 144 ~~neerlandica~~ ~~Koretsky and Peters, 2008~~, from the early to middle Tortonian (8 – 11.5 Ma) of
18
19 145 the Netherlands, and *Praepusa boeska* ~~Koretsky, Peters and Rahmat, 2015~~, from the late
20
21 146 Miocene to late Pliocene of Belgium and the Netherlands (~~Koretsky and Peters 2008~~;
22
23 147 ~~Koretsky et al. 2015~~). However, the fossil record of these taxa is extremely scarce and the
24
25 148 attribution of the various specimens to each taxon is questionable (e.g., Koretsky and Peters
26
27 149 2008, Koretsky et al. 2015, Dewaele et al. 2017a). Tomographic (CT) data for *B. neerlandica*
28
29 150 and *Pr. boeska* are of moderate quality. Distinction between the internal structures of the bone
30
31 151 and the sediment infill proved unpractical, and both taxa are only considered qualitatively.
32
33 152 Additional data (from either classical thin sections or micro-CT scans) already published by
34
35 153 Buffrénil and Schoevaert (1989), Buffrénil et al. (2010), Canoville and Laurin (2010),
36
37 154 Canoville et al. (2016), and Amson et al. (2014) about the inner structure of long bones in
38
39 155 various extant and extinct aquatic mammals (otters, marine sloths, polar bear, and sirenians)
40
41 156 were also considered for the comparisons (~~Tab-Table~~ 3). In extinct phocid taxa, the
42
43 157 osteohistological dataset is limited to three species, in addition to ~~Nanophoca-N.~~ *vitulinoides*:
44
45 158 the monachine *Callophoca obscura*, and the phocines *Leptophoca proxima* and *Phocanella*
46
47 159 *pumila* (~~Tab-Table~~ 3). The bone samples for these taxa include femora, humeri, radii, ribs,
48
49 160 tibiae, and lumbar vertebrae with both transverse and longitudinal sections. These bones are
50
51 161 also known in the fossil record of *N. vitulinoides* and can therefore allow detailed
52
53 162 comparisons.

1
2
3
4
5
6
7 164 **PROCESSING OF THE SPECIMENS**
8

9
10 165 **Morphometric features.** Buffrénil et al.'s (2010) study focused on the discrimination of
11 166 pachyostosis sensu stricto (cortical hyperplasy) in ribs and used, among other measurements,
12 167 rib length. Unfortunately, very few entire ribs are available for fossil seals, and the so-called
13 168 Cortical Development index used by these authors (the calculation of this index requires
14 169 measurements of total length, chord, and mean circumference of the ribs) could not be applied
15 170 to ~~the ribs of *Nanophoca-N. vitulinoides* ribs~~; conversely, this index, called here “bulkiness
16 171 index” or BI, could be used for the humeri and femora in the same conditions as for the other
17 172 phocid specimens (Fig. 2). For the humerus, two measurements were taken: A) absolute
18 173 sagittal length of the bone between the most proximal point and most distal point, or BL, and
19 174 B) transverse width at mid-shaft, or TW. For the femur, three measurements were taken: A)
20 175 absolute sagittal length (BL), B) transverse width at the narrowest portion of the diaphysis
21 176 (TW), and C) anteroposterior width of the diaphysis in the same portion (APW), which is
22 177 perpendicular to transverse width. For the humerus, the calculated ratio is $BI = TW/BL$. A
23 178 low BI value indicates a relatively narrow diaphysis, and a high value indicates a relatively
24 179 thick diaphysis. For the femur, the ratio is $BI = [0.5(TW+APW)]/BL$. Similarly, a low value
25 180 of BI indicates a relatively narrow diaphysis, and a high value indicates a relatively thick
26 181 diaphysis.

27
28 182 **Thin section analysis (microanatomy and histology).** Thin section preparation was carried
29 183 out according to the classical procedures used for this kind of preparations (Lamm 2013). All
30 184 the sections made for this study are now part of the Histothèque (i.e., thin section collection)
31 185 housed in the Muséum national d'Histoire naturelle in Paris, where they are recorded under
32 186 various numbers within the Histos database. These sections include transverse mid-diaphyseal
33 187 and metaphyseal sections, with additional longitudinal sections through the epiphyses.

34 188 Microscopy was performed using a Zeiss Axioskop microscope, with ordinary and polarized
35
36
37
38
39
40

Formatted: Font: Not Italic

Formatted: Font: Not Italic

Formatted: Font: Not Italic

Formatted: Font: Not Italic

1
2
3
4
5
6
7 189 transmitted light at low (x25) to medium (x400) magnifications. All measurements of
8
9 190 sectional dimensions were performed with the software ImageJ (National Institute of Health,
10
11 191 USA) on microphotographs. For microanatomy, only mid-diaphyseal transverse sections were
12
13 192 considered. The terminology used in microanatomical and histological descriptions refers to
14
15 193 Francillon-Vieillot et al. (1990) and Prondvai et al. (2014).
16
17 194 **X-ray computed microtomography (micro-CT).** A part of the biological sample (see
18
19 195 [Tab:Table 4–8](#)) consists of specimens scanned at the Ghent University Centre for X-ray
20
21 196 Tomography (www.ugct.ugent.be) with a custom-built microtomograph HECTOR
22
23 197 (Masschaele et al. 2013). Depending on the sample, the tube was operated at 140 to 160 kV
24
25 198 and 40 to 45 W. A 1 mm Al filter was applied to reduce beam hardening, which was then
26
27 199 further filtered during the reconstruction process. The reconstruction was performed with
28
29 200 OCTOPUS RECONSTRUCTION (XRE Belgium). Resulting images had a voxel size of
30
31 201 approximately 30 μm , 46 μm , or 84 μm , depending on the magnification (see [Tab:Table 4–8](#)).
32
33 202 **Cross-section analysis using BONE PROFILER**—All cross-sections (be they material thin
34
35 203 sections or virtual micro-CT Scan sections) were analyzed using BONE PROFILER Version
36
37 204 4.5.8 (Girondot and Laurin 2003). BONE PROFILER is a freeware dedicated to the analysis
38
39 205 of bone compactness in sections, i.e., the area actually occupied by mineralized bone tissue
40
41 206 divided by total sectional area, and designed to calculate relevant parameters describing the
42
43 207 compactness profile. To do so, the entire cross-section is divided in 3060 cells created by the
44
45 208 intersection of 60 sectors ($360^\circ/60 = 6^\circ$ per sector) and 51 concentric rings parallel to the
46
47 209 section outline (Laurin et al., 2004: fig. 3). Compactness distribution and variation from the
48
49 210 ontogenetic center of the sections to cortical surface are presented as the ‘compactness
50
51 211 profile’. The compactness profile is characterized by four parameters S, P, Min, and Max. S is
52
53 212 the reciprocal of the slope at the curve inflection point, and it is proportional to the relative
54
55 213 width of the transition zone between the medulla and the cortical regions. P is the position of

1
2
3
4
5
6
7²¹⁴ the curve inflection point on the x-axis, and it represents the position of the transition area
8
9²¹⁵ between the medulla and the cortical region. Min and Max are the minimum and maximum
10
11²¹⁶ asymptotes, respectively, representing the minimum and maximum values of bone
12
13²¹⁷ compactness in a section. Other parameters can be calculated using BONE PROFILER
14
15²¹⁸ (Laurin et al. 2004; Quemeneur et al. 2013), but these were not used in the current study.
16
17²¹⁹ More elaborate analyses with BONE PROFILER including parameters Minrad, Maxrad, Srad,
18²²⁰ and Prad are not used in the present study, but are provided as Supporting Information
19
20²²¹ (Appendix 1). These are similar to the abovementioned parameters, but are the radial
21
22²²² versions, i.e., the average values of the measurements for the 60 sectors. Hence, standard
23
24²²³ deviations (SD) are also calculated for these values.
25

26²²⁴
27
28
29²²⁵ **PHYLOGENETIC FRAMEWORK**

30
31²²⁶ For the phylogenetic position of *Nanophoca N. vitulinoides* in the current study, we follow the
32
33²²⁷ phylogenetic analysis by Dewaele et al. (2017a), which is, to date, the only published analysis
34
35²²⁸ including this species (Fig. 3). According to Dewaele et al. (2017a: fig. 25; Fig 3. in the
36
37²²⁹ current study), *N. vitulinoides* is a relatively late-branching stem-phocine; it is the closest
38
39²³⁰ known relative of crown Phocinae. Evidently, it should be noted that this phylogenetic
40
41²³¹ position is only relative to the other Operational Taxonomic Units (OTUs) included in this
42
43²³² analysis. The phylogenetic relationships of other small phocids, such as *Batavipusa*
44
45²³³ *neerlandica*, *Pontophoca sarmatica*, *Praepusa boeska*, or –most notably– *Monachopsis*
46
47²³⁴ *pontica* has been studied by Koretsky (2001) and Koretsky and Rahmat (2013). However,
48
49²³⁵ their fossil record is too scarce (e.g., *B. neerlandica* is only known from one isolated humerus,
50
51²³⁶ an isolated ilium, and an isolated partial femur tentatively assigned to it; *M. pontica* is only
52
53²³⁷ known from multiple isolated humeri and femora) to be confident about their phylogenetic
54
55²³⁸ position. Not surprisingly, previous phylogenetic analyses including those taxa show little

1
2
3
4
5
6
7²³⁹ consensus and confidence on their phylogenetic position (Koretsky 2001; Koretsky and
8
9²⁴⁰ Rahmat 2013). For the phylogeny of other, extant Pinnipedia included in this study, we refer
10
11²⁴¹ to Higdon et al. (2007). The extinct *Callophoca obscura*, *Leptophoca proxima*, and
12
13²⁴² *Phocanella pumila* have all been considered in phylogenetic analyses. There is little
14
15²⁴³ consensus about the phylogenetic position of the monachine *C. obscura*. Some researchers
16
17²⁴⁴ consider *C. obscura* most closely related to the extant elephant seal *Mirounga*, while others
18
19²⁴⁵ group it with the late Pliocene *Pliophoca etrusca* from Italy, or consider it as a stem
20
21²⁴⁶ monachine (compare Muizon 1981; Koretsky and Ray 2008; Koretsky and Rahmat 2013;
22
23²⁴⁷ Amson and Muizon 2014; Berta et al. 2015). Therefore, we consider *C. obscura* a monachine
24
25²⁴⁸ phocid, but we do not make genus-level phylogenetic inferences for this taxon. The
26
27²⁴⁹ phylogenetic position of *L. proxima* (or as *Leptophoca lenis*) has been first analyzed by
28
29²⁵⁰ Koretsky (2001) and Koretsky and Rahmat (2013), but without consensus. Cozzuol (2001)
30
31²⁵¹ interpreted *L. lenis* as an early-branching phocine, while Berta et al. (2015) suggested that the
32
33²⁵² taxon was an early-branching stem monachine. However, the latter expressed doubt over their
34
35²⁵³ phylogenetic results for *Leptophoca*. More recent studies by Dewaele et al. (2017a, b) placed
36
37²⁵⁴ *L. proxima* as a stem phocine with strong statistical support. The phylogenetic position of *P.*
38
39²⁵⁵ *pumila* has only been analyzed once, by Koretsky and Rahmat (2013). However, they neither
40
41²⁵⁶ present the character matrix nor a list of synapomorphies to support their analysis. In addition,
42
43²⁵⁷ this analysis differs on key nodes from other, widely-accepted phylogenetic analyses (e.g.
44
45²⁵⁸ Bininda-Emonds and Russell 1996), inhibiting us of considering this analysis to elucidate the
46
47²⁵⁹ phylogenetic position of ~~*Phocanella*~~ *pumila*. The phylogenetic position of the latter remains
48
49²⁶⁰ unclear, pending future discoveries of more complete material and new analyses. This
50
51²⁶¹ information is provided only as contextual information; we did not perform any phylogeny-
52
53²⁶² informed statistical tests in this study given that the focus is on only three early pinniped taxa.

1
2
3
4
5
6
7
8
9
10
11
12
13
14
15
16
17
18
19
20
21
22
23
24
25
26
27
28
29
30
31
32
33
34
35
36
37
38
39
40
41
42
43
44
45
46
47
48
49
50
51
52
53
54
55
56
57
58
59
60
61
62
63
64
65

INSTITUTIONAL ABBREVIATIONS

IRSNB/RBINS, Institut royal des Sciences naturelles de Belgique, Brussels, Belgium; MAB, Oertijdmuseum Groene Poort, Boxtel, the Netherlands; MNHN, Muséum national d’Histoire naturelle, Paris, France; MSC, Smithsonian Institution Museum Support Center, Suitland, Maryland, USA; USNM, National Museum of Natural History, Washington, DC, USA.

DATA AVAILABILITY

All data used in this study is presented within the main text. Additional results from the radial analysis with BONE PROFILER are provided as Supporting Information (Appendix 1). Thin sections that are used in this study are housed at the MNHN. Specimens that have been CT-scanned are housed at the IRSNB. Specimens are available for consultation and access should be requested at the respective institutions.

RESULTS

MORPHOMETRIC DATA

Although no complete ribs of *Nanophoca-N. vitulinoides* are preserved to perform morphometric measurements, the sub-circular morphology of the cross-section from these bones differs from that of related taxa (Fig. 5A versus Fig. 5B, C). For a similar rib length (a parameter that unfortunately lacks), it could possibly be indicative of some incipient tendency toward pachyostosis. Morphometric results for the humerus and femur are listed as Tab-Tables 1 and 2. The diaphysis of the humerus of *Nanophoca* humerus is relatively slender, as compared to other extant and extinct Phocidae. BI ratio for the humerus of two specimens of *N. vitulinoides* is 0.121 and 0.135, which is at the lower half of the range of the

Formatted: Space After: 0 pt

1
2
3
4
5
6
7 287 29 calculated values (0.109 – 0.210) ([Tab-Table 1](#)). Apart from the extinct *Batavipusa*
8
9 288 *neerlandica* (0.182), *Monachopsis pontica* (0.169), and *Pachyphoca ukrainica* (0.210), extinct
10
11 289 Phocidae in our sample tend to have a relatively slender humeral diaphysis, as compared to
12
13 290 extant forms. This rules out the eventual occurrence of pachyostosis in the humerus of *N.*
14
15 291 *vitulinoides*.

16
17 292 Bulkiness index values indicate that the femoral diaphysis of *Nanophoca N.*
18
19 293 *vitulinoides* (0.200, 0.207, and 0.208) and other extinct Phocidae (0.173 – 0.240) is overall
20
21 294 relatively thick, as compared to extant Phocidae (0.158 – 0.187) ([Tab-Table 2](#)). This contrasts
22
23 295 with the measurements of the humeri. As for the humerus, the taxon with the bulkiest femur is
24
25 296 *Pachyphoca P. ukrainica*, based on the average of
26
27 297 three specimens presented by Koretsky and Rahmat (2013), and a value of 0.229 for one
28
29 298 specimen of *Pachyphoca chapskii*. Given that the femora of the extinct taxa in our sample
30
31 299 have consistently higher values, i.e., suggestive of pachyostosis, it remains difficult to find
32
33 300 conclusive evidence on the presence or absence of pachyostosis in the femur of *N. vitulinoides*
34
35 301 in comparison to contemporaneous taxa.

36 37 38 303 **MICROANATOMY**

39 40 304 ***Vertebrae***

41
42 305 [Table 4]

43
44
45 306 [Figure 4]

46
47 307 Bone compactness in the centra of the two lumbar vertebrae of *Nanophoca N. vitulinoides*,
48
49 308 ranges from 93.8% for the adult, to 63.6% for the juvenile. ([Tab-Table 4](#); Fig. 4). These values
50
51 309 are much higher than those observed in the other pinnipeds and semi-aquatic mammals
52
53 310 included in this study ([Tab-Table 4](#)): compactness values indeed range for these taxa from

Formatted: Indent: First line: 0.5"

1
2
3
4
5
6
7 311 22.3% (hooded seal, *Cystophora cristata*) to 44.3% (sea otter, *Enhydra lutris*). Apart from *N.*
8
9 312 *vitulinoides*, the compactness values for the vertebrae of the Phocinae (22.3% for *C. cristata*
10
11 313 and 29.3% for the harp seal, *Pagophilus groenlandicus*) are lower than the values calculated
12
13 314 for Monachinae and Otariidae.

14
15 315
16
17 316 **Rib**

18
19
20 317 [Table 5]

21
22 318 [Figure 5]

23
24 319 With an overall compactness of 99.8%, the rib of ~~*Nanophoca*~~ *N. vitulinoides* is almost
25
26 320 completely ossified, and much more compact than that of other semi-aquatic mammals
27
28 321 (~~Tab. Table~~ 5; Fig. 5). The Cape fur seal *Arctocephalus pusillus* and the Californian sea lion
29
30 322 *Zalophus californianus* have the second and third most compact ribs in the biological sample,
31
32 323 with compactnesses of 78.4% and 78.2%, respectively. While there is no differentiated
33
34 324 medullary cavity in the rib of *N. vitulinoides* (Fig. 5A), the medullary cavity in the ribs of
35
36 325 other taxa in the biological sample is occupied by loose spongiosa and surrounded by a
37
38 326 compact cortex (Fig. 5B, C).

39
40 327

41
42 328 **Humerus**

43
44 329 [Table 6]

45
46
47 330 [Figure 6]

48
49 331 [Figure 7]

50
51
52
53
54
55
56
57
58
59
60
61
62
63
64
65

1
2
3
4
5
6
7
8
9
10
11
12
13
14
15
16
17
18
19
20
21
22
23
24
25
26
27
28
29
30
31
32
33
34
35
36
37
38
39
40
41
42
43
44
45
46
47
48
49
50
51
52
53
54
55
56
57
58
59
60
61
62
63
64
65

With an overall compactness of 99.7% for one specimen and 99.9% for the other, the humerus of *Nanophoca N. vitulinoides* is almost completely solid (Table 6; Fig. 6). Only the humerus of *Phocanella pumila* has a comparably (though somewhat lesser) high compactness (95.9%); but unlike *Phocanella P. pumila*, there is no discernable medullary cavity in the two specimens of *N. vitulinoides* (Fig. 6A, B versus Fig. 6C). Given the poor density differentiation between the mineralized bone tissue and the sediment infill in *Batavipusa neerlandica* and *Praepusa boeska*, quantitative microanatomical analysis using BONE PROFILER was precluded. A qualitative analysis reveals the presence of a porous medullary cavity framed by compact cortices in both taxa (Fig. 7A, B).

Femur

[Table 7]

[Figure 8]

Compactness values for the two femora of *Nanophoca N. vitulinoides*, i.e., 97.1% and 99.4%, are much higher than those of all extant and most extinct semi-aquatic taxa considered in this study (Table 7; Fig. 8A, B versus Fig. 8C, D, F-I). Only the femur of *Phocanella pumila* shows a compactness approaching the condition in *N. vitulinoides* (Table 7; Fig. 8A, B versus Fig. 8E).

Other bones

[Table 8]

[Figure 9]

1
2
3
4
5
6
7
8
9
10
11
12
13
14
15
16
17
18
19
20
21
22
23
24
25
26
27
28
29
30
31
32
33
34
35
36
37
38
39
40
41
42
43
44
45
46
47
48
49
50
51
52
53
54
55
56
57
58
59
60
61
62
63
64
65

Other long bones of *Nanophoca vitulinoides*, i.e., the radius and the tibia, have been studied as well and show very high compactness ratios, similar to the condition observed in the rib, humerus, and femur (Table 8; Fig. 9). There is no discernable medullary cavity present, unlike, for example, the extant *Phoca vitulina* (Table 8; Fig. 9A, C versus Fig. 9B, D).

BONE HISTOLOGY

In cross and sagittal sections, all bones of *Nanophoca N. vitulinoides* examined in this study share the same basic histological features (in addition to their microanatomical similarity), with only few differences most likely related to ontogenetic age. In most of the bones, except one of the radii (Histos 2142) and one of the vertebral centra (Histos 2150), Haversian remodeling is mild in the cortex; the characteristics of primary periosteal deposits thus remain visible (Fig.10A, B). They consist in layers of woven-parallel tissue (according to Prondvai et al.'s 2014 terminology) with longitudinal primary osteons, separated by very birefringent annuli made of parallel-fibered or lamellar bone (Fig.10C). Short Sharpey's fibers (60-80 µm long) colonize the basal parts of the woven-parallel layers (Fig.10C). The annuli are wide (up to 180 µm) in the cortical depth, and thinner (some 60-70 µm) towards the cortical periphery. The bone displaying the greatest number of visible growth marks is the humerus, with five sharp annuli (Fig.10A) associated with lines of arrested growth. Of course, in this specimen, several annuli were erased by remodeling in the depth of the cortex. In the long bones where they occur, the annuli tend to be more tightly spaced towards the cortical periphery, but they nevertheless maintain a significant spacing, e.g., 320 µm between the fourth and fifth annuli in the humerus (Fig.10A). In the femur and the humerus, in which cortical structure is perfectly preserved up to the outer margin of the diaphysis, the last growth mark is an annulus (Fig.10A). The nature of the last growth mark is less evident in the other long bones, due to the impregnation of superficial layers by a dark substance during

Formatted: Space After: 0 pt

Formatted: Font: Not Italic

Formatted: Font: Not Italic

Formatted: Font: Not Italic

Formatted: Font: Not Italic

Formatted: Font: Not Italic

Formatted: Font: Not Italic

Formatted: Font: Not Italic

1
2
3
4
5
6
7 379 fossilization. However, there is no clear indication of the presence of an external fundamental
8
9 380 system (EFS) that could have shown that the growth of the bones, at least in diameter, had
10
11 381 dropped to a very low level and that skeletal growth was ending by the time the animals died.
12
13 382 In the two specimens (radius Histos 2142 and centrum of the vertebra Histos 2150) where the
14
15 383 structure of primary periosteal deposits is no longer visible, bone cortices are entirely
16
17 384 occupied by a particularly dense Haversian tissue (Fig.10E) that extends continuously towards
18
19 385 the central (medullary) region of the bones.

20 386 The medullary territory of all bones is entirely compact, with the exception of some
21
22 387 scarce, vaguely circular cavities measuring generally less than 300-400 µm in diameter. The
23
24 388 dense Haversian tissue occupying this region (Fig.10F) has three basic characteristics: A) Its
25
26 389 secondary osteons are roughly longitudinal, but their orientation can be locally variable;
27
28 390 moreover, their central canals (Havers' canals) develop numerous transversal anastomoses
29
30 391 (Wolkman's canals), suggesting high BMU (Bone Multicellular Units, i.e., the populations of
31
32 392 cells responsible for the formation of secondary osteons; Frost 1969) activation frequency,
33
34 393 i.e., parameter *Ac.f* in classical histomorphometric nomenclature (cf. Dempster 2013). B)
35
36 394 Most of the secondary osteons show evidence of particularly intense remodeling (Fig.10G,
37
38 395 H), with the presence of two2 to four4 cycles of resorption and reconstruction centered on the
39
40 396 Haversian canal. By this process, several generations of osteons with decreasing diameters
41
42 397 were formed inside ontogenetically older secondary osteons. This situation is general in
43
44 398 *Nanophoca-N. vitulinoides*; it occurs in all secondary bone deposits, be they localized in the
45
46 399 medullary or cortical regions of the bones. C) Such a process resulted in extreme thinning of
47
48 400 the lumens of Havers' canals, which are very seldom wider than 10 µm, and most often less
49
50 401 than 5 µm. Havers' canals in numerous osteons are so drastically reduced that they seem to be
51
52 402 completely occluded (Fig.10H).

Formatted: Indent: First line: 0.5", Space After: 0 pt

1
2
3
4
5
6
7
8
9
10
11
12
13
14
15
16
17
18
19
20
21
22
23
24
25
26
27
28
29
30
31
32
33
34
35
36
37
38
39
40
41
42
43
44
45
46
47
48
49
50
51
52
53
54
55
56
57
58
59
60
61
62
63
64
65

This special Haversian tissue, characteristic of the medullary (and occasionally cortical) region, can be observed in all parts of the long bones: in the mid-diaphyseal region as well as in metaphyses, from which it extends continuously into the whole epiphyseal regions, up to the proximal and distal extremities of the bones, where it merges into the thin layers of calcified cartilage covering articular surfaces (Fig.11A-C). None of the longitudinal sections (which were made in all specimens) reveal the presence of a functional growth plate or a lack of fusion of primary and secondary centers of ossification (Fig.11A, B). We thus conclude that the growth in length of long bone specimens in our sample was complete.

With the exception of the vertebral centra (considered below), there is only one variation to this general pattern. In the radius Histos 2174, the medullary territory (51% of the total area in cross section) is occupied by a compacted spongiosa whose former trabeculae, still clearly distinguishable, show numerous reversion lines (created by a strong resorption – reconstruction activity), but no secondary osteons (Fig.11D, E). Conversely, inter-trabecular spaces are entirely filled by endosteal lamellar tissue showing evidence of intense Haversian substitution. This process resulted in several generations of concentric secondary osteons (Fig.10E). Such a detailed topographical difference in remodeling patterns, through which the initial architecture of the medullary spongiosa was preserved, is unknown in all other specimens studied here.

The femur, humerus, and ulna examined here display a strong off-centering of growth (Fig.11F) that provoked, on the one hand, the development of a thick primary cortex on the lateral side of these bones and, on the other hand, the superficial outcropping of remodeled medullary regions, due to extensive resorption on their medial side. The result of this double process was a lateral drift of growth. Moreover, several of the long bones show, on cross sections, variably oriented fissures 120 to 200 μm long (Fig.11E). These cracks are observed only in deep cortical regions and in the medullary territory; they never reach the peripheral

1
2
3
4
5
6
7 428 margins of the bones. Their possible nature and the causes of their occurrence are discussed
8
9 429 below (see Discussion).

10
11 430 The trabeculae occupying the centrum of the largest vertebra (specimen IRSNB prov.
12
13 431 16), as well as the lamellar bone that partly fills inter-trabecular spaces, have a histological
14
15 432 structure similar to that observed in the medullary region of long bones: they are formed of
16
17 433 intensively-remodeled tissue (Fig.11G). Remodeling is less intensive in the smaller vertebra;
18
19 434 therefore, the growth pattern of this bone remains legible. It was a normal endochondral
20
21 435 osteogenesis, with complete resorption of epiphyseal calcified cartilages; and active
22
23 436 remodeling of primary trabeculae, at a small distance away from the zone of cartilage
24
25 437 hypertrophy. In general, none of the bones examined in this study displays the slightest
26
27 438 residue of calcified cartilage outside a narrow band (200 to 400 µm) localized just under the
28
29 439 epiphyseal surface (Fig.11C). The largest centrum retains only a thin layer of primary
30
31 440 periosteal bone tissue spared by remodeling on the walls of the neural arch (Fig.11I). Six
32
33 441 tightly spaced growth marks (mean spacing < 50 µm) forming an external fundamental
34
35 442 system are visible in this layer: the bone was thus reaching the end of its growth.

36 37 38 444 **Comparative data**

39
40 445 The vertebrae of pinniped taxa other than *Nanophoca N. vitulinoides* show relatively little
41
42 446 microanatomical or histological differences from other mammals. Moreover, the diaphyses of
43
44 447 their long bones, though presenting some few, slender medullary trabeculae, do not display
45
46 448 typical microanatomical or histological peculiarities (very high or very low global
47
48 449 compactness, lack of a medullary cavity, cortical hyperplasy, diaphyseal persistence of
49
50 450 calcified cartilage, etc.) likely to distinguish these taxa unambiguously from other mammals
51
52 451 (see also the Introduction). The only exception is the small development of the medullary
53
54 452 cavity in the femur of *Phocanella pumila* (Fig.12A). When primary periosteal cortices in long

Formatted: Indent: First line: 0.5"

1
2
3
4
5
6
7
8
9
10
11
12
13
14
15
16
17
18
19
20
21
22
23
24
25
26
27
28
29
30
31
32
33
34
35
36
37
38
39
40
41
42
43
44
45
46
47
48
49
50
51
52
53
54
55
56
57
58
59
60
61
62
63
64
65

bones, are partly spared by Haversian substitution (as observed in the femur of *P-Phocanella pumila* and a rib from *Monachus monachus*), they are composed, like those of *N. vitulinoides*, of a woven-parallel complex containing longitudinal primary osteons, annuli and lines of arrested growth (Fig.12B–D). Otherwise, remodeling is intense and spreads to the totality of bone cortices; however, extreme remodeling resulting in the closure of vascular canals does not occur (Fig.12D, E). In all taxa, except *Phocanella-P. pumila*, the thin trabeculae occurring in the medullary cavity are made of remodeled lamellar bone, framing wide inter-trabecular spaces (Fig.12E, F). In *Phocanella- pumila*, medullary trabeculae are also intensely remodeled, but they are much thicker than in other pinnipeds (compare Fig.12A and 12F). As a consequence, they divide the medullary cavity into small lacunae and strongly increase its compactness (on cross sections).

DISCUSSION

MORPHOMETRICS AND MICROANATOMY

Based on the sample of specimens used for the morphometric analysis, the diaphysis of the humerus of extinct Phocidae is generally more slender than in extant specimens, apart from the late Miocene *Pachyphoca ukrainica*, which shows pachyostotic ‘swelling’ of the humeral diaphysis. However, the femoral diaphysis of the sampled extinct Phocidae is generally a little thicker than that of extant Phocidae. The femoral diaphysis in *Pachyphoca* and, to a lesser extent, *N. vitulinoides* is also relatively bulky, without appearing swollen. Thus, we detected no clear pachyostotic trend in our sample.

Despite the absence of pachyostosis in the humerus and the femur of *Nanophoca N. vitulinoides*, osteosclerosis appears to be extreme in this taxon, and occurs also in *Phocanella pumila*. For the studied specimens of *N. vitulinoides*, namely one rib, two humeri, one radius,

Formatted: Font: Not Italic

Formatted: Space After: 0 pt

Formatted: Indent: First line: 0.5", Space After: 0 pt

1
2
3
4
5
6
7 477 two femora, and one tibia, actual bone compactness (0.971 – 0.999) approaches 1 (100%).
8
9 478 Similarly, although slightly lower (0.959 – 0.977), compactness values in the humerus and
10
11 479 femur of *P-hocanella pumila* are much above the common situation of other specimens. The
12
13 480 relatively high compactness of the lumbar vertebrae of both the juvenile and the adult
14
15 481 specimens of *N. vitulinoides* shows that osteosclerosis in the taxon extends to the entire
16
17 482 postcranial skeleton. Moreover, differences in compactness between the adult (93.8%) and the
18
19 483 juvenile (63.6%) suggest that the increase in compactness is an ongoing process during the
20
21 484 growth of the animal. In addition to that, it is noteworthy that the compactness observed in the
22
23 485 vertebrae of Phocinae (excluding *N. vitulinoides*) is noticeably lower than the compactness
24
25 486 observed in Monachinae and Otariidae. This may hypothetically be related to differences in
26
27 487 locomotion (Pierce et al. 2011; Kühn and Prey 2012) or differences in maternal care (Boness
28
29 488 and Bowen 1996). However, this is beyond the scope of the current study and should be
30
31 489 treated in a future studies.

32
33 490 Considering the entire set of microanatomical observations made on the bones of
34
35 491 *Nanophoca* ~~bones~~, it seems obvious that osteosclerosis touches most (and perhaps all) of the
36
37 492 appendicular elements. This contrasts with the situation prevailing in the sirenian *Dugong*
38
39 493 *dugon*, in which there is a gradual decrease in compactness from the more proximal portion of
40
41 494 the forelimb towards its distal portion (Buffrénil and Schoevaert 1989). A similar condition
42
43 495 has been described in the marine sloth *Thalassocnus* (Amson et al. 2014) in which the radius
44
45 496 is noticeably less compact than the humerus.

46 498 **GROWTH PATTERN OF THE BONES AND MECHANISM OF THEIR COMPACTION**

47
48
49 499 ***Growth pattern of bone cortices.*** According to the experimental data presently available
50
51 500 about the relationship between the structure of periosteal bone deposits and their accretion
52
53 501 rate, the so-called Amprino's (1947) rule, the growth in thickness of *Nanophoca-N.*

Formatted: Space After: 0 pt

1
2
3
4
5
6
7 502 *vitulinoides* bone cortices proceeded at relatively moderate speed. The woven-parallel bone
8
9 503 with longitudinal primary osteons that compose them is generally associated, in extant
10
11 504 mammals and birds, ~~to~~-with apposition rates ranging between 4 and 8 μm per day (Castanet et
12
13 505 al. 1996, 2000). All other forms of woven-parallel bone, i.e., reticular, plexiform, laminar, or
14
15 506 radial tissues, correspond to higher growth rates. This question is nevertheless complex; it
16
17 507 remains incompletely settled and contrasting results have been presented by Margerie et al.
18
19 508 (2002). To our knowledge, there are neither experimental data on bone apposition rate in
20
21 509 pinnipeds, nor precise histological descriptions of the structure of periosteal cortices in their
22
23 510 bones. The comparative observations made in the present study suggest that, despite its
24
25 511 modest size, *N. vitulinoides* did not grow at a rate very different from that of larger species.

26 512 The growth of primary bone cortices was cyclic in *Nanophoca* with, as in most
27
28 513 mammals for which accurate data exist, the yearly alternation of a fast growth phase
29
30 514 (accretion of the woven-parallel layers) when food was abundant, and a slow growth phase,
31
32 515 corresponding to unfavorable environmental conditions, during which the annuli were
33
34 516 formed. In one specimen at least, the humerus Histos 2139, a total arrest of growth occurred
35
36 517 each year, resulting in the formation of lines of arrested growth. The comparative sample
37
38 518 reveals that *Nanophoca* did not differ from other pinnipeds for these characteristics. More
39
40 519 generally, several recent studies (e.g., Castanet 2006; Köhler et al. 2012) show that the
41
42 520 presence of growth cycles of annual periodicity (supposed so in fossils) is a general,
43
44 521 plesiomorphic feature in vertebrates (it primarily depends on endogenous rhythms), whatever
45
46 522 their phylogenetic position, physiological characteristics, or ecological adaptations, as shown
47
48 523 by the occurrence of cyclic growth marks in Silurian placoderms (Giles et al. 2013).

49 524 The ontogenetic transformation of primary cortices in *Nanophoca* was basically due to
50
51 525 intense Haversian remodeling, a situation also observed in other pinnipeds and otherwise
52
53 526 common to most mammals. Cortical remodeling presented some delay as compared to that

Formatted: Indent: First line: 0.5", Space After: 0 pt

Formatted: Font: Not Italic

1
2
3
4
5
6
7 527 occurring in the medullary region, which explains that non-remodeled primary cortices co-
8
9 528 existed with a densely remodeled medulla in most bones.
10
11 529 ***Mechanism of medullary compaction.*** Our histological observations suggest that the
12
13 530 fundamental process of endochondral osteogenesis was not significantly modified in
14
15 531 *Nanophoca-N. vitulinoides*. Contrary to the situation prevailing in numerous secondarily
16
17 532 aquatic tetrapods (reviewed in e.g., Ricqlès and Buffrénil 2001), the calcified cartilage formed
18
19 533 in growth plates was entirely eroded and the formation of primary trabeculae was apparently
20
21 534 normal. Compaction of the medullary region basically resulted from the mode of remodeling
22
23 535 of these trabeculae. The erosion and reconstruction process involved in bone remodeling is
24
25 536 generally balanced, the amount of bone resorbed by osteoclasts being approximately
26
27 537 compensated by an equivalent amount of reconstructive (secondary) osseous tissue (Parfitt
28
29 538 1981, 1982). In *N. vitulinoides*, imbalance visibly existed in favor of the reconstructive stage:
30
31 539 the amount of secondary deposits produced by endosteal osteoblasts exceeded the volume of
32
33 540 tissue previously eroded by the osteoclasts. The detailed histogenetical mechanism controlling
34
35 541 this peculiar functioning of the osteoblasts is, of course, beyond reach of this study. The
36
37 542 regulation of osteoblast activity during Haversian remodeling is a complex, still poorly
38
39 543 elucidated question (e.g., Martin 2000; Burr and Allen 2014). It nevertheless remains that the
40
41 544 cause responsible for osteosclerosis in *N. vitulinoides* obviously resided in a modification of
42
43 545 this regulation mechanism. Occlusion of intra-osseous cavities due to this process was
44
45 546 extremely pronounced because several, successive peri-vascular remodeling cycles occurred
46
47 547 locally (over-remodeling), up to a quasi-total closure of vascular canals. Vascular canals
48
49 548 reduced to diameters less than 10 μm , and a fortiori the thinner capillaries housed in them, are
50
51 549 unlikely to have remained functional, ~~since-as~~ the mean diameter of mammalian erythrocytes
52
53 550 (not to speak of other blood cells) is 7 to 8 μm (e.g., Fawcett and Jensch 1997). In humans, the
54
55 551 lumen of the Haversian canal of a normal, fully developed, secondary osteon is 20 – 50 μm in
56
57
58
59
60
61
62
63
64
65

Formatted: Space After: 0 pt

Formatted: Font: Not Italic

1
2
3
4
5
6
7 552 diameter (Jaworski 1993; Fiala 1980; see also Polig and Jee 1990). For example, in the ribs of
8
9 553 male humans aged 20 – 25 years, mean Haversian canal perimeter (variable *Hc.Pm* in
10
11 554 classical nomenclature) is 0.165 mm, and Haversian canal area (*Hc.Ar*) is 0.002 mm² (Qiu et
12
13 555 al. 2003); these parameters indeed correspond to a diameter of some 50 µm.

14
15 556 The compaction process described here in *Nanophoca-N. vitulinoides* is known also
16
17 557 from other marine tetrapods; it was observed in the femur and humerus of *Clausiosaurus*
18
19 558 *germaini* (Buffrénil and Mazin, 1989), the rostral region of the skull of several ziphiid whales
20
21 559 (Buffrénil and Casinos, 1995; Zylberberg et al. 1998; Lambert et al. 2011; Dumont et al.
22
23 560 2016), and the five species of the xenarthran genus *Thalassocnus* (Amson et al. 2014).
24
25 561 Conversely, it was not observed in other pinnipeds, albeit our data suggest that *Phocanella*
26
27 562 *pumila* might have displayed a similar specialization, though far less pronounced than in *N.*
28
29 563 *vitulinoides*.

30 564 **Remark on the timing of somatic growth in *Nanophoca vitulinoides***—The results of the
31
32 565 present study reveal a paradoxical situation in which two conditions, which can be considered
33
34 566 contradictory, coexist. A) In several long bones (humerus, femur, ulna), primary periosteal
35
36 567 cortices display rather broadly spaced annuli up to bone periphery and, although the outer
37
38 568 margins of the bones are bordered by an annulus, there is no clearly characterized external
39
40 569 fundamental system. This situation should normally indicate that, on the one hand, the growth
41
42 570 of the bones was still actively progressing when the animals died and that, on the other hand,
43
44 571 death occurred during the unfavorable season, when annuli were formed. B) However, in all
45
46 572 long bones, growth plates are entirely erased by remodeling; therefore, no further growth in
47
48 573 length could occur. A possible explanation for these contrasted data is that the growth in
49
50 574 diameter of the bones remained active by the time their growth in length was already stopped.
51
52 575 This hypothesis is not convincing because such a process would have created a great diversity
53
54 576 in the shape of the bones of *Nanophoca-N. vitulinoides* ~~bones~~, a situation that does not exist

Formatted: Indent: First line: 0.5"

Formatted: Space After: 0 pt

Formatted: Font: Not Italic

Formatted: Font: Not Italic

Formatted: Font: Not Italic

1
2
3
4
5
6
7
8
9
10
11
12
13
14
15
16
17
18
19
20
21
22
23
24
25
26
27
28
29
30
31
32
33
34
35
36
37
38
39
40
41
42
43
44
45
46
47
48
49
50
51
52
53
54
55
56
57
58
59
60
61
62
63
64
65

(see Dewaele et al. 2017a). Another hypothesis is to consider that growth ceased abruptly, with both the destruction of growth plates and a sudden stop in periosteal apposition, when a certain size was reached. In this situation, peripheral annuli should be viewed as functional equivalents of EFS. For each individual, this double process of growth cessation is likely to have occurred during the unfavorable season, when annuli were deposited. Depending on the age when this process normally occurred (this age cannot be determined because early growth marks were erased by remodeling) it could explain the small size of *N. vitulinoides*. This issue requires the examination of a larger sample of *Nanophoca* bones and cannot be settled for the present. Moreover, slight local differences in the timing of the growth dynamics are not to be excluded, as suggested by the occurrence of an EFS in the largest vertebra.

Possible consequence of compaction on bone biomechanics—The unusual frequency of the short fissures observed in several ~~specimens of *Nanophoca*~~ *N. vitulinoides* ~~specimens~~ cannot be readily explained by the effect of taphonomic constraints ~~since because~~ *N. vitulinoides* fossils do not show traces of crushing or deformation (although they can be broken). Moreover, the cracks are restricted to the central region of the bones, and never extend towards their peripheral margins; such extensions should nevertheless have occurred if an external constraint had been exerted on the bones. The aspect of the fissures observed here is strongly reminiscent of the fatigue micro-fractures, as they are classically described and illustrated in the skeleton of *Homo* (e.g., Schaffer et al. 1995; Lee et al. 2003; Landrigan et al. 2011) and numerous domestic and wild animals ~~like~~ such as, e.g., dogs (Burr et al. 1985), rats (Voide et al. 2011), sheep (Mohsin et al. 2006), etc. In the absence of another plausible interpretation, the fissures observed in bones of *N. vitulinoides* ~~bones~~ are considered as genuine fatigue micro-fractures. The accumulation and coalescence of these small lesions, caused by long-lasting, repetitive mechanical stress, constitute the major processes responsible for the degradation of bone mechanical properties (Danova et al. 2003). Their

Formatted: Font: Not Italic

1
2
3
4
5
6
7 602 relative abundance in *N. vitulinoides* could have been indirectly induced by the compaction of
8
9 603 bone tissue that occurred in this taxon. It is indeed possible that the pronounced reduction, or
10
11 604 even the total occlusion, of the lumen of vascular canals by excessive secondary deposits
12
13 605 resulted in a local cessation of Haversian remodeling, ~~since-as~~ the precursors of the
14
15 606 osteoclasts (monocytes), cells of the blood lineage, arrive in situ via vascular networks
16
17 607 (syntheses in Marks and Popoff 1988; Charles and Aliprantis 2014; see also Lafage-Proust et
18
19 608 al. 2015). It is therefore likely that the extreme and imbalanced remodeling in bones of *N.*
20
21 609 *vitulinoides* ~~bones~~ was a self-blocking process, a hypothesis that could additionally explain
22
23 610 why open resorption cavities are so scarce in the bones of *N. vitulinoides* ~~bones~~ observed in
24
25 611 this study. One of the functions most commonly attributed to remodeling, be it of the
26
27 612 Haversian type or not, is precisely to operate a local replacement of the osseous tissue
28
29 613 damaged by the proliferation of fatigue micro-fractures (Burr 1993; Burr et al. 1995;
30
31 614 Lieberman et al. 2003). In *N. vitulinoides*, this process might have been hampered by local
32
33 615 restriction to blood supply. If a strong increase in bone compactness in this taxon was
34
35 616 positively selected for the functional benefit that it could provide, the “price to pay” was a
36
37 617 decrease in the mechanical resistance of the bones. This result is maladaptive because a total
38
39 618 closure of vascular canals actually provided negligible gain in mass (which was not the case
40
41 619 for the closure of larger bone cavities). This situation suggests that such an extreme degree of
42
43 620 bone compaction might have resulted from developmental constraints that could have
44
45 621 prevented compaction of the skeleton to be optimal throughout. Several, relatively common,
46
47 622 disorders of the skeleton likely to have a genetic origin provoke increased and imbalanced
48
49 623 remodeling, e.g., Paget’s disease, osseous mastocytosis, etc. (Ralston 2008; Michou and
50
51 624 Brown 2011; see also Evans et al. 1983), and can produce symptoms reminiscent of, though
52
53 625 not strictly identical to, the situation observed in *N. vitulinoides*. It seems possible that the
54
55 626 peculiarities of bone structure in *Nanophoca* could have initially resulted from a process akin

Formatted: Font: Not Italic

1
2
3
4
5
6
7 627 to such pathological processes. Pending an actual genetic causality, the latter could have been
8
9 628 selected and subsequently increased during evolution for its adaptive consequences, if the
10
11 629 resulting general compactness increase of the skeleton of *N. vitulinoides* ~~skeleton~~ was
12
13 630 advantageous. Such a process might have occurred also in other aquatic tetrapods showing the
14
15 631 same bone structural peculiarities as *Nanophoca*. Future studies should address this issue and
16
17 632 point out the frequency of this putative process.
18

19 633
20
21 634 **FUNCTIONAL CONSIDERATIONS**
22

23
24 635 One of the obvious consequences of the osteosclerotic-like process described here was to
25
26 636 increase the overall mass of the ~~*Nanophoca*~~ *N. vitulinoides* skeleton. In the absence of
27
28 637 pachyostosis, this increase was relatively moderate, as compared to the extreme situations
29
30 638 encountered in the Sirenia (Kaiser 1974; Buffrénil et al. 2010) or the marine squamates (the
31
32 639 so-called limbed snakes) from the Cenomanian of Europe and North Africa (Buffrénil and
33
34 640 Rage 1993; Houssaye, 2013). Nevertheless, it necessarily provoked an increase in the density
35
36 641 and inertia of the body, and proportionally reduced its buoyancy and maneuverability in the
37
38 642 water as well as on land (Taylor 2009; Domning and Buffrénil 1991). It is thus likely that, as
39
40 643 compared to the other pinnipeds devoid of osteosclerosis, (e.g., *Arctocephalus*, *Phocarcetos*,
41
42 644 and *Zalophus*: Godfrey 1985; Beentjes 1990; Fish et al. 2003), the locomotor capabilities of
43
44 645 *N. vitulinoides* were characterized by a lower swimming speed and a poor aptitude for steep
45
46 646 accelerations or sudden direction changes (maneuverability). Until now, no skull of this taxon
47
48 647 has been discovered; thus, its feeding strategy and food preferences cannot be determined.

49 648 The extreme compactness of postcranial elements strongly suggests that *N. vitulinoides* was
50
51 649 not adapted to the capture of fast and mobile prey in open seas. Rather, it must have fed upon
52
53 650 benthic or fixed animals in coastal shallow waters. One well-known extant benthic feeder is
54
55 651 the walrus, *Odobenus rosmarus* (e.g., Fay 1982; Gjertz and Wiig 1992; Dehn et al. 2006).
56

Formatted: Font: Not Italic

1
2
3
4
5
6
7
8
9
10
11
12
13
14
15
16
17
18
19
20
21
22
23
24
25
26
27
28
29
30
31
32
33
34
35
36
37
38
39
40
41
42
43
44
45
46
47
48
49
50
51
52
53
54
55
56
57
58
59
60
61
62
63
64
65

652 However, bone densification in the walrus is limited to pachyostosis in certain cranial regions
653 (Kaiser 1967), while the postcranial skeleton is largely untouched by pachyosteosclerosis
654 (e.g., Canoville et al. 2016: fig. 7O). In addition, Deméré (1994a, b) showed that the skeleton
655 of the extinct walrus *Valenictus* was pachyosteosclerotic and that this taxon most likely had
656 an even more pronounced benthic foraging lifestyle than the extant *Odobenus*. Moreover, the
657 interpretation of *N. vitulinoides* as a benthic feeder closely fits the conclusions drawn by
658 Dewaele et al. (2017a) from extensive anatomical clues and reconstructions of the
659 appendicular musculature: pectoral and pelvic girdles were used by *N. vitulinoides* in a
660 different way than in other Phocidae, “presumably for grasping and crawling on the
661 substrate.”²² For instance, the strong development of the greater tubercle of the humerus, the
662 weak development of the lesser tubercle of the latter, and the strong development of the
663 olecranon process on the ulna point toward powerful extension and abduction of the
664 foreflippers, contrasting with the conditions displayed by extant phocids. In this functional
665 context, even a limited buoyancy decrease (as compared to other taxa such as the sirenians or
666 some Cenomanian aquatic squamates; the bone ballast of *Nanophoca* is moderate) must have
667 facilitated a passive control, with little energy expense, of body position and trim in the water
668 column. The same may apply to the contemporaneous late Miocene–early Pliocene
669 *Phocanella pumila*, given the similar trend toward density increase in the humerus and femur.
670 Hence, a comparable feeding pattern might have existed in these two taxa. Unfortunately, no
671 dental remains are known from ~~PP-~~*hocanella pumila*, which precludes elucidating the
672 feeding habits of this species and, indirectly, that of *N. vitulinoides*. Both are nevertheless
673 found in the same geological context, and might therefore have shared close ecological
674 adaptations. Although our analysis includes only two specimens of the latter taxon (the extent
675 of bone compaction in the rest of the skeleton cannot be assessed), a similar ecology to that of
676 *N. vitulinoides* can be expected. The presence of a (thick) spongy trabecular network in the

1
2
3
4
5
6
7 677 medullary cavity of *Batavipusa neerlandica* and *Praepusa boeska*, two small, roughly
8
9 678 contemporaneous (late Miocene–early Pliocene) species from the southern margin of the
10
11 679 North Sea Basin, shows that the extreme compactness of the long bones of *N. vitulinoidea*
12
13 680 ~~long bones~~ is not strictly correlated ~~with~~ the small body size of the taxon.
14
15 681

17 682 **CONCLUSIONS**

19
20 683 *Nanophoca vitulinoidea* from the middle Miocene of the North Sea Basin is the first extinct
21
22 684 phocid taxon to undergo a detailed microanatomical and osteohistological description. Its long
23
24 685 bones are extremely compact, lacking a differentiated medullary cavity and exhibiting
25
26 686 compactness values close to 100%. Apart from the extinct phocine seal *Phocanella pumila*,
27
28 687 such structural peculiarities are unknown among pinnipeds. The spine of *Nanophoca* was also
29
30 688 touched by this process, which is a unique case among mammals. The high compactness is
31
32 689 not observed in any other semi-aquatic mammal. The high compactness observed in the
33
34 690 skeleton of *Nanophoca* ~~skeleton visibly~~ resulted from an imbalanced remodeling process
35
36 691 located in the medullary region. Positively selected during evolution, this process might have
37
38 692 been rooted in an initial genetic condition akin to one form of the so-called “metabolic bone
39
40 693 diseases.” It increased body density, thus reducing buoyancy and facilitating long-lasting
41
42 694 underwater stays. Conversely, it limited speed and maneuverability. Although more complete
43
44 695 fossils, and especially cranial remains, are needed to draw definite conclusions on *Nanophoca*
45
46 696 ecology, the results of this study strongly suggest that *N. vitulinoidea* was a bottom-dwelling
47
48 697 seal, living in shallow waters close to the shore in the Miocene North Sea Basin, and feeding
49
50 698 on benthic prey.

51 52 700 **ACKNOWLEDGEMENTS**

1
2
3
4
5
6
7
8
9
10
11
12
13
14
15
16
17
18
19
20
21
22
23
24
25
26
27
28
29
30
31
32
33
34
35
36
37
38
39
40
41
42
43
44
45
46
47
48
49
50
51
52
53
54
55
56
57
58
59
60
61
62
63
64
65

The research presented in this study is in partial fulfillment of the PhD research of LD, conducted at Ghent University, Ghent, Belgium, and in collaboration with the Royal Belgian Institute of Natural Sciences, Brussels, Belgium. This PhD research is funded by the Research Foundation – Flanders (FWO) through an FWO PhD Fellowship to LD. This research is also partly funded by the Society of Vertebrate Paleontology’s 2016 Steven Cohen Award for Excellent Student Research, awarded to LD. TDK holds a postdoctoral Fellowship at the FWO.

We also want to thank S Bruaux, C Cousin, and A Folie from the RBINS for providing access to the collections. We thank R Fraaije and N Peters from the Oertijdmuseum Groene Poort, Boxtel, Netherlands, ~~to allow~~ for allowing access to the holotypes of *Batavipusa neerlandica* and *Praepusa boeska*. We are grateful to M Bosselaers for donating specimens from his private collection for the elaboration of thin sections. Special thanks to JRJ Wible (editor-in-chief of *Journal of Mammalian Evolution*), A Houssaye (reviewer), and a second anonymous reviewer for helpful comments that improved the quality of this work.

REFERENCES CITED

Amprino R (1947) La structure du tissu osseux envisagée comme expression de différences dans la vitesse de l'accroissement. Arch Biol 58:315–330.

Amson E, Muizon C de (2014) A new durophagous phocid (Mammalia: Carnivora) from the late Neogene of Peru and considerations on monachine seal phylogeny. J Syst Paleontol 12:523–548. doi: 10.1080/14772019.2013.799610

Amson E, Muizon C de, Laurin M, Argot C, Buffrénil V de (2014) Gradual adaptation of bone structure to aquatic lifestyle in extinct sloths from Peru. Proc Biol Soc 281:20140192. doi: 10.1098/rspb.2014.0192

1
2
3
4
5
6
7 725 Beentjes MP (1990) Comparative terrestrial locomotion of the Hooker's sea lion (*Phocarcotos*
8
9 726 *hookeri*) and the New Zealand fur seal (*Arctocephalus forsteri*): evolutionary and
10
11 727 ecological implications. Zool J Linn Soc 98:307–325. doi: 10.1111/j.1096-
12
13 728 3642.1990.tb01204.x
14
15 729 Berta A, Kienle S, Bianucci G, Sorbi S (2015) A reevaluation of *Pliphoca etrusca*
16
17 730 (Pinnipedia, Phocidae) from the Pliocene of Italy: phylogenetic and biogeographic
18
19 731 implications. J Vertebr Paleontol 35:e88944. doi: 10.1080/02724634.2014.889144.
20
21 732 Bininda-Emonds ORP, Russell AP (1996) A morphological perspective on the phylogenetic
22
23 733 relationships of the extant phocid seals (Mammalia: Carnivora: Phocidae). Bonn Zool
24
25 734 Monograph 41:1–256.
26
27 735 Boness DJ, Bowen WD (1996) The evolution of maternal care in pinnipeds. ~~Biosci~~
28
29 736 Bioscience 46:645–654.
30
31 737 Buffrénil V de, Canoville A, D'Anastasio R, Domning DP (2010) Evolution of sirenian
32
33 738 pachyosteosclerosis, a model-case for the study of bone structure in aquatic tetrapods.
34
35 739 ~~J Mamm Mammal~~ Evol 17:101–120. doi: 10.1007/s10914-010-9130-1
36
37 740 Buffrénil V de, Casinos A (1995) Observations histologiques sur le rostre de *Mesoplodon*
38
39 741 *densirostris* (Mammalia, Cetacea, Ziphiidae): le tissu osseux le plus dense connu. Ann
40
41 742 Sci Nat Zool 13ème Ser 16:21–32.
42
43 743 Buffrénil V de, Mazin J-M (1989) Bone histology of *Claudiosaurus germaini* (Reptilia,
44
45 744 Claudiosauridae) and the problem of pachyostosis in aquatic tetrapods. Hist Biol
46
47 745 2:311–322. doi: 10/1080/08912968909386509
48
49 746 Buffrénil V de, Rage J-C (1993) La 'pachyostose' vertébrale de *Simoliophis* (Reptilia,
50
51 747 Squamata): données comparatives et considérations fonctionnelles. Ann Paleontol
52
53 748 (Vertebr) 79:315–335.
54
55
56
57
58
59
60
61
62
63
64
65

1
2
3
4
5
6
7 749 Buffrénil V de, Ricqlès A de, Ray CE, Domning, DP (1990) Bone histology of the ribs of the
8
9 ~~750~~ ~~a~~Archaeocetes (Mammalia: Cetacea). J Vertebr Paleontol 10:455–466.doi:
10
11 10/1080/02724634.1990.10011828
12
13 752 Buffrénil V de, Schoevaert D (1989) Données quantitatives et observations histologiques sur
14
15 753 la pachyostose du squelette du dugong, *Dugong dugon* (Müller) (Sirenia,
16
17 754 Dugongidae). Can J Zool 67:2107-2119. doi: 10.1139/z89-300
18
19 755 Burr DB (1993) Remodeling and the repair of fatigue damage. Calcif Tissue Internatl 53
20
21 756 (suppl_1):S75–S81. doi: 10.1007/BF01673407
22
23 757 Burr DB, Allen MR, (eds.) (2014) Basic and Applied Bone Biology. Elsevier/Academic
24
25 758 Press, London.
26
27 759 Burr DB, Martin RB, Schaffler MB, Radin EL (1985) Bone remodeling in response to *in vivo*
28
29 760 fatigue microdamage. J Biomech 18:189–200. doi:10.1016/0021-9290(85)90204-0
30
31 761 Canoville A, Buffrénil V de, Laurin M (2016) Microanatomical diversity of amniote ribs: an
32
33 762 exploratory quantitative study. Biol J Linn Soc 118:706–733. doi: 10.1111/bij.12779
34
35 763 Canoville A, Laurin M (2010) Evolution of humeral microanatomy and lifestyle in amniotes,
36
37 764 and some comments on palaeobiological inferences. Biol J Linn Soc 100:384–406.
38
39 765 doi: 10.1111/j.1095-8312.2010.01431.x
40
41 766 ~~Canoville A, Buffrénil V de, Laurin M (2016) Microanatomical diversity of amniote ribs: an~~
42
43 767 ~~exploratory quantitative study. Biol J Linn Soc 118:706–733. doi: 10.1111/bij.12779~~
44
45 768 Castanet J (2006) Time recording in bone microstructures of endothermic animals; functional
46
47 769 relationships. CR Palevol 5:629–636. doi: 10.1016/j.crpv.2005.10.006
48
49 770 Castanet J, Grandin A, Abourachid A, Ricqlès A de (1996) Expression de la dynamique de
50
51 771 croissance dans la structure de l’os périostique chez *Anas platyrhynchos*. CR Acad Sci
52
53 772 Paris, Sci Vie 319:301–308.
54
55
56
57
58
59
60
61
62
63
64
65

1
2
3
4
5
6
7
773 Castanet J, Curry Rogers C, Cubo J, Boisard J (2000) Periosteal bone growth rates in extant
8
9
974 ratites (ostrich and emu). Implications for assessing growth in dinosaurs. CR Acad Sci
10
11775 Paris, Sci Vie 323:543–550. doi: 10.1016/S0764-4469(00)00181-5
12
13
13776 Charles JF, Aliprantis AO (2014) Osteoclasts: more than ‘bone eaters’. Trends Mol Med
14
15777 20:449–459. doi: 10.1016/j.molmed.2014.06.001
16
17
17778 Cozzuol MA (2001) A “northern” seal from the Miocene of Argentina: implications for
18
19779 phocid phylogeny and biogeography. J Vertebr Paleontol 21:415–421. doi:
20
21780 10.1671/0272-4634(2001)021[0415:ANSFTM]2.0.CO;2
22
23
23781 Danova NA, Colopy SA, Radtke CL, Kalscheur VL, Markel MD, Vanderby R Jr, McCabe
24
25782 RP, Escarcega AJ, Muir P (2003) Degradation of bone structural properties by
26
27783 accumulation and coalescence of microcracks. Bone 33:197–205. doi: 10.1016/S8756-
28
29784 3282(03)00155-8
30
31
31785 Dehn L-A, Sheffield GG, Follmann EH, Duffy LK, Thomas DL, O’Hara TM (2006) Feeding
32
33786 ecology of phocid seals and some walrus in the Alaskan and Canadian Arctic as
34
35787 determined by stomach contents and stable isotope analysis. Polar Biol 30:167–181.
36
36788 doi: 10.1007/s00300-006-0171-0
37
38
39789 Deméré TA (1994a) Two new species of fossil walruses (Pinnipedia: Odobenidae) from the
40
41790 upper Pliocene San Diego Formation. Proc ~~San~~ Diego Soc Nat Hist 29:77–98.
42
43791 Deméré TA (1994b) The family Odobenidae: ~~a~~A phylogenetic analysis of fossil and living
44
45792 taxa. Proc ~~San~~S Diego Soc Nat Hist 29:99–123.
46
47
47793 Dempster, DW, Compston JE, Drezner MK, Glorieux FH, Kanis JA, Malluche H, Meunier
48
49794 PJ, Ott SM, Recker RR, Parfitt AM (2013) Standardized nomenclature, symbols, and
50
51795 units for bone histomorphometry: ~~a~~A 2012 update of the report of the ASBMR
52
53
54
55
56
57
58
59
60
61
62
63
64
65

1
2
3
4
5
6
7 796 Histomorphometry Nomenclature Committee. J Bone Miner Res 28:1–16. doi:
8
9 997 10.1002/jbmr.1805
10
11 798 Dewaele L, Amson E, Lambert O, Louwye S (2017a) Reappraisal of the extinct seal “*Phoca*”
12
13 799 *vitulinoides* from the Neogene of the North Sea Basin, with bearing on its geological
14
15 800 age, phylogenetic affinities, and locomotion. PeerJ 5:e3316. doi: 10.7717/peerj.3316
16
17 801 Dewaele L, Lambert O, Louwye S (2017b) On *Prophoca* and *Leptophoca* (Pinnipedia,
18
19 802 Phocidae) from the Miocene of the North Atlantic realm: redescription, phylogenetic
20
21 803 affinities and paleobiogeographic implications. PeerJ 5:e3024. doi: 10.7717/peerj.3024
22
23 804 Domning D, Buffrénil V de (1991) Hydrostasis in the Sirenia: quantitative data and functional
24
25 805 interpretation. Mar Mammal Sci 7:331–368. doi: 10.1111/j.1748-7692.1991.tb00111.x
26
27 806 Dumont M, Buffrénil V de, Mijan I, Lambert O (2016) Structure and growth pattern of the
28
29 807 bizarre hemispheric prominence of the rostrum of the fossil beaked whale *Globicetus*
30
31 808 *huberus* (Mammalia, Cetacea, Ziphiidae). J Morphol 277:1292–1308. doi:
32
33 809 10.1002/jmor.20575
34
35 810 Dumont M, Laurin M, Jacques F, Pellé E, Dabin W, Buffrénil V de (2013) Inner architecture
36
37 811 of vertebral centra in terrestrial and aquatic mammals: a two-dimensional comparative
38
39 812 study. J Morphol 274:570–584. doi: 10.1002/jmor.20122
40
41 813 Evans RA, Hughes WG, Dunstan CR, Lennon WP, Kohan L, Hills E, Wong SYP (1983)
42
43 814 Adult osteosclerosis. Metab Bone Dis Relat 5:111–117. doi: 10.1016/0221-
44
45 815 8747(83)90011-5
46
47 816 Fawcett DW, Jensch RP (1997) Bloom and Fawcett: Concise Histology. Chapman and Hall,
48
49 817 New York-

1
2
3
4
5
6
7 818 Fay FH (1982) Ecology and ~~b~~Biology of the Pacific ~~w~~Walrus, *Odobenus rosmarus divergens*
8
9 819 Illiger. N Am Fauna 74:1–279. doi: 10.3996/nafa.74.0001
10
11 820 Fiala P (1980) Structure of the long limb bones and its significance in determining age in
12
13 821 man. Folia Morphol 28:259–263.
14
15 822 Fish FE, Stein BR (1991) Functional correlates of differences in bone density among
16
17 823 terrestrial and aquatic genera in the family Mustelidae (Mammalia). ~~Zoomorphol~~
18
19 824 ~~Zoomorphol~~ Zoomorphology 110:339–345. doi: 10.1007/BF01668024
20
21 825 Fish FE, Hurley J, Costa DP (2003) Maneu~~v~~erability by the sea lion *Zalophus californianus*:
22
23 826 turning performance of an unstable body design. J Exp Biol 206:667–674. doi:
24
25 827 10.1242/jeb.00144
26
27 828 Francillon-Vieillot H, de Buffrénil V, Castanet J, Geraudie J, Meunier JF, Sire JY, Zylberberg
28
29 829 L, Ricqlès A de (1990) Microstructure and mineralization of vertebrate skeletal
30
31 830 tissues. In: Carter JG (ed) Skeletal Biomineralizations: Patterns, Processes and
32
33 831 Evolutionary Trends, Vol. 1. Van Nostrand Reinhold, New York, pp 471–530.
34
35 832 Frost HM (1969) Tetracycline-based histological analysis of bone remodeling. Calc Tiss Res
36
37 833 33:211–237. doi: 10.1007/BF02058664
38
39 834 Fulton TL, Strobeck C (2010) Multiple markers and multiple individuals refine true seal
40
41 835 phylogeny and bring molecules and morphology back in line. ~~Proc~~ Roy Soc B–Biol
42
43 836 Sci 277:1065–1070. doi: 10.1098/rspb.2009.1783.
44
45 837 Germain D, Laurin M (~~2005~~) Microanatomy of the radius and lifestyle in amniotes
46
47 838 (Vertebrata, Tetrapoda). Zool Scr 34:335–350. doi: 10.1111/j.1463-
48
49 839 6409.2005.00198.x
50
51
52
53
54
55
56
57
58
59
60
61
62
63
64
65

1
2
3
4
5
6
7 840 Giles S, Rücklin M, Donoghue PCJ (2013) Histology of “~~p~~Placoderm” dermal skeletons:
8
9 841 implications for the nature of the ancestral gnathostomes. *J Morphol* 274:627–644.
10
11 842 doi: 10.1002/jmor.20119
12
13 843 Girondot M, Laurin M (2003) Bone Profiler: a tool to quantify, model and statistically
14
15 844 compare bone section compactness profiles. *J Vertebr Paleontol* 23:458-461. doi:
16
17 845 10.1671/0272-4634(2003)023[0458:BPATTQ]2.0.CO;2
18
19 846 Gjertz I, Wiig Ø (1992) Feeding of walrus *Odobenus rosmarus* in Svalbard. *Polar Record*
20
21 847 28:57–59. doi: 10.1017/S0032247400020283
22
23 848 Godfrey SJ (1985) Additional observations of subaqueous locomotion in the California Sea
24
25 849 Lion (*Zalophus californianus*). *Aquat Mamm-Mammal* 11:53–57.
26
27 850 Gray N-M, Kainec K, Madar SI, Tomko L, Wolfe S (2007) Sink or swim? Bone density as a
28
29 851 mechanism for buoyancy control in early cetaceans. *Anat Rec* 290:638–653. doi:
30
31 852 10.1002/ar.20533
32
33 853 Higdon JW, Bininda-Emonds ORP, Beck RMD, Ferguson SH (2007) Phylogeny and
34
35 854 divergence of the pinnipeds (Carnivora: Mammalia) assessed using a multigene
36
37 855 dataset. *BMC Evol Biol* 7 :216. doi: 10.1186/1471-2148-7-216.
38
39 856 Houssaye A (2009) “Pachyostosis” in aquatic amniotes: a review. *Integr Zool* 4:325–340. doi:
40
41 857 10.1111/j.1749-4877.2009.00146.x
42
43 858 Houssaye A (2013) Palaeoecological and morphofunctional interpretation of bone mass
44
45 859 increase: an example in Late Cretaceous shallow marine squamates. *Biol Rev* 88:117–
46
47 860 139.
48
49
50
51
52
53
54
55
56
57
58
59
60
61
62
63
64
65

1
2
3
4
5
6
7
8
9
10
11
12
13
14
15
16
17
18
19
20
21
22
23
24
25
26
27
28
29
30
31
32
33
34
35
36
37
38
39
40
41
42
43
44
45
46
47
48
49
50
51
52
53
54
55
56
57
58
59
60
61
62
63
64
65

861 Houssaye A, Fish FE (2016) Functional (secondary) adaptation to an aquatic life in
862 ~~y~~Vertebrates: an introduction to the symposium. Integr Comp Biol 56:1266–1270. doi:
10.1093/icb.icw129

864 Houssaye A, Lindgren J, Pellegrini R, Lee AH, Germain D, Polcyn MJ (2013)
865 Microanatomical and histological features in the long bones of mosasaurine mosasaurs
866 (Reptilia, Squamata)—~~H~~Implications for aquatic adaptation and growth rates. PLoS One
867 8:e76741. doi: 10.1371/journal.pone.0076741

868 Houssaye A, Sander PM, Klein N (2016) Adaptive patterns in aquatic amniote bone
869 microanatomy—more complex than previously thought. Integr Comp Biol 56:1349–
870 1369. doi: 10.1093/icb/icw120

871 Houssaye A, Tafforeau P, Muizon C de, Gingerich PD (2015). Transition of Eocene ~~w~~Whales
872 from ~~l~~Land to ~~s~~Sea: ~~e~~Evidence from ~~b~~Bone ~~m~~Microstructure. PLoS One 10:e0118409.
873 doi: 10.1371/journal.pone.0118409

874 Jaworski ZFG (1992) Haversian system and Haversian bone. In: Hall BK (ed) Bone
875 ~~M~~etabolism and ~~M~~ineralization. CRC Press, Boca Raton, pp 21–45.

876 Jefferson TA, Webber MA, Pitman RL (2008) Marine Mammals of the World: A
877 Comprehensive Guide to their Identification. Elsevier/Academic Press, Amsterdam

878 Kaiser HE (1974) Morphology of the Sirenians. A ~~M~~acroscopic X-Ray ~~A~~tlas of the
879 ~~M~~orphology of ~~R~~ecent ~~S~~pecies. S. Karger, Basel.

880 Köhler M, Marin-Moratalla N, Jordana X, Aanes R (2012) Seasonal bone growth and
881 physiology in endotherms shed light on dinosaur physiology. Nature 487:358–361.
882 doi: 10.1038/nature11264

1
2
3
4
5
6
7 883 Koretsky IA (2001) Morphology and systematics of the Miocene Phocinae (Mammalia:
8
9 884 Carnivora) from Paratethys and the North Atlantic Region. Geol Hung Ser Palaeontol
10
11 885 54:1–109.
12
13 886 Koretsky IA, Grigorescu D (2002) The fossil monk seal *Pontophoca sarmatica* (Aleksiev)
14
15 887 (Mammalia: Phocidae: Monachinae) from the Miocene of eastern Europe. Smithson
16
17 888 Contrib Paleobiol 93:149–162.
18
19 889 Koretsky IA, Peters N (2008) *Batavipusa* (Carnivora, Phocidae, Phocinae): a new genus from
20
21 890 the eastern shore of the North Atlantic Ocean (Miocene seals of the Netherlands, part
22
23 891 II). Deinsea 12:53–62.
24
25 892 Koretsky IA, Peters N, Rahmat SJ (2015) New species of *Praepusa* (Carnivora, Phocidae,
26
27 893 Phocinae) from the Netherlands supports east to west Neogene dispersal of true seals.
28
29 894 Vestn Zool 49:57–66.
30
31 895 Koretsky IA, Rahmat SJ (2013) First record of fossil Cystophorinae (Carnivora, Phocidae):
32
33 896 middle Miocene seals from the northern Paratethys. Riv Ital Paleontol S 119:325–350.
34
35 897 doi: 10.13130/2039-4942/6043
36
37 898 Koretsky IA, Rahmat SJ (2017). Preliminary ~~r~~Report of ~~p~~Pachyosteosclerotic ~~b~~Bones in
38
39 899 ~~s~~Seals. Open Acc Res Anat 1:1–3.
40
41 900 Koretsky IA, Ray CE (2008) Phocidae of the Pliocene of Eastern North America. Virginia
42
43 901 Mus Nat Hist; Spec Pub 14:81–140.
44
45 902 Krilloff A, Germain D, Canoville A, Vincent P, Sache M, Laurin M (2008) Evolution of bone
46
47 903 microanatomy of the tetrapod tibia and its use in palaeobiological inference. J Evol
48
49 904 Biol 21:807–826. doi: 10.1111/j.1420-9101.2008.01512.x
50
51 905 Kühn C, Frey E (2012) Walking like caterpillars, flying like bats—pinniped locomotion.
52
53
54
55
56
57
58
59
60
61
62
63
64
65

1
2
3
4
5
6
7
906 Palaeobio Palaeoenv 92:197–210. doi: 10.1007/s12549-012-0077-5
8
9
10
907 Lafage-Proust M-H, Roche B, Langer M, Cleret D, Vanden Bossche A, Olivier T, Vico L
11
908 (2015) Assessment of bone vascularization and its role in bone remodeling. BoneKEY
12
909 Rep 4, art. no. 662:1–8. doi: 10.1038/bonekey.2015.29
14
15
910 Lambert O, Muizon C de, Buffrénil V de (2011) Hyperdense rostral bones of ziphiid whales:
17
911 diverse processes for a similar pattern. CR Palevol 10:453–468. doi:
18
912 10.1016/j.crpv.2011.03.012
20
21
913 Lamm ET (2013) Preparation and sectioning of specimens. In: Padian K, Lamm ET (eds)
22
914 Bone ~~H~~istology of ~~F~~ossil ~~T~~etrapods: ~~A~~dvancing ~~M~~ethods, ~~A~~nalysis, and
24
915 ~~I~~nterpretation. University of California Press, Berkeley, pp 55–160
26
27
916 Landrigan MD, Li J, Turnbull TL, Burr DB, Niebur GL, Roeder RK (2011) Contrast-
28
917 enhanced micro-computed tomography of fatigue microdamage accumulation in
30
918 human cortical bone. Bone 48:443–450. doi: 10.1016/j.bone.2010.10.160
32
33
919 Laurin M, Canoville A, Germain D (2011) Bone microanatomy and lifestyle: ~~a~~A descriptive
34
920 approach. CR Palevol 10:381–402. doi: 10.1016/j.crpv.2011.02.003
36
37
921 Laurin M, Girondot M, Loth M-M (2004) The evolution of long bone microanatomy and
38
922 lifestyle in lissamphibians. Paleobiology 30:589–613. doi: 10.1666/0094-
40
923 8373(2004)030<0589:TEOLBM>2.0.CO;2
42
43
924 Lee TC, Mohsin S, Taylor D, Parkesh R, Gunnlaugsson T, O’Brien FJ, Giehl M, Gowin W
44
925 (2003) Detecting microdamage in bone. J Anat 203:161–172. doi: 10.1046/j.1469-
46
926 7580.2003.00211.x
48
49
927 Lieberman DE, Pearson OM, Polk JD, Demes B, Crompton AW (2003) Optimization of bone
50
928 growth and remodeling in response to loading in tapered mammalian limbs. J Exp Biol
52
929 206:3125–3138. doi: 10.1242/jeb.00514
54
55
56
57
58
59
60
61
62
63
64
65

1
2
3
4
5
6
7 930 Liu XS, Bevill G, Keaveny TM, Sajda P, Guo XE (2009) Micromechanical analyses of
8
9 931 vertebral trabecular bone based on individual trabeculae segmentation of plates and
10
11 932 rods. *J Biomech* 42:249–256. doi: 10.1016/j.biomech.2008.10.035
12
13 933 Margerie E de, Cubo J, Castanet J (2002) Bone typology and growth rate: testing and
14
15 934 quantifying “Amprino’s rule” in the mallard (*Anas platyrhynchos*). *CR Biol* 325:221–
16
17 935 230. doi: 10.1016/S1631-0691(02)01429-4
18
19 936 Marks SC, Popoff SN (1988) Bone cell biology: the regulation of development, structure and
20
21 937 function of the skeleton. *Am J Anat* 183:1–44. doi: 10.1002/aja.1001830102
22
23 938 Martin RB (2000) Toward a unifying theory of bone remodeling. *Bone* 26:1–6. doi:
24
25 939 10.1016/S8756-3282(99)00241-0
26
27 940 Masschaele B, Dierick M, Loo DV, Boone MN, Brabant L, Pauwels E, Cnudde V, Hoorebeke
28
29 941 LV (2013) HECTOR: A 240kV micro-CT setup optimized for research. *J Phys Conf*
30
31 942 Ser 463:012012. doi: 10.1088/1742-6596/463/1/012012.
32
33 943 Michou L, Brown JP (2011) Genetics of bone diseases: Paget’s disease, fibrous dysplasia,
34
35 944 osteopetrosis and osteogenesis imperfecta. *Joint Bone Spine* 78: 252–258. doi:
36
37 945 10.1016/j.bspin.2010.07.010
38
39 946 Mohsin S, O’Brien FJ, Lee TC (2006) Osteonal crack barriers in ovine compact bone. *J Anat*
40
41 947 208: 81-89.
42
43 948 Muizon C de (1981) Les vertébrés fossiles de la Formation Pisco (Pérou). Première partie:
44
45 949 deux nouveaux Monachinae du Pliocène de Sud Sacaco. *Inst Franc Etud Andines*
46
47 950 Mem 6 20–161-
48
49 951 Nakajima Y, Endo H (2013). Comparative humeral microanatomy of terrestrial, semiaquatic,
50
51 952 and aquatic carnivorans using micro-focus CT scan. *Mammal Study* 38:1–8-
52
53
54
55
56
57
58
59
60
61
62
63
64
65

- 1
2
3
4
5
6
7
953 Parfitt AM (1981) Bone effect of spaceflight: analysis by quantum concept of bone
8
954 remodeling. *Acta Astronaut* 8:1083–1090. doi: 10.1016/0094-5765(81)90082-5
10
11
955 Parfitt AM (1982) The coupling of bone formation to bone resorption: a critical analysis of
12
1356 the concept and of its relevance to the pathogenesis of osteoporosis. *Metab Bone Dis*
14
1557 *Relat* 4:1–6. doi: 10.1016/022-8747(82)90002-9
16
17
958 Pierce SE, Clack JA, Hutchinson JR (2011) Comparative axial morphology in pinnipeds and
18
1959 its correlation with aquatic locomotory behaviour. *J Anat* 219:502–514. doi:
20
2160 10.1111/j.1469-7580.2011.01406.x
22
2361 Polig E, Jee WSS (1990) A model of osteon closure in cortical bone. *Calcif Tissue Int+Internat*
24
2562 47:261–269. doi: 10.1007/BF02555907
26
27
963 Prondvai E, Stein KHW, Ricqlès A de, Cubo J (2014) Development-based revision of bone
28
2964 tissue classification: the importance of semantics for science. *Biol J Linn Soc*
30
3165 112:799–816. doi: 10.1111/bio.12323
32
3366 Pyenson, ND, Kelley NP, Parham JF (2014) Marine tetrapod macroevolution: pPhysical and
34
3567 biological drivers on 250 Ma of invasions and evolution in ocean ecosystems.
36
3768 *Palaeogeogr Palaeoclimatol Palaeoecol* 400:1–8. doi:10.1016/j.palaeo.2014.02.18
38
3969 Qiu S, Fyhrie DP, Palnitkar S, Sudhaker Rao D (2003) Histomorphometric assessment of
40
4170 Haversian canal and osteocyte lacunae in different-sized osteons in human ribs. *Anat*
42
4371 *Rec* 272A:520–525. doi: 10.1002/ar.a.10058
44
4572 Quemeneur S, Buffrénil V de, Laurin M (2013) Microanatomy of the amniote femur and
46
4773 inference of lifestyle in limbed vertebrates. *Biol J Linn Soc* 109:644–655. doi:
48
4974 10.1111/bij.12066
50
51
52
53
54
55
56
57
58
59
60
61
62
63
64
65

- 1
2
3
4
5
6
7 975 Ralston SH (2008) Pathogenesis of Paget's disease of Bone. Bone 43: 819–825. doi:
8
9 976 10.1016/j.bone.2008.06.015
10
11
12 977 Ricqlès A de (1989). Les mécanismes hétérochroniques dans le retour des tétrapodes au
13
14 978 milieu aquatique. Geobios Mem Spec 12:337–348. doi: 10.1016/S0016-
15
16 979 6995(89)80034-8
17
18 980 Ricqlès A de, Buffrénil V de (1995) Sur la présence de pachyostéose chez la rhytine de
19
20 981 Steller [*Rhytina (Hydrodamalis) gigas*], sirénien récent éteint. Ann Sci Nat Zool Paris,
21
22 982 13e Ser 16:47–53.
23
24 983 Ricqlès A de, Buffrénil V de (2001) Bone histology, heterochronies and the return of
25
26 984 Tetrapods to life in water: w[h]ere are we? In: Mazin J-M, Buffrénil V de
27
28 985 (eds) Secondary Aadaptation of Ttetrapods to Life in Water. Verlag Dr. Friedrich
29
30 986 Pfeil, München, pp 289–310
31
32 987 Schaffler MB, Choi K, Milgrom C (1995) Aging and matrix microdamage accumulation in
33
34 988 human compact bone. Bone 17:521–527. doi: 10.1016/8756-3282(95)00370-3
35
36 989 Stein BR (1989) Bone density and adaptation in semiaquatic mammals. J Mammal 70:467–
37
38 990 476. doi: 10.2307/1381418
39
40 991 Storå J (2000) Skeletal development in the Grey seal *Halichoerus grypus*, the Ringed seal
41
42 992 *Phoca hispida botnica*, the Harbour seal *Phoca vitulina vitulina* and the Harp seal
43
44 993 *Phoca groenlandica*. Epiphyseal fusion and life History. ~~Archaeozoolog~~
45
46 994 Archaeozoologia 11:199–222.
47
48 995 Taylor MA (2009) Functional significance of bone ballast in the evolution of buoyancy
49
50 996 control strategies by aquatic tetrapods. Hist Biol 14:15–31. doi:
51
52 997 10.1080/10292380009380550
53
54
55
56
57
58
59
60
61
62
63
64
65

1
2
3
4
5
6
7 998 Thompson DW (1961) On Growth and Form. Cambridge University Press, Cambridge
8
9 999 Turner CH (1998) Three rules for bone adaptation to mechanical stimuli. *Bone* 23:399–407.
10
11 doi: 10.1016/S8756-3282(98)00118-5
12
13 1001 Uhen MD (2007) Evolution of marine mmammals: back to the sea after 300 million
14
15 years. *Anat Rec* 290:514–522. doi:10.1002/ar.20545
16
17 1003 Van Beneden P-J (1871) Les phoques de la mer scaldisienne. *Bul Acad R Sci Let b-Arts Belg*
18
19 2^{ième} Ser 32:5–19.
20
21
22 1005 Van Beneden P-J (1877) Description des ossements fossiles des environs d’Anvers, première
23
24 partie. *Pinnipèdes ou amphithériens. Ann Mus R Hist Nat Belg* 1:1–88.
25
26 1007 Voide R, Schneider P, Stauber M, van Lenthe GH, Stampanoni M, Müller R (2011) The
27
28 importance of murine cortical bone microstructure for microcrack initiation and
29
30 propagation. *Bone* 49:1186–1193. doi: 10.1016/j.bone.2011.08.011
31
32 1010 Wall WP (1983) The correlation between high limb-bone density and aquatic habits in recent
33
34 mammals. *J Paleontol* 57:197–207.
35
36 1012 Webb P, Buffrénil V de (1990) Locomotion in the biology of large aquatic vertebrates.
37
38 Trans Am Fish Soc 119:629–641. doi: 10.1577/1548-
39
40 8659(1990)119<0629:LITBOL>2.3.CO;2
41
42 1015 Zylberberg L, Traub W, Buffrénil V de, Alizard F, Arad T, Weiner S (1998) Rostrum of a
43
44 toothed whale: ultrastructural study of a very dense bone. *Bone* 23:241–247. doi:
45
46 10.1016/S8756-3282(98)00101-X
47
48
49
50
51
52
53
54
55
56
57
58
59
60
61
62
63
64
65

1
2
3
4
5
6
7
8
9
10
11
12
13
14
15
16
17
18
19
20
21
22
23
24
25
26
27
28
29
30
31
32
33
34
35
36
37
38
39
40
41
42
43
44
45
46
47
48
49
50
51
52
53
54
55
56
57
58
59
60
61
62
63
64
65

LEGENDS OF THE FIGURES

Fig. 1 – Reconstruction of the skeleton of the phocid *Nanophoca vitulinoides* from the middle Miocene of the southern North Sea, with the partial skeleton of specimen IRSNB M2276 superimposed. Light gray indicates bone types that have been subjected to micro-CT scanning exclusively; dark gray indicates bone types that have been subjected to thin sectioning exclusively; and intermediate gray indicates bones that have been subjected to both micro-CT scanning and thin sectioning. Thin sectioning includes transverse sections and longitudinal sections. Note: thin sectioning has been performed on other specimens than IRSNB M2276. Modified from Dewaele et al. (2017a: fig. 1).

Fig. 2 – Line drawing of a humerus and femur of the *Nanophoca vitulinoides* neotype specimen IRSNB M2276 showing the measurements taken for the basic morphometric analysis. Gray lines on the humerus show total length of the humerus and least transverse width of the humeral diaphysis. Gray lines on the femur show total length of the femur and least transverse width across the diaphysis. Anteroposterior width is shown as an arrow perpendicular to the field of view (circle with diagonal cross).

Fig. 3 – Phylogeny of *Nanophoca vitulinoides*, as presented by Dewaele et al. (2017a). Both *Leptophoca proxima* and *N. vitulinoides* are ~~returned-shown~~ as stem phocines. Based on the literature, the phylogenetic position of *Callophoca obscura* is difficult to ascertain. The phylogenetic position of *Batavipusa neerlandica*, *Phocanella pumila*, and *Praepusa boeska* remains unclear, in part due to the incompleteness of their respective fossil records.

Fig.4 – Microanatomy of the vertebra of *Nanophoca vitulinoides*. Longitudinal microanatomical drawings of an **A**) adult (Histos 2150, thin section) and **B**) juvenile (Histos

Formatted: Font: Bold
Formatted: Font: Bold

1
2
3
4
5
6
7
8
9
10
11
12
13
14
15
16
17
18
19
20
21
22
23
24
25
26
27
28
29
30
31
32
33
34
35
36
37
38
39
40
41
42
43
44
45
46
47
48
49
50
51
52
53
54
55
56
57
58
59
60
61
62
63
64
65

2147, thin section) lumbar vertebra. The compactness in the adult specimen is clearly much higher than in the juvenile specimen. Scale bars equal 5 mm.

Fig. 5 – Microanatomy of the rib of *Nanophoca vitulinoides*. Microanatomical drawings of the transverse sections through the ribs of **A)** *N. vitulinoides* (Histos 2152, thin section), **B)** *Callophoca obscura* (Histos 168, thin section), and **C)** *Phoca vitulina* (specimen from Canoville et al. 2016, thin section), and the corresponding compactness profiles. Scale bars equal 5 mm.

Formatted: Font: Bold
Formatted: Font: Bold
Formatted: Font: Bold

Fig.6 – Microanatomy of the humerus of *Nanophoca vitulinoides*. Microanatomical drawings of the transverse sections through the humerus of **A)** *N. vitulinoides* (IRSNB M2276c, micro-CT), **B)** *N. vitulinoides* (Histos 2136, thin section), **C)** *Phocanella pumila* (Histos 163, thin section), **D)** *Phoca vitulina* (IRSNB 1157E, micro-CT), **E)** *Mirounga leonina* (specimen from Canoville and Laurin 2010, thin section), **F)** *Otaria byronia* (specimen from Canoville and Laurin 2010, thin section), and **G)** *Lutra lutra* (specimen from Canoville and Laurin 2010, thin section), and the corresponding compactness profiles. Scale bars equal 5 mm.

Formatted: Font: Bold
Formatted: Font: Bold
Formatted: Font: Bold
Formatted: Font: Bold
Formatted: Font: Bold
Formatted: Font: Bold

Fig.7 – Micro-CT scans of the holotype humeri of *Batavipusa neerlandica* and *Praepusa boeska* from the middle Miocene of the southern North Sea basin. Scans show the diaphyseal cross sections of holotype humeri of **A)** *B. neerlandica* (MAB 3798) and **B)** *P. boeska* (MAB 4686). Anterior end up. White arrows point toward different concentric cortical layers. A spongy medullary region is clearly visible in *B. neerlandica*, but less conspicuous in *P. boeska*. Scale bars equal 5 mm.

Formatted: Font: Bold
Formatted: Font: Bold

Fig.8 – Microanatomy of the femur of *Nanophoca vitulinoides*. Microanatomical drawings of the transverse sections through the femur of **A)** *N. vitulinoides* (Histos 1935, thin section), **B)** *N. vitulinoides* (IRSNB M2276d, micro-CT), **C)** *Leptophoca proxima* (Histos 166, thin

Formatted: Font: Bold
Formatted: Font: Bold
Formatted: Font: Bold

1
2
3
4
5
6
7 section), **D**) *Callophoca obscura* (Histos 170, thin section), **E**) *Phocanella pumila* (Histos
8
9 160, thin section), **F**) *Phoca vitulina* (IRSNB 1157E, micro-CT), **G**) *Otaria byronia*
10
11 (specimen from Quemeneur et al. 2013, thin section), and **H**) and **I**) *Lutra lutra* (specimen
12
13 from Quemeneur et al. 2013, thin section), and the corresponding compactness profiles.

14
15 Scale bars equal 5 mm.

16
17 **Fig.9** – Microanatomy of the radius and tibia of *Nanophoca vitulinoides*. Microanatomical

18 drawings of the transverse sections through the radius of **A**) *N. vitulinoides* (Histos 2142,
19
20 thin section), and **B**) *Phoca vitulina* (IRSNB 1157E, micro-CT), and through the tibia **C**) *N.*
21
22 *vitulinoides*(IRSNB M2276g, micro-CT), and **D-F**) *P. vitulina* (IRSNB 1157E, micro-CT),
23
24 and the corresponding compactness profiles. Scale bars equal 5 mm.

25
26 **Fig.10** – Bone structure in the cortex and medulla of *Nanophoca vitulinoides*-bones. **A**) The

27
28 cortex of the humeral diaphysis (cross section) is composed of a woven-parallel complex
29
30 with longitudinal primary osteons and conspicuous, broadly spaced annuli (arrows). Left
31
32 half: ordinary transmitted light, right half: polarized light. **B**) Longitudinal section in the
33
34 same bone in the metaphyseal region. The primary osteons appear brightly birefringent. **C**)
35
36 Closer view at the diaphyseal cortex between annuli 2 and 4. The arrows point to short
37
38 Sharpey's fibers. **D**) Lines of arrested growth (arrows) in the humeral cortex. **E**) Cross-
39
40 section in the larger radius (Histos 2174). The whole bone area is occupied by a dense
41
42 Haversian tissue, and no medullary cavity is visible. **F**) Closer view at the remodeled
43
44 medullary of the radius shown in Fig.10E. **G**) Detail of the structure of the dense Haversian
45
46 tissue in the medulla of the radius. Remark that vascular canals are extremely thin or
47
48 occluded. **H**) Close view at over-remodeled bone in the medulla of the radius. The two
49
50 arrows point at occluded Haversian canals. Scale bars equal 5 μm, except E) 5 mm, and H)
51
52 50 μm.

Formatted: Font: Bold

Formatted: Font: Bold

Formatted: Font: Bold

Formatted: Font: Bold

Formatted: Font: Bold

Formatted: Font: Bold

Formatted: Font: Bold

Formatted: Font: Bold

Formatted: Font: Bold

Formatted: Font: Bold

Formatted: Font: Bold

Formatted: Font: Not Italic

Formatted: Font: Bold

Formatted: Font: Bold

Formatted: Font: Bold

Formatted: Font: Bold

Formatted: Font: Bold

Formatted: Font: Bold

Formatted: Font: Bold

1
2
3
4
5
6
7
8
9
10
11
12
13
14
15
16
17
18
19
20
21
22
23
24
25
26
27
28
29
30
31
32
33
34
35
36
37
38
39
40
41
42
43
44
45
46
47
48
49
50
51
52
53
54
55
56
57
58
59
60
61
62
63
64
65

Fig.11 – Inner bone remodeling in long bones and vertebrae. **A)** Longitudinal section in the proximal metaphyseal and epiphyseal regions of the femur. The whole bone is compact and composed of densely remodeled osseous tissue. **B)** Longitudinal section in the proximal metaphysis and epiphysis of a rib. Same comment as for the femur. **C)** Longitudinal section in the epiphysis of the larger radius (Histos 2174). Epiphyseal surface is covered by a thin layer of calcified cartilage. Under it, the metaphyseal medulla is already compact and densely remodeled (right half: polarized light). **D)** Cross section in the diaphysis of the smaller radius (Histos 2142). The architecture of the spongiosa that once occupied the medulla is still visible, though inter-trabecular spaces are filled. **E)** Detail of the medullar of the smaller radius. The endosteal deposits filling inter-trabecular spaces are densely remodeled and vascular canals (arrows) tend to be occluded. The asterisks indicate micro-cracks. **F)** Off-centered growth of Humeral diaphysis. One face of the bone is under resorption (hollow arrow) while accretion occurs on the other (solid arrow). **G)** Cross section in the centrum of the larger vertebra. Polarized light reveals that the thick trabeculae filling the centrum are densely remodeled. **H)** Longitudinal section in the same specimen (polarized light) showing densely remodeled osseous tissue. **I)** External fundamental system on the outer wall of the neural arch (cross section) in polarized light. Scale bars equal 5 mm for A) and B); 1 mm for D), F), G), H), and I); and 500µm for C), and E).

Formatted: Font: Bold

Formatted: Font: Bold

Formatted: Font: Bold

Formatted: Font: Bold

Formatted: Font: Bold

Formatted: Font: Bold

Formatted: Font: Bold

Formatted: Font: Bold

Formatted: Font: Bold

Fig.12 – Comparative data in extant and extinct pinnipeds. **A)** Cross section in the femur of *Phocanella pumila*. Remark the relatively high compactness of this bone, and its non-remodeled cortex. White rectangle: field shown in Fig.11B. **B)** Detail of the cortex showing a woven-parallel tissue with longitudinal primary osteons and annuli. Right half: polarized light. **C)** lines of arrested growth in the femoral cortex of *P-Phocanella pumila*. **D)** Non-remodeled part of the cortex of a rib in *Monachus monachus* (polarized light). Histology of primary cortices is comparable to that prevailing in *P-Phocanella pumila* and *Nanophoca*

Formatted: Font: Bold

Formatted: Font: Bold

Formatted: Font: Not Italic

Formatted: Font: Bold

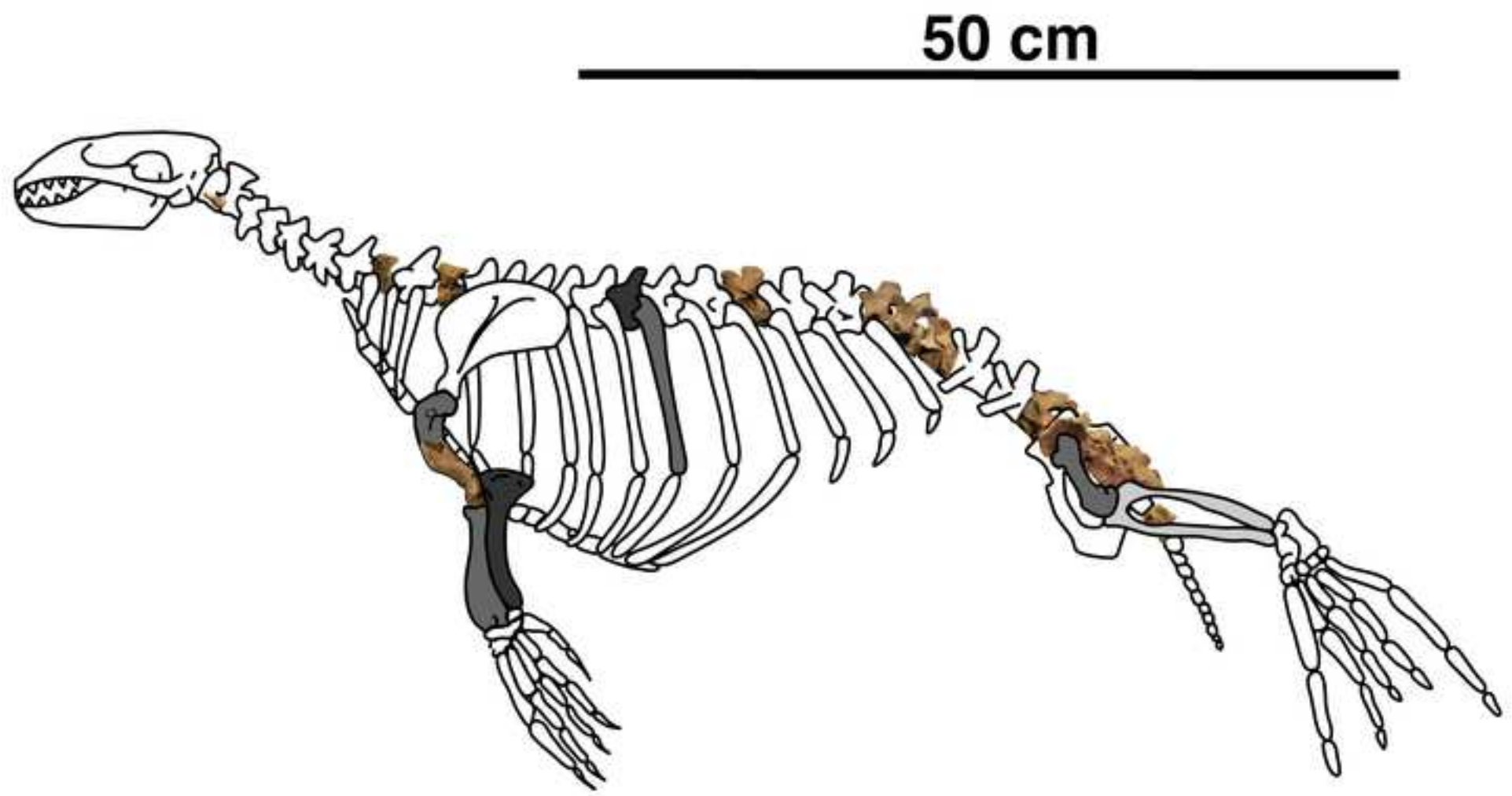
Formatted: Font: Bold

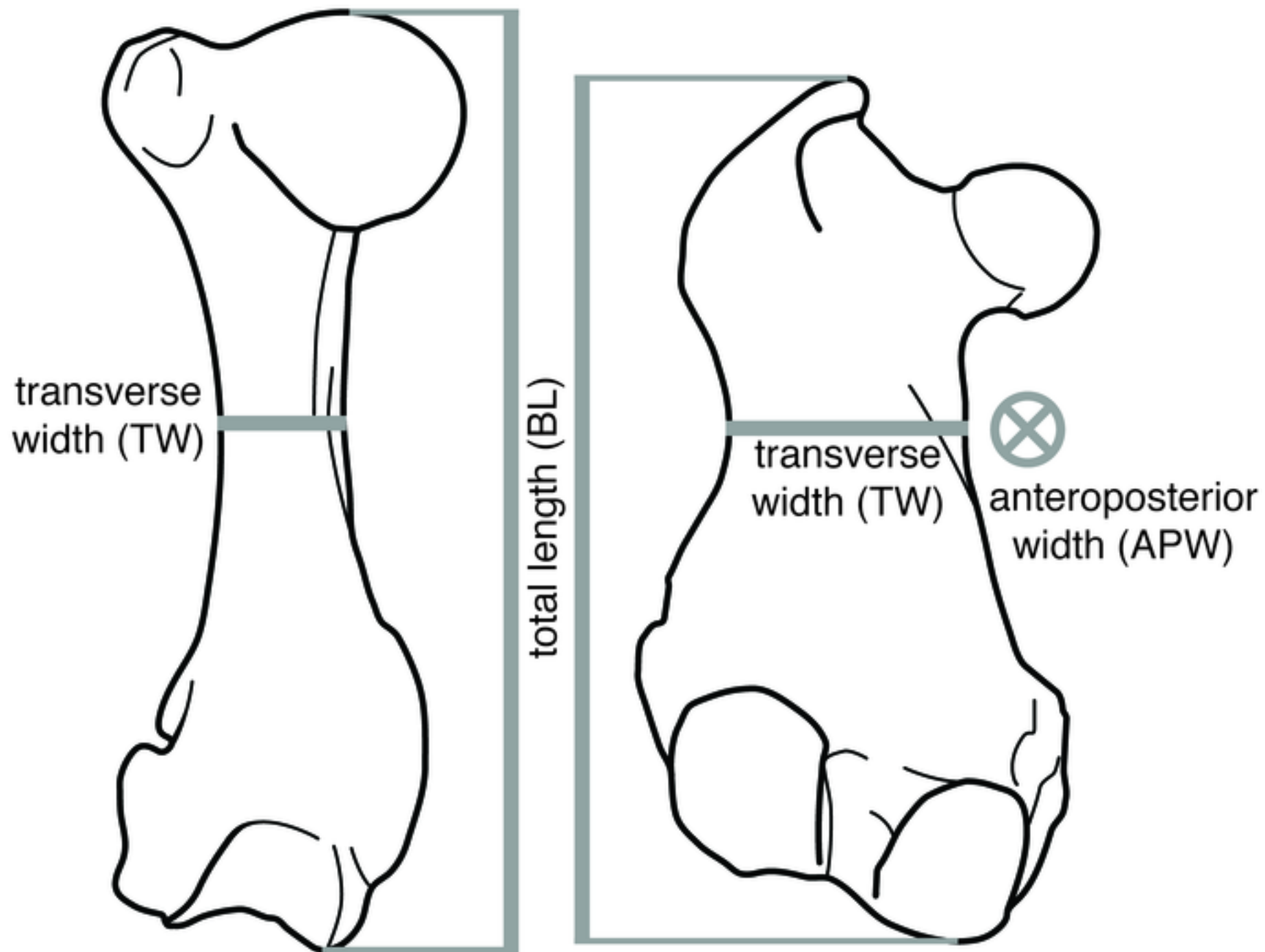
1
2
3
4
5
6
7
8
9
10
11
12
13
14
15
16
17
18
19
20
21
22
23
24
25
26
27
28
29
30
31
32
33
34
35
36
37
38
39
40
41
42
43
44
45
46
47
48
49
50
51
52
53
54
55
56
57
58
59
60
61
62
63
64
65

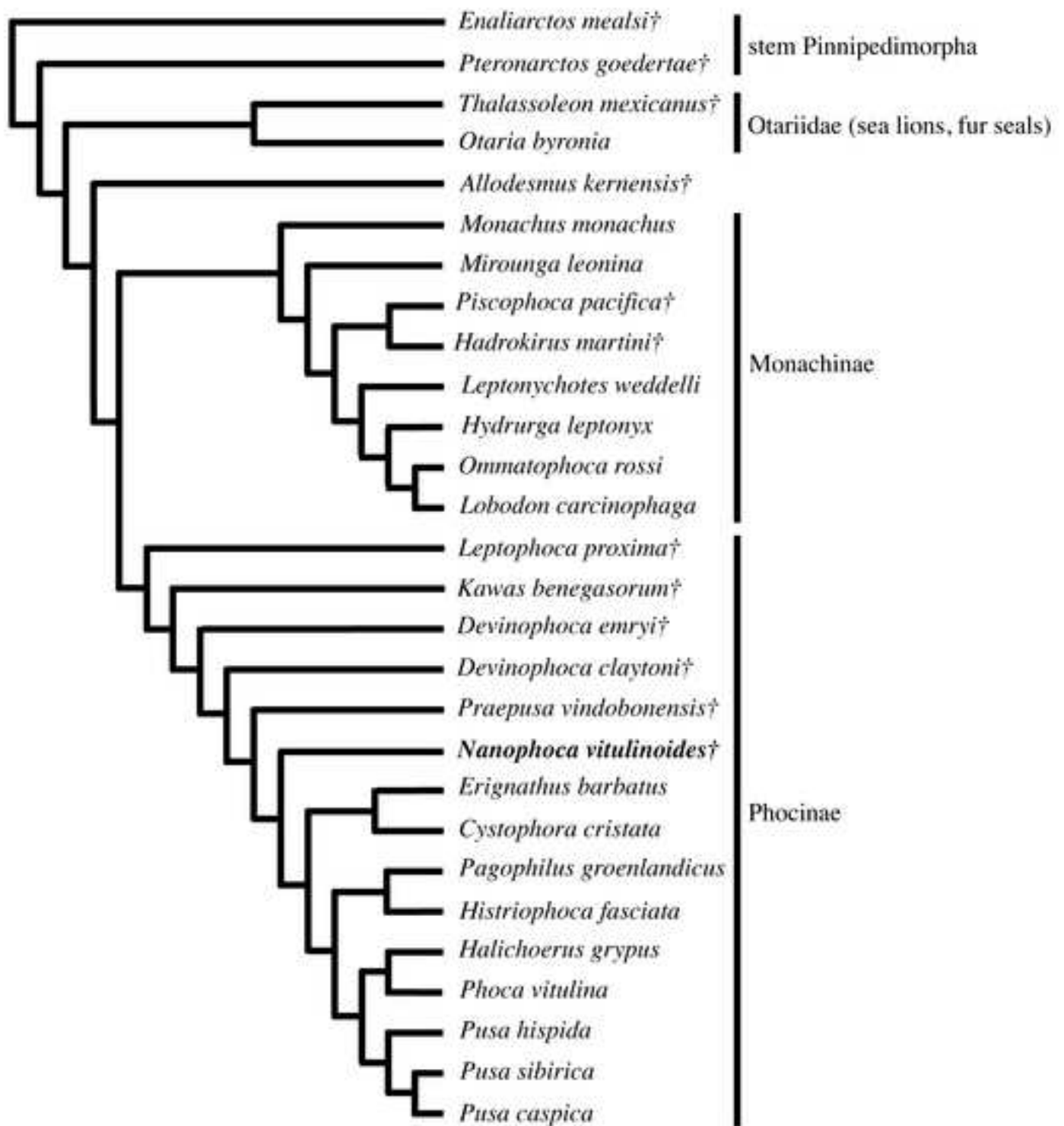
vitulinoides. **E**) Remodeling in the deep femoral cortex of *Callophoca obscura*. Remodeling is intense, but Havers' canals remain widely open. **F**) Normal (most frequent) bone architecture in extant and some extinct pinnipeds (here: femur of *Callophoca obscura*). The medullary region is hollow, and contains only a loose spongiosa with thin trabeculae. Scale bars equal 10 mm for A) and F); 1 mm for the inset of F); and 500 μ m for B), C), D), and E).

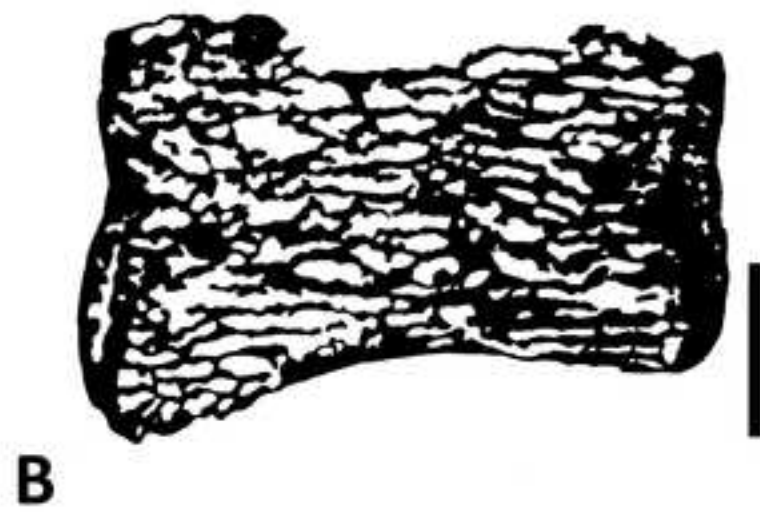
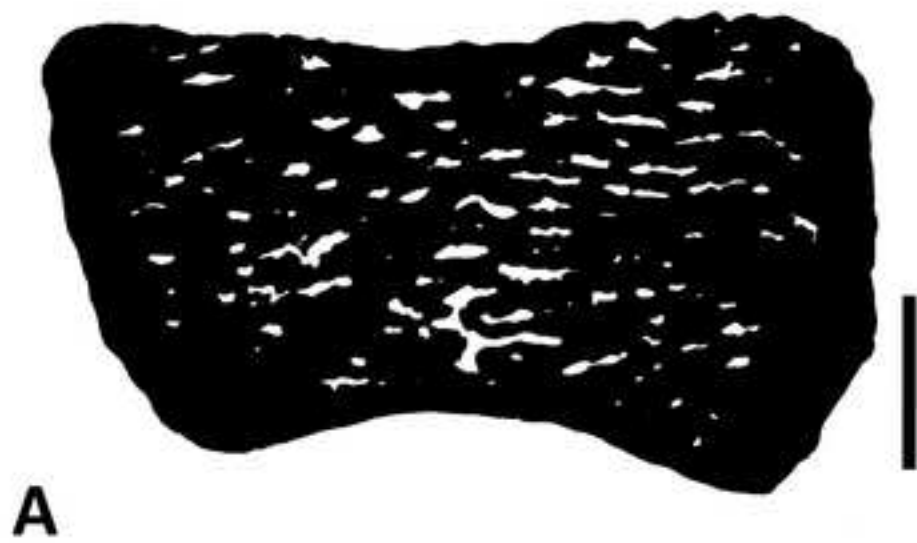
Formatted: Font: Bold

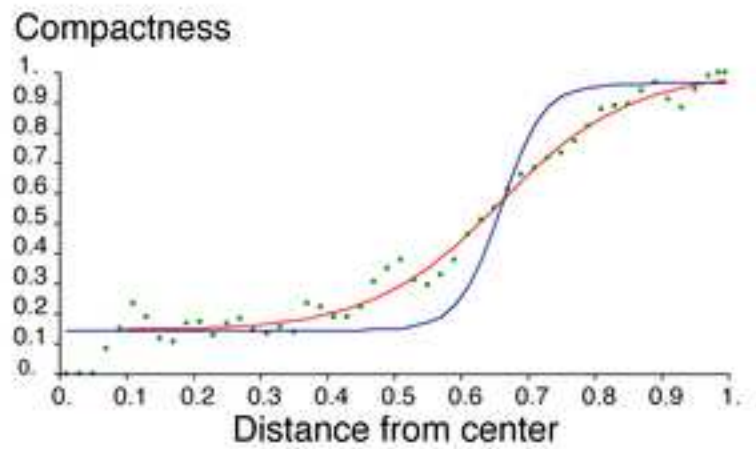
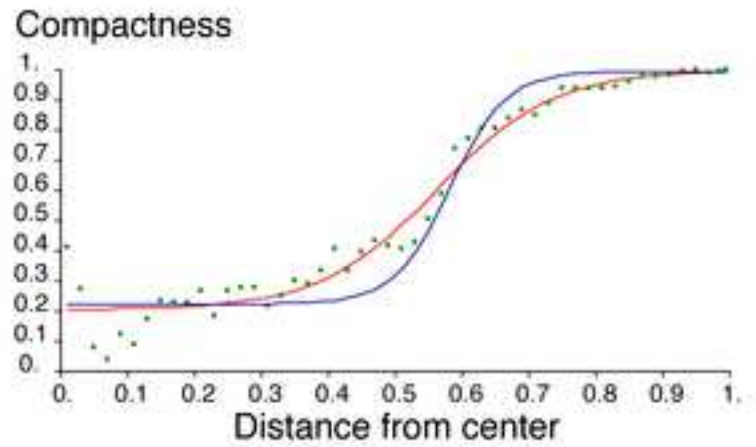
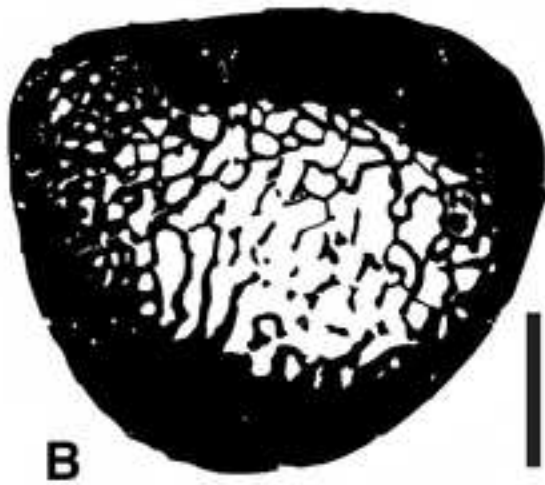
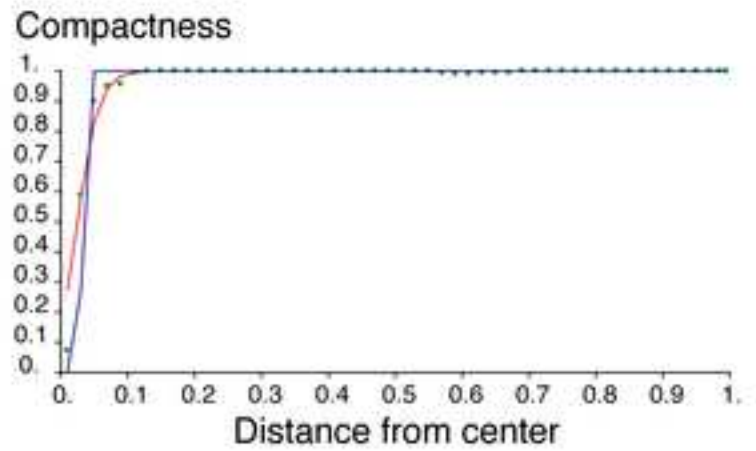
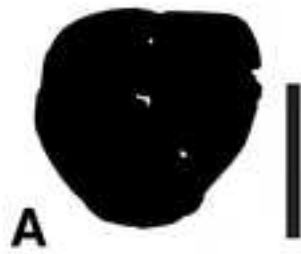
Formatted: Font: Bold

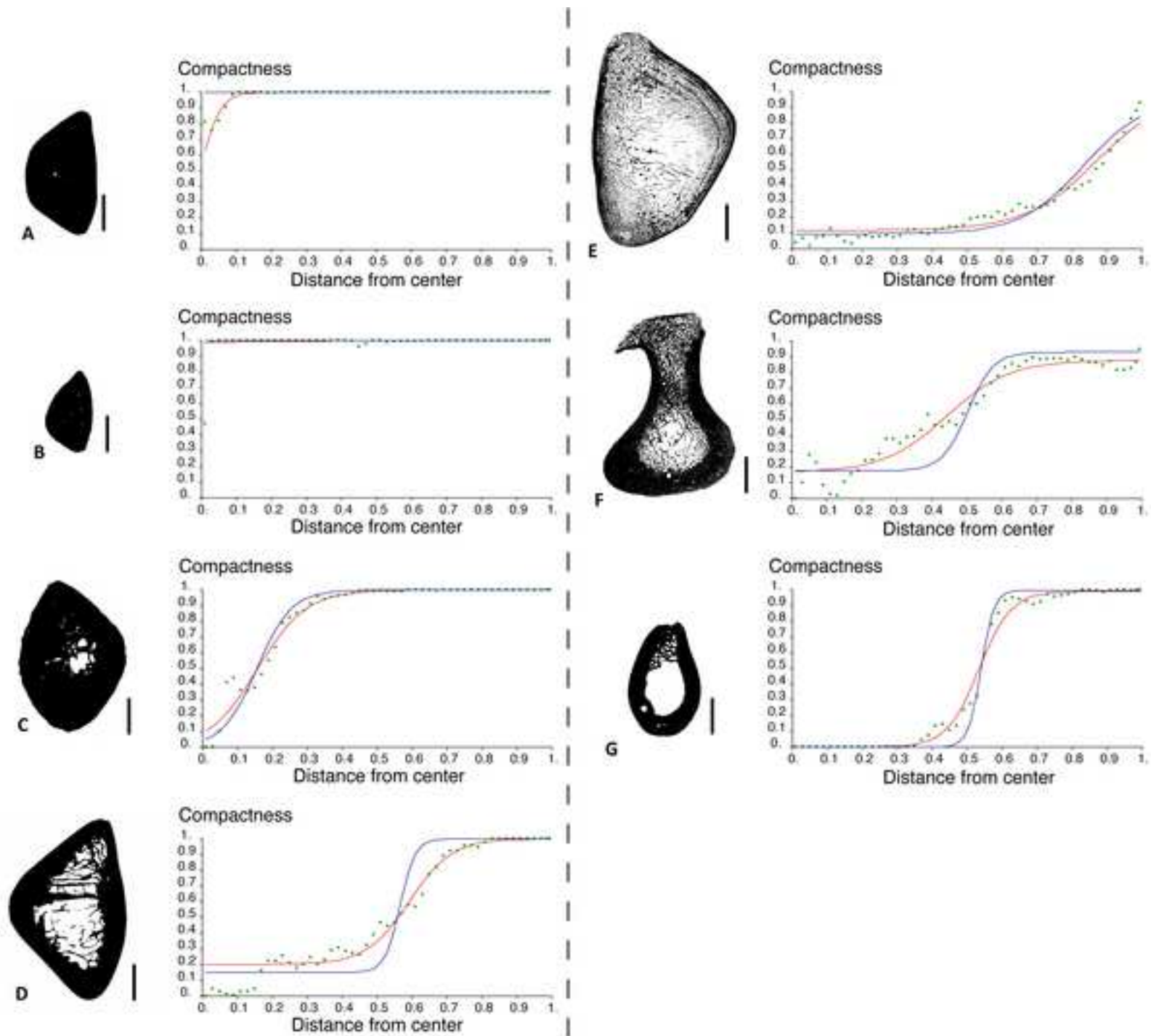


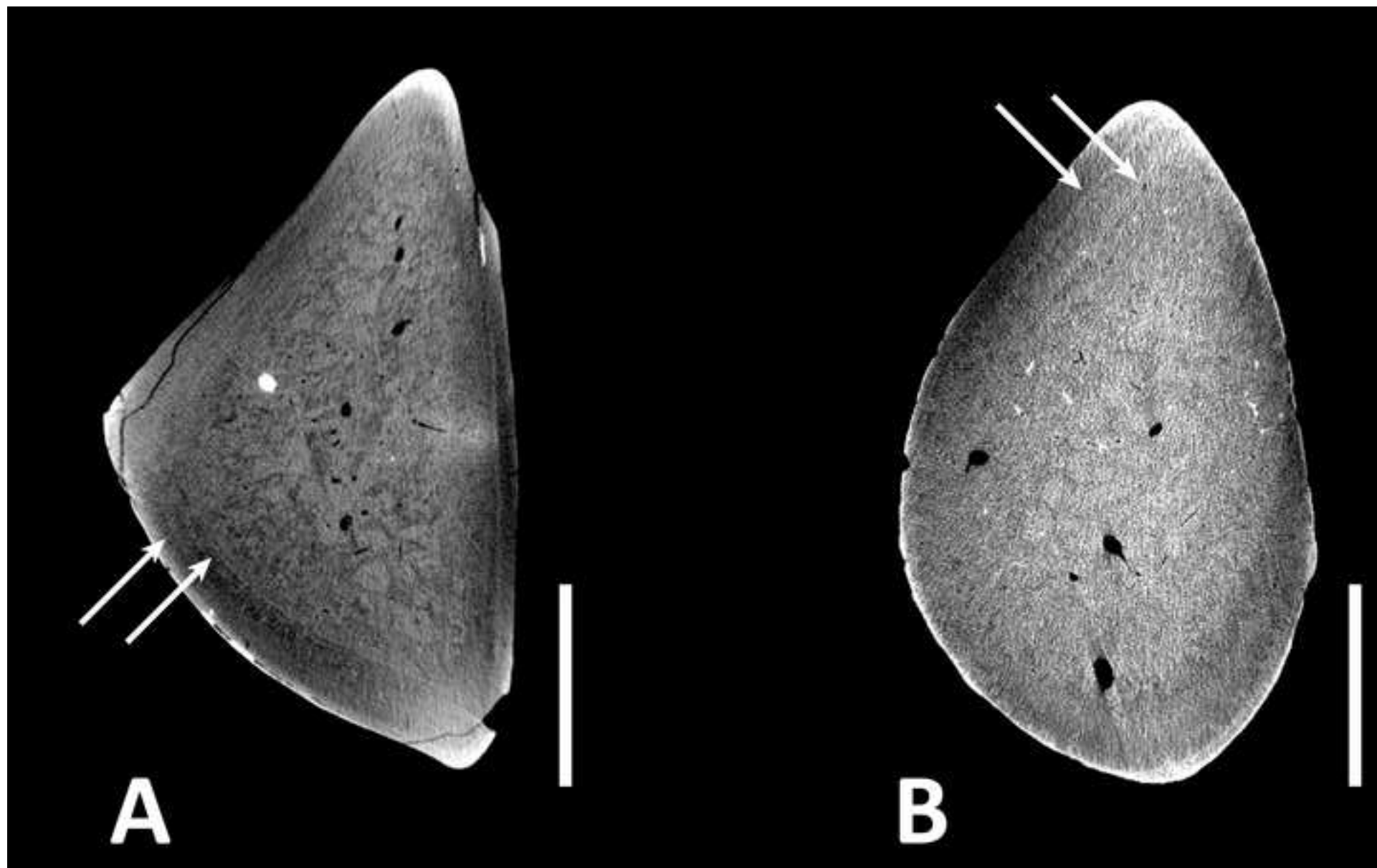


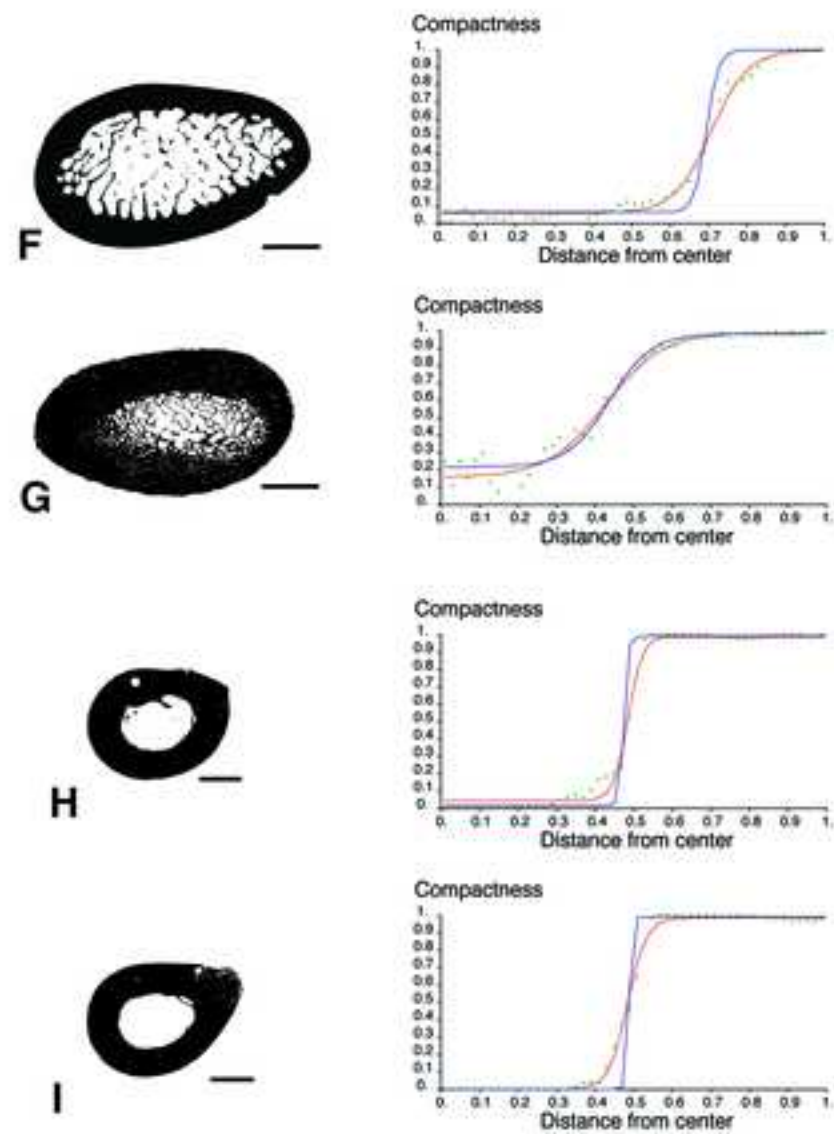
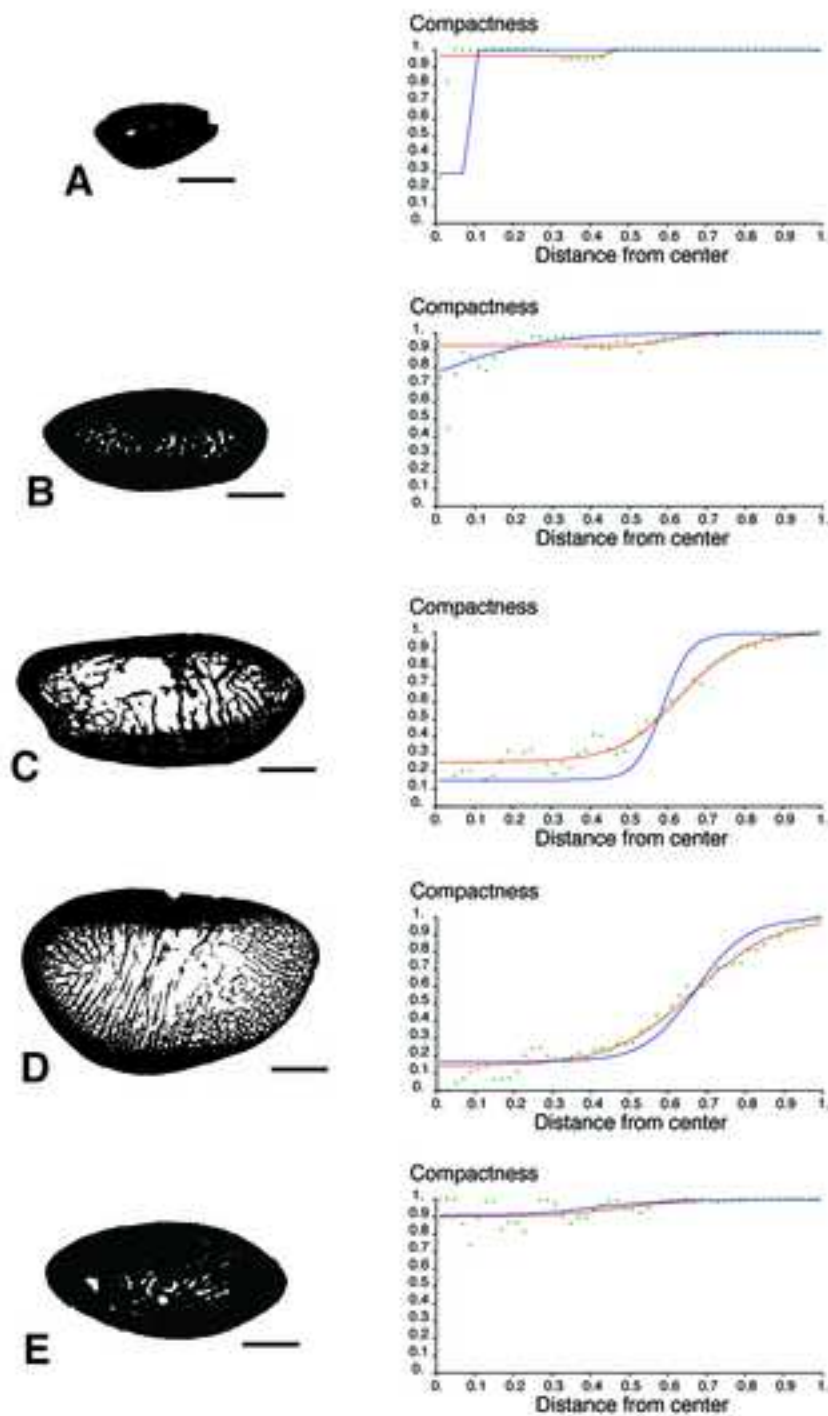


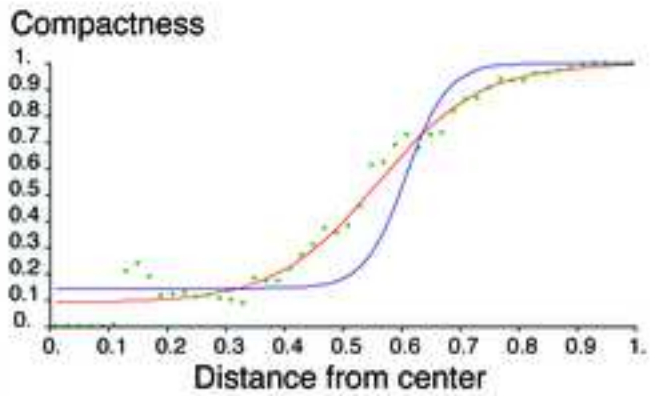
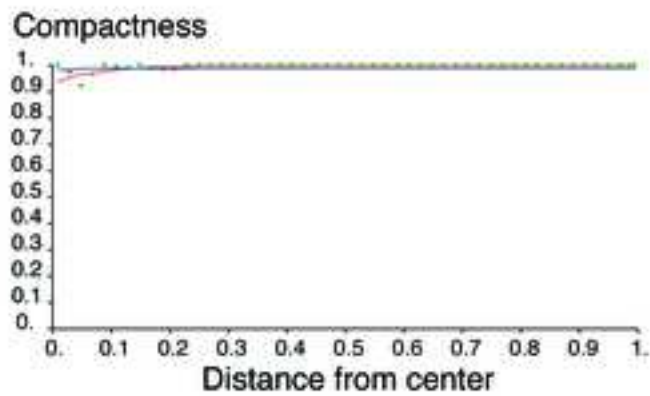
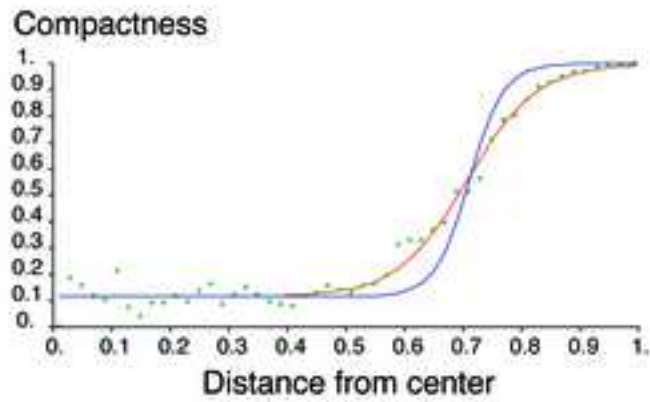
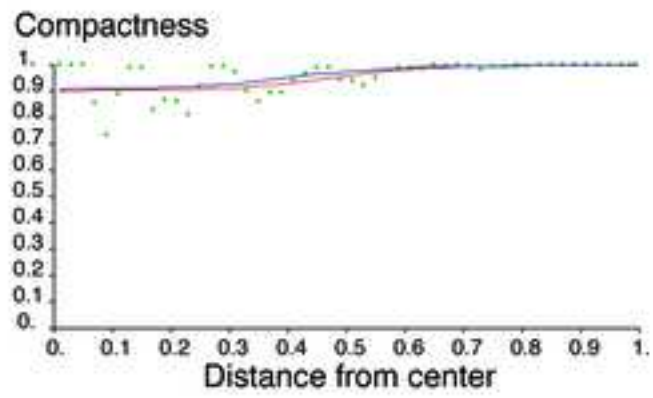


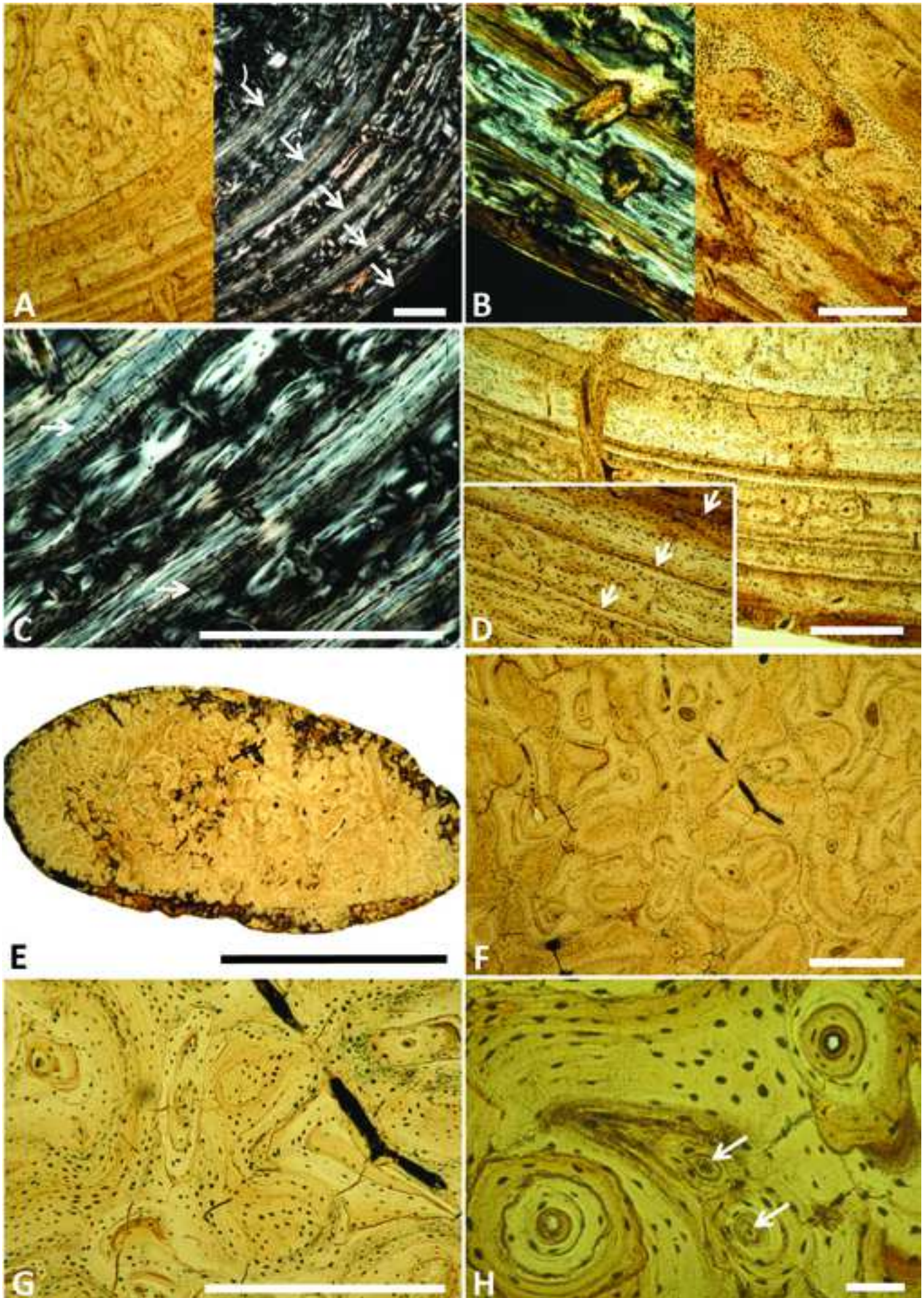


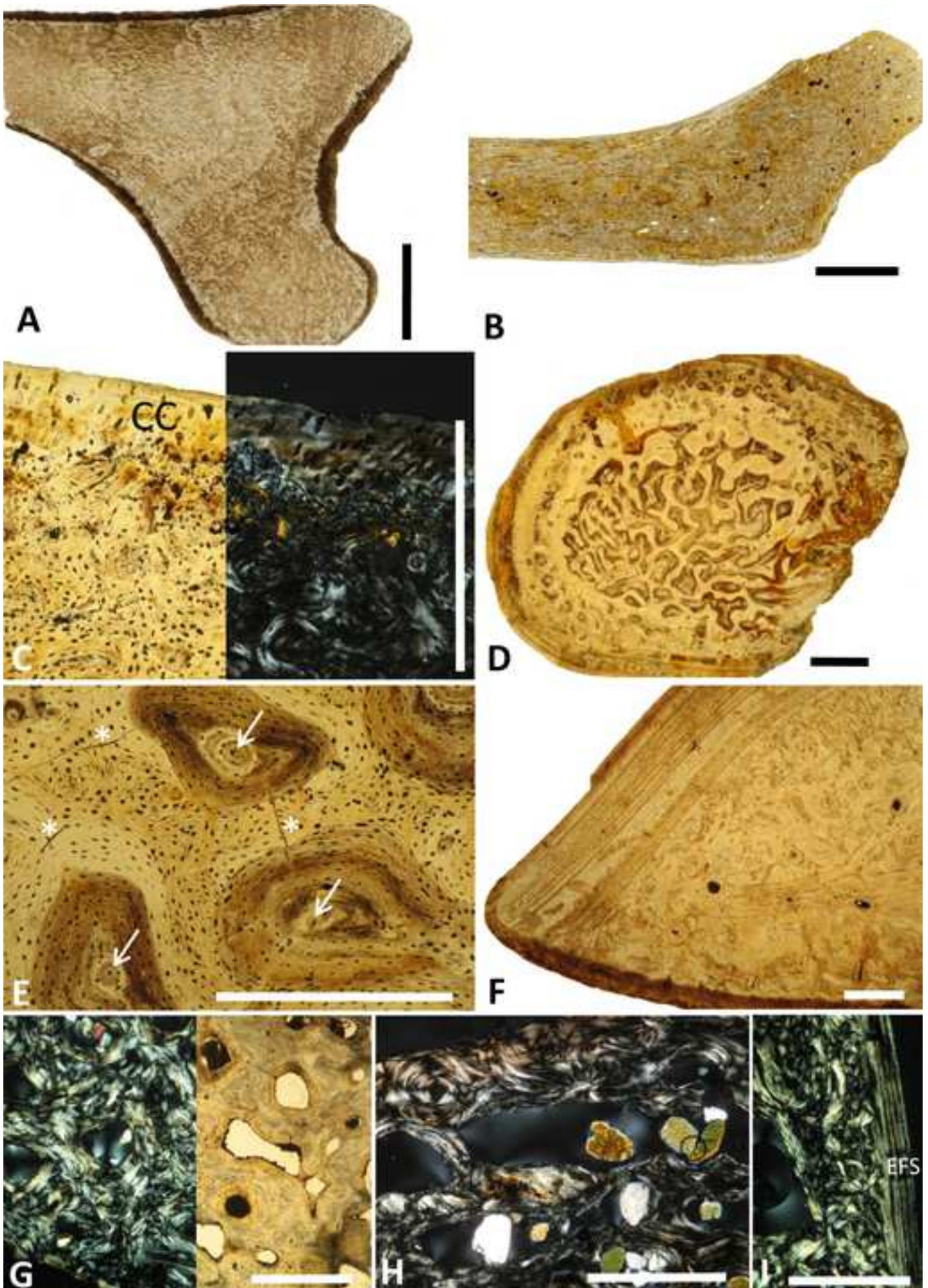












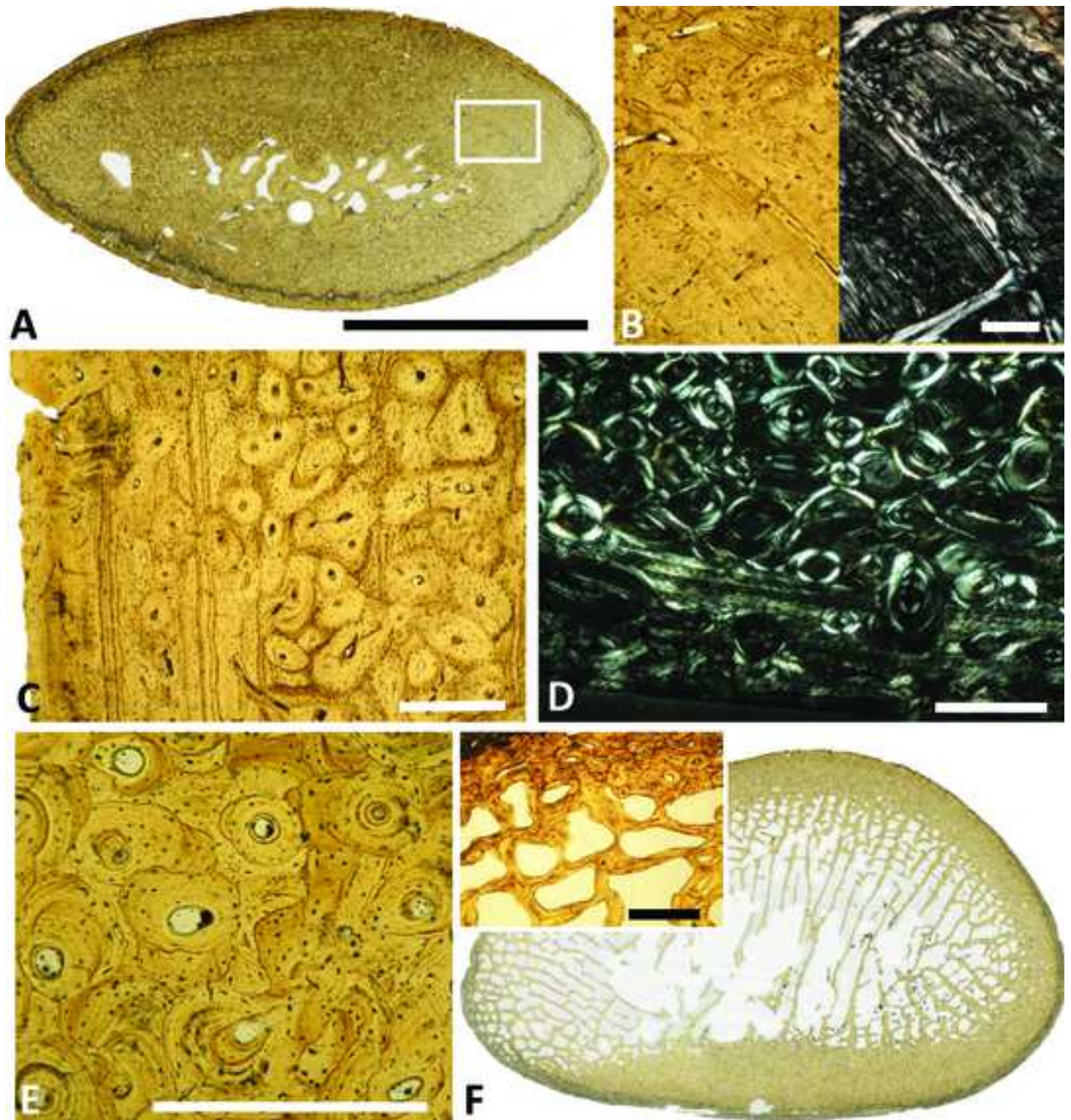


Table 1. Basic morphometric analysis of the humerus. Table showing the specimen numbers of the used specimens, including averages retrieved from the literature. The third and fourth column present the measurements, with the absolute sagittal length (BL) in the third column and the least transverse width of the diaphysis (TW) in the fourth column. The resulting ratio is presented in the final column. Color coding from red (low values, suggesting no pachyostosis) via yellow (medium values) to green (high values, suggesting pachyostosis) for easy visual differentiation.

Taxon	Specimen number	Humerus		
		Absolute sagittal length (mm)(BL)	Least transverse width diaphysis (mm)(TW)	Ratio TW/BL
<i>Halichoerus grypus</i>	MSC 1978-48	142.0	24.2	0.170
<i>Pusa sibirica</i>	IRSNB 14210	75.7	10.0	0.132
<i>Pusa sibirica</i>	IRSNB 15264	79.4	11.8	0.149
<i>Pusa sibirica</i>	IRSNB 21170	74.7	10.9	0.146
<i>Pusa sibirica</i>	IRSNB 21171	91.4	12.6	0.138
<i>Pusa sibirica</i>	MSC 504941	85.5	11.6	0.136
<i>Phoca vitulina</i>	IRSNB 1165S	109.6	16.2	0.148
<i>Phoca vitulina</i>	IRSNB 1157C	111.0	16.8	0.151
<i>Phoca vitulina</i>	IRSNB 7605	110.4	18.0	0.163
<i>Phoca vitulina</i>	IRSNB 35247	110.0	15.2	0.138
<i>Phoca vitulina</i>	IRSNB 36548	122.9	18.8	0.153
<i>Leptophoca proxima</i>	USNM 5359	124.5	14.9	0.120

<i>Leptophoca proxima</i>	USNM 23450	113.4	13.5	0.119
<i>Leptophoca proxima</i>	USNM 284721	126.2	15.0	0.119
<i>Leptophoca proxima</i>	USNM 412115	131.7	14.4	0.109
<i>Cryptophoca maeotica</i>	Average Koretsky (2001)	107.1	14.5	0.135
<i>Praepusa vindobonensis</i>	Average Koretsky (2001)	86.3	10.6	0.123
<i>Pachyphoca ukrainica</i>	Average Koretsky & Rahmat (2013)	87.0	18.3	0.210
<i>Sarmatonectes sintsovi</i>	USNM unspecified cast	90.4	13.9	0.154
<i>Monachopsis pontica</i>	Average Koretsky (2001)	80.5	13.6	0.169
<i>Praepusa boeska</i>	MAB 4686 (holotype)	81.1	11.3	0.139
<i>Batavipusa neerlandica</i>	MAB 3798	64.9	11.8	0.182
<i>Phocanella pumilla</i>	USNM 171151	128.8	15.8	0.123
<i>Phocanella pumilla</i>	USNM 305304	131.9	15.4	0.117
<i>Phocanella pumilla</i>	USNM 329059	127.8	15.8	0.124
<i>Phocanella pumilla</i>	USNM 421544	124.6	16.6	0.133
<i>Phocanella pumilla</i>	USNM 437762	125.1	13.9	0.111
<i>Nanophoca vitulinoides</i>	IRSNB 1063-M242	78.2	9.5	0.121
<i>Nanophoca vitulinoides</i>	IRSNB M2276c	72.4	9.8	0.135

Table 2. Basic morphometric analysis of the femur. Table showing the specimen numbers of the used specimens, including averages retrieved from the literature. The third, fourth, and fifth column present the measurements, with the absolute sagittal length (BL) in the third column, the least transverse width of the diaphysis (TW) in the fourth column, and the anteroposterior width of the diaphysis (APW) in the fifth column. The resulting ratio is presented in the final column. Color coding from red (low values, suggesting no pachyostosis) via yellow (medium values) to green (high values, suggesting pachyostosis) for easy visual differentiation.

Taxon	Specimen number	Femur			
		Absolute sagittal length (mm)(BL)	Least transverse width diaphysis (mm)(TW)	Anteroposterior width diaphysis (mm)(APW)	Ratio [0.5(TW+APW)] /BL
<i>Halichoerus grypus</i>	MSC 1978-48	120.4	30.7	14.4	0.187
<i>Pusa sibirica</i>	IRSNB 14210	68.5	14.7	7.0	0.158
<i>Pusa sibirica</i>	IRSNB 15264	72.4	15.1	8.2	0.161
<i>Pusa sibirica</i>	IRSNB 21170	67.8	15.6	6.7	0.164
<i>Pusa sibirica</i>	IRSNB 21171	86.1	17.1	9.9	0.157
<i>Pusa sibirica</i>	MSC 504941	76.7	16.1	8.2	0.158
<i>Phoca vitulina</i>	IRSNB 1157C	99.4	22.6	13.9	0.184
<i>Phoca vitulina</i>	IRSNB 7605	106.4	21.8	14.0	0.168
<i>Phoca vitulina</i>	IRSNB 35247	98.4	18.7	13.7	0.165
<i>Phoca vitulina</i>	IRSNB 36548	109.3	21.5	15.2	0.168
<i>Leptophoca proxima</i>	USNM 263648	107.8	27.0	15.1	0.195

<i>Leptophoca proxima</i>	USNM 347348	118.9	28.9	17.2	0.194
<i>Leptophoca proxima</i>	USNM 559330	115.8	27.6	17.0	0.193
<i>Cryptophoca maeotica</i>	Average from Koretsky (2001)	106.0	27.6	12.4	0.189
<i>Praepusa vindobonensis</i>	Average from Koretsky (2001)	72.8	18.4	10.4	0.198
<i>Pachyphoca ukrainica</i>	Average from Koretsky & Rahmat (2013)	80.3	24.3	14.3	0.240
<i>Pachyphoca chapskii</i>	NMNHU-P 64-706	120.0	33.5	21.5	0.229
<i>Sarmatonectes sintsovi</i>	Specimen Koretsky (2001)	89.5	21.0	13.0	0.190
<i>Sarmatonectes sintsovi</i>	Specimen Koretsky (2001)	94.5	22.5	13.0	0.188
<i>Monachopsis pontica</i>	Average from Koretsky (2001)	68.3	18.1	9.7	0.204
<i>Phocanella pumilla</i>	USNM 181649	124.1	29.5	15.9	0.183
<i>Phocanella pumilla</i>	USNM 481569	115.0	27.4	12.3	0.173
<i>Nanophoca vitulinoides</i>	IRSNB1049-M246	73.6	19.8	9.7	0.200
<i>Nanophoca vitulinoides</i>	IRSNB M2271	71.5	20.3	9.5	0.208
<i>Nanophoca vitulinoides</i>	IRSNB M2276d	69.4	19.6	9.1	0.207

Table 3. Taxa and specimens considered for the micro-anatomic and osteohistological parts of the study. Specimens that have exclusively been considered for microanatomy are indicated by an asterisk (*) and specimens that have exclusively been considered for osteohistology are indicated by a dagger (†). For institutional abbreviations, see ‘materials and methods’ section. Other abbreviations: Av. = “average of”; Histos = collection of osteohistological sections at the Muséum national d’Histoire naturelle.; Sp. = “specimen from”. Note that, for cells containing multiple specimens, asterisks and daggers apply to all specimens in that cell.

Taxon	Rib	Humerus	Radius	Ulna	Femur	Tibia	Vertebra
<i>Arctocephalus pusillus</i>	Sp. Canovile et al. (2016)*						Sp. Dumont et al. (2013)*
<i>Callophoca obscura</i>	Histos 168				Histos 170		
	Histos 169†						
<i>Cystophora cristata</i>	Sp. Canovile et al. (2016)*						Sp. Dumont et al. (2013)*
<i>Enhydra lutris</i>	Sp. Canovile et al. (2016)*						Sp. Dumont et al. (2013)*
<i>Eumetopias jubatus</i>	Sp. Canovile et al. (2016)*						
<i>Halichoerus grypus</i>					Sp. Quemeneur et al (2013)*		
<i>Leptophoca lenis</i>					Histos 166		
<i>Lutra lutra</i>		Sp. Canoville and Laurin (2010)*			Av. 8 sp. Quemeneur et al (2013)*		Sp. Dumont et al. (2013)*
<i>Mirounga leonina</i>		Specimen from Canoville and Laurin (2010)*					Sp. Dumont et al. (2013)*
<i>Monachus monachus</i>	Sp. Canovile et						

	al. (2016)*						
<i>Nanophoca vitulinoides</i>	Histos 2152	Histos 2135, 2137–2140†	Histos 2142	Histos 2143, 2144†	Histos 1934, 1936–1941†	IRSNB M2276g*	Histos 2147, 2150
	Histos 2153–2156†	Histos 2136	Histos 2174†		Histos 1935		Histos 2148, 2149, 2151†
		IRSNB M2276c*			IRSNB M2276d*		
<i>Odobenus rosmarus</i>	Sp. Canovile et al. (2016)*						
<i>Otaria byronia</i>		Sp. Canoville and Laurin (2010)*			Sp. Quemeneur et al (2013) *		Sp. Dumont et al. (2013)*
<i>Pagophilus groenlandicus</i>							Sp. Dumont et al. (2013)*
<i>Phoca vitulina</i>	Sp. Canovile et al. (2016)*	IRSNB 1157E*	IRSNB 1157E*		IRSNB 1157E*	IRSNB 1157E*	
<i>Phocanella pumila</i>		Histos 162, 164†			Histos 159, 161†		
		Histos 163			Histos 160		
<i>Ursus maritimus</i>	Histos 42*						Sp. Dumont et al. (2013)*
<i>Zalophus californianus</i>	Sp. Canovile et al. (2016)*						Sp. Dumont et al. (2013)*

Table 4. Histomorphometry of the vertebrae with BONE PROFILER.

Taxon	Specimen number / Collection	Global compactness
Carnivora		
Ursidae		
<i>Ursus maritimus</i>	Specimen from Dumont et al. (2013)	0.294
Phocidae		
Phocinae		
<i>Cystophora cristata</i>	Specimen from Dumont et al. (2013)	0.223
<i>Nanophoca vitulinoides</i>	Histos 2150	0.938
<i>Nanophoca vitulinoides</i>	Histos 2147	0.636
<i>Pagophilus groenlandicus</i>	Specimen from Dumont et al. (2013)	0.293
Monachinae		
<i>Hydrurga leptonyx</i>	Specimen from Dumont et al. (2013)	0.380
<i>Mirounga leonina</i>	Specimen from Dumont et al. (2013)	0.341
Otariidae		
<i>Arctocephalus pusillus</i>	Specimen from Dumont et al. (2013)	0.411
<i>Otaria byronia</i>	Specimen from Dumont et al. (2013)	0.354
<i>Zalophus californianus</i>	Specimen from Dumont et al. (2013)	0.363
Mustelidae		
<i>Enhydra lutris</i>	Specimen from Dumont et al. (2013)	0.443
<i>Lutra lutra</i>	Specimen from Dumont et al. (2013)	0.412

Table 5. Histomorphometry of the ribs with BONE PROFILER. Analyses were conducted on thin sections. Min, Max, S, and P values are global values for each bone. Abbreviation: Comp., global compactness.

Taxon	Specimen number / Collection	Min	Max	S	P	Comp.
Carnivora						
Ursidae						
<i>Ursus maritimus</i>	Histos 42	0.129	1.000	0.049	0.707	0.554
Phocidae						
Phocinae						
<i>Cystophora cristata</i>	Specimen from Canoville et al. (2016)	0.138	1.000	0.037	0.895	0.307
<i>Nanophoca vitulinoides</i>	Histos 2152	0.000	0.999	0.015	0.025	0.998
<i>Phoca vitulina</i>	Specimen from Canoville et al. (2016)	0.000	0.963	0.135	0.624	0.603
Monachinae						
<i>Callophoca obscura</i>	Histos 168	0.205	1.000	0.087	0.562	0.727
<i>Monachus monachus</i>	Specimen from Canoville et al. (2016)	0.017	1.000	0.127	0.517	0.687
Otariidae						
<i>Arctocephalus pusillus</i>	Specimen from Canoville et al. (2016)	0.154	1.000	0.136	0.445	0.784
<i>Eumetopias jubatus</i>	Specimen from Canoville et al. (2016)	0.032	0.942	0.122	0.506	0.666
<i>Zalophus californianus</i>	Specimen from Canoville et al. (2016)	0.000	1.000	0.125	0.410	0.782
Odobenidae						
<i>Odobenus rosmarus</i>	Specimen from Canoville et al. (2016)	0.084	1.000	0.119	0.765	0.449
Mustelidae						
<i>Enhydra lutris</i>	Specimen from Canoville et al. (2016)	0.694	0.957	0.044	0.421	0.908

Table 6. Histomorphometry of the humeri with BONE PROFILER. Min, Max, S, and P values are global values. Abbreviations: TS, Thin section; CT, micro-CT; Comp., global compactness.

Taxon	Specimen number / Collection	TS / CT	Resolution (µm)	Min	Max	S	P	Comp.
Carnivora								
Phocidae								
Phocinae								
<i>Nanophoca vitulinoides</i>	Histos 2136	TS	—	0.007	0.998	0.113	-0.486	0.997
<i>Nanophoca vitulinoides</i>	IRSNB M2276c	CT	45.8	0.000	1.000	0.028	-0.005	0.999
<i>Phoca vitulina</i>	IRSNB 1157E	CT	45.7	0.202	1.000	0.061	0.591	0.706
<i>Phocanella pumilla</i>	Histos 162	TS	—	0.000	1.000	0.069	0.158	0.959
Monachinae								
<i>Mirounga leonina</i>	Specimen from Canoville and Laurin (2010)	TS	—	0.118	1.000	0.101	0.870	0.348
Otariidae								
<i>Otaria byronia</i>	Specimen from Canoville and Laurin (2010)	TS	—	0.167	0.879	0.090	0.442	0.720
Mustelidae								
<i>Lutra lutra</i>	Specimen from Canoville and Laurin (2010)	TS	—	0.000	0.990	0.046	0.534	0.697

Table 7. Histomorphometry of the femora with BONE PROFILER. Min, Max, S, and P values are global values. Abbreviations: TS, Thin section; CT, micro-CT; Comp., Global compactness.

Taxon	Specimen number / Collection	TS / CT	Resolution (µm)	Min	Max	S	P	Comp.
Carnivora								
Phocidae								
Phocinae								
<i>Halichoerus grypus</i>	From Quemeneur et al. (2013)	TS	—	0.109	0.980	0.045	0.638	0.615
<i>Leptophoca proxima</i>	Histos 166	TS	—	0.225	1.000	0.076	0.605	0.700
<i>Nanophoca vitulinoides</i>	Histos 1935	TS	—	0.969	1.000	0.002	0.451	0.994
<i>Nanophoca vitulinoides</i>	IRSNB M2276d	CT	45.8	0.574	1.000	0.207	0.001	0.971
<i>Phoca vitulina</i>	IRSNB 1157E	CT	45.7	0.061	1.000	0.048	0.706	0.520
<i>Phocanella pumilla</i>	Histos 170	TS	—	0.902	1.000	0.083	0.476	0.977
Monachinae								
<i>Callophoca obscura</i>	Histos 170	TS	—	0.143	1.000	0.106	0.667	0.591
Otariidae								
<i>Otaria byronia</i>	From Quemeneur et al. (2013)	TS	—	0.159	0.992	0.074	0.426	0.824
Mustelidae								
<i>Lutra lutra</i>	From Quemeneur et al. (2013)	TS	—	0.043	0.991	0.018	0.485	0.764
<i>Lutra lutra</i>	From Quemeneur et al. (2013)	TS	—	0.000	0.988	0.024	0.484	0.751
<i>Lutra lutra</i>	From Quemeneur et al. (2013)	TS	—	0.003	0.995	0.034	0.517	0.722
<i>Lutra lutra</i>	From Quemeneur et al. (2013)	TS	—	0.000	1.000	0.009	0.574	0.666
<i>Lutra lutra</i>	From Quemeneur et al. (2013)	TS	—	0.024	0.994	0.013	0.473	0.773
<i>Lutra lutra</i>	From Quemeneur et al. (2013)	TS	—	0.043	0.991	0.018	0.485	0.764

<i>Lutra lutra</i>	From Quemeneur et al. (2013)	TS	—	0.000	0.998	0.024	0.484	0.751
<i>Lutra lutra</i>	From Quemeneur et al. (2013)	TS	—	0.000	1.000	0.009	0.574	0.666

Table 8. Histomorphometry of the radii and tibiae with BONE PROFILER. Min, Max, S, and P values are global values. Abbreviations: TS, Thin section; CT, micro-CT; Comp., Global compactness.

Taxon	Specimen number / Collection	TS / CT	Resolution (µm)	Min	Max	S	P	Comp.
Carnivora								
Phocidae								
Phocinae								
<i>Nanophoca vitulinoides</i>	Histos 2142	TS	—	0.974	1.000	0.070	0.676	0.986
<i>Nanophoca vitulinoides</i>	IRSNB M2276g	CT	83.9	0.000	1.000	0.064	-0.154	0.999
<i>Phoca vitulina</i>	IRSNB 1157E	CT	45.7	0.115	1.000	0.060	0.707	0.541
<i>Phoca vitulina</i>	IRSNB 1157E	CT	46.3	0.091	1.000	0.087	0.559	0.691



Click here to access/download

Supplemental Material

Dewaele et al. Supplemental Table.docx

